NASA CR-135184

BORON/ALUMINUM FAN BLADES FOR SCAR ENGINES

FINAL REPORT

by

R.G. Stabrylla
R.G. Carlson

GENERAL ELECTRIC COMPANY

Prepared For

National Aeronautics and Space Administration

NASA Lewis Research Center
Contract NAS3-18910

1. Report No.	2. Government Accession No.	3. Recipient's Catalog No.
NASA CR-135184		

4. Title and Subtitle	5. Report Date
Boron/Aluminum Fan Blades for SCAR Engines	June 1977
	6. Performing Organization Code

7. Author(s)	8. Performing Organization Report No.
R.G. Stabrylla, R.G. Carlson	
	10. Work Unit No.

9. Performing Organization Name and Address	11. Contract or Grant No.
General Electric Company Aircraft Engine Group Cincinnati, Ohio 45215	NAS3-18910
	13. Type of Report and Period Covered
12. Sponsoring Agency Name and Address	Contractor Final Report
National Aeronautics and Space Administrations Washington, D.C. 20546	14. Sponsoring Agency Code

15. Supplementary Notes

Project Manager, D. McDaniels
NASA Lewis Research Center, Cleveland, Ohio 44135

16. Abstract

This report covers the technological developments to evaluate advanced fan blades of boron/aluminum to demonstrate Supersonic Cruise Aircraft Research (SCAR) type engines.

The program has been divided into four tasks. In Task I, processing procedures have been developed to enhance boron/aluminum bond behavior and foreign object damage (FOD) tolerance. In Task II, design and analysis have indicated that the J101 Stage 1 fan blade will meet the required frequencies without a midspan shroud. Task III has assessed the fabricability of full size J101 blades, while in Task IV six blades have been fabricated and finished machined.

The results demonstrate that components for fan blades are extremely attractive, and advancement as a result of this program will encourage the support of their applications.

17. Key Words (Suggested by Author(s))	18. Distribution Statement
Boron Aluminum Composite Material Impact Testing Fan Blades	Unclassified - Unlimited

19. Security Classif. (of this report)	20. Security Classif. (of this page)	21. No. of Pages	22. Price*
UNCLASSIFIED	UNCLASSIFIED	129	

* For sale by the National Technical Information Service, Springfield, Virginia 22151

TABLE OF CONTENTS

LIST OF ILLUSTRATIONS

LIST OF ILLUSTRATIONS (Continued)

LIST OF ILLUSTRATIONS (Continued)

LIST OF ILLUSTRATIONS (Concluded)

LIST OF TABLES

LIST OF TABLES (Concluded)

SECTION 1.0

INTRODUCTION

For several years, metal matrix composite materials have been recognized as having significant potential as replacement material for titanium fan and compressor blades used in high temperature, supersonic applications. For example, cost and weight reductions on the order of 35% relative to a standard metal blade are projected for a typical Supersonic Cruise Aircraft Research (SCAR) fan through the use of boron/aluminum composite materials. An aerodynamic performance improvement, resulting from the removal of the titanium blade mid-span shroud, is also anticipated with the advent of boron/aluminum fan blades.

Although these potential benefits are extremely attractive, the lack of impact resistance of boron/aluminum fan blades represents a major deterrent to the application of this material. Accordingly, this program was undertaken with the following objectives in mind:

Task I - Fabricate and characterize boron/aluminum composite panels made with uniaxial and angle plied reinforcement.

Task II - Refine the J101 F/Al composite fan blade design to successfully convey the design loads and resist the FOD anticipated in service.

Task III - Assess the fabricability (using non-destructive techniques) of full size J101 B/Al fan blades.

Task IV - Fabricate additional J101 B/Al fan blades for eventual dynamic impact rig testing.

These objectives have been accomplished during the period of performance of this contract and the results are summarized in the following section. Although these results are encouraging, future applications of B/Al fan blades in high temperature, supersonic engines must be predicated on consistently demonstrating the weight, cost and impact resistance benefits of this material in an actual service environment. General Electric remains enthusiastic about this technology and is confident of its ultimate success and acceptance.

SECTION 1.0

SUMMARY

This program was initiated to evaluate J101 Stage 1 fan blades fabricated in high impact resistant boron/aluminum materials to demonstrate application in Supersonic Cruise Aircraft Research (SCAR) type engines. The program is divided into four tasks. The scope of work within this reporting period includes the Task I and Task II efforts and initiation of Task III.

In the Task I - Advanced Process Development, initial attempts to use 1100 series aluminum matrix resulted in poorly bonded panels and delamination during machining of the specimens. A new material ATAC (Aluminum Two Alloy Composite), which uses alternating foils of 1100 and 2024 series aluminum, was devised to achieve improved bonding. Subsequent efforts to improve the bonding of the 1100 aluminum have been successful and both the 1100 aluminum and ATAC material systems remain potential candidates for fabricating J101 blades.

The highest impact energy of both the 1100 aluminum and ATAC was obtained in the [0/22/0-22] layup whereas the greatest impact energy of the 2024 aluminum was obtained in a [±15] layup. The 1100 aluminum material specimens exhibited highest impact strength while the 2024 Al was the lowest. The tensile and compressive testing was also completed.

Design and analysis of the J101 Stage 1 B/Al fan blade in Task II indicated that the blade will meet the required frequencies without a mid-span shroud, using 0.2 mm (8-mil) diameter boron filament material. All rotor component detail drawings were released. Design of the blade tooling was released and lofting of the blade patterns completed.

Within the Task III effort, the fabrication of the blade pressing die was completed and all other rotor components were fabricated.

Six J101 B/Al Stage 1 Fan Blades were fabricated in Task IV. Four of these blades have been machined and finished and are available for structural and FOD resistance evaluations on subsequent programs.

SECTION 3.0

DISCUSSION

3.1 ADVANCED PROCESS DEVELOPMENT

This section details the materials and processes selection approach taken during this program. The overall purpose of this program approach is to obtain quality blades with the highest impact strength possible. In fact, the recognition of the importance of FOD resistance requirement has dominated the direction of this program. This direction has been largely brought about by the recognized shortcomings of earlier B/Al blades and thus predicates the need for the FOD resistance priority.

The effort described herein consists of fabrication and characterization of boron/aluminum (B/Al) composite panels with uniaxial and angle cross-plied reinforcements to determine tensile, compression and impact properties. Boron filaments of both 0.14 mm (5.6 mil) and 0.2 mm (8.0 mil) diameter have beem composited with two matrix materials of 1100 aluminum and 2024 aluminum. This dual matrix composite is termed "Aluminum Two Alloy Composite" (ATAC). These composite elements have been combined into a continuous roll bonded (CRB) tape prior to forming the panels and blades. Both eight-ply panels of 12.7 cm × 17.8 cm (5 in. × 7 in) and the 46-ply panels of 7.6 cm × 12.7 cm (3 in. × 5 in.) have been fabricated at 767 K/5.5kN/cm^2/20 minutes (920° F/8 ksi/20 minutes), sectioned, tested and evaluated. The program on the eight-ply panel has been divided into three parts consisting of (1) evaluation of the alternate matrix ply layered approach, (2) characterization of the filament orientation on impact, and 3) determination of the aluminum reinforced stainless steel wire mesh influence on impact behavior. Additional eight-ply panels have been to evaluate the all-2024 Al and all-1100 Al matrix composites.

From test results, the ATAC composite system exhibited the best combination of properties and 46-ply panels have been fabricated for evaluation of both compression and Charpy impact behavior. Charpy test results showed impact strength for the [0], [0/22/0/-22], and [±15] orientations of only 35 ft-lbs, 20.5 ft-lbs, and 12 ft-lbs, respectively. These values were lower than desired and, consequently, greater emphasis was directed at improving the all-1000 Aluminum composite by varying the process parameters to achieve a more uniform bond with, hopefully, concomitant impact strength increases. These results have been translated into blade fabrication, but, as described later, these blades were of poor quality. Hence, this approach to consolidation of 1100 Al was unsuccessful and the program efforts were curtailed. An internally funded program had previously been initiated with the objective of identifying surface treatment procedures for achieving higher bond quality. This internal program successfully developed surface treatments which led to high quality bonding along with superior impact

characteristics. As a result of this program effort, surface treatments have been identified and then used to fabricate six additional blades.

3.1.1 Materials Screening

In the initial program effort, the materials evaluated were the 1100 Al and 2024 Al matrices along with the 5.6 mil and the 8.0 mil diameter boron filaments. In addition, the behavior of stainless steel reinforced aluminum and nickel plating were also evaluated.

The purpose of this task was to fabricate and characterize boron/aluminum (B/Al) composite panels with uniaxial and angle-plied orientations at [+15], [0/22] and [0/22/0/-22] to determine tensile, compression, and impact properties. As shown in the program flow diagrams in Figures 1 and 2, both 12.7 cm × 17.8 cm (5" × 7") × 8-ply panels and 7.6 cm × 12.7 cm (3" × 5") × 46-ply panels were fabricated. Panels, as well as blades, fabricated were designated by a coding system as outlined below:

Coding Sequence

5 5 8 2/1 - u

i ii iii iv v

i = volume percent, v/o
- 5 = 55 v/o

ii = orientation
- 0 - 0° filament orientation
- 1 - [±10] filament orientation
- 2 - [0/22/0/-22] filament orientation
- (0/2) - [0/-22] filament orientation
- 5 - [±15] filament orientation

iii = filament diameter
- 5 - 5.6 mil diameter filament
- 8 - 8 mil diameter filament

iv = matrix
- 1 - 1100 Al
- 2 - 2024 Al
- 2/1 - 2024 Al/1100 Al (ATAC)

v = designated panel number

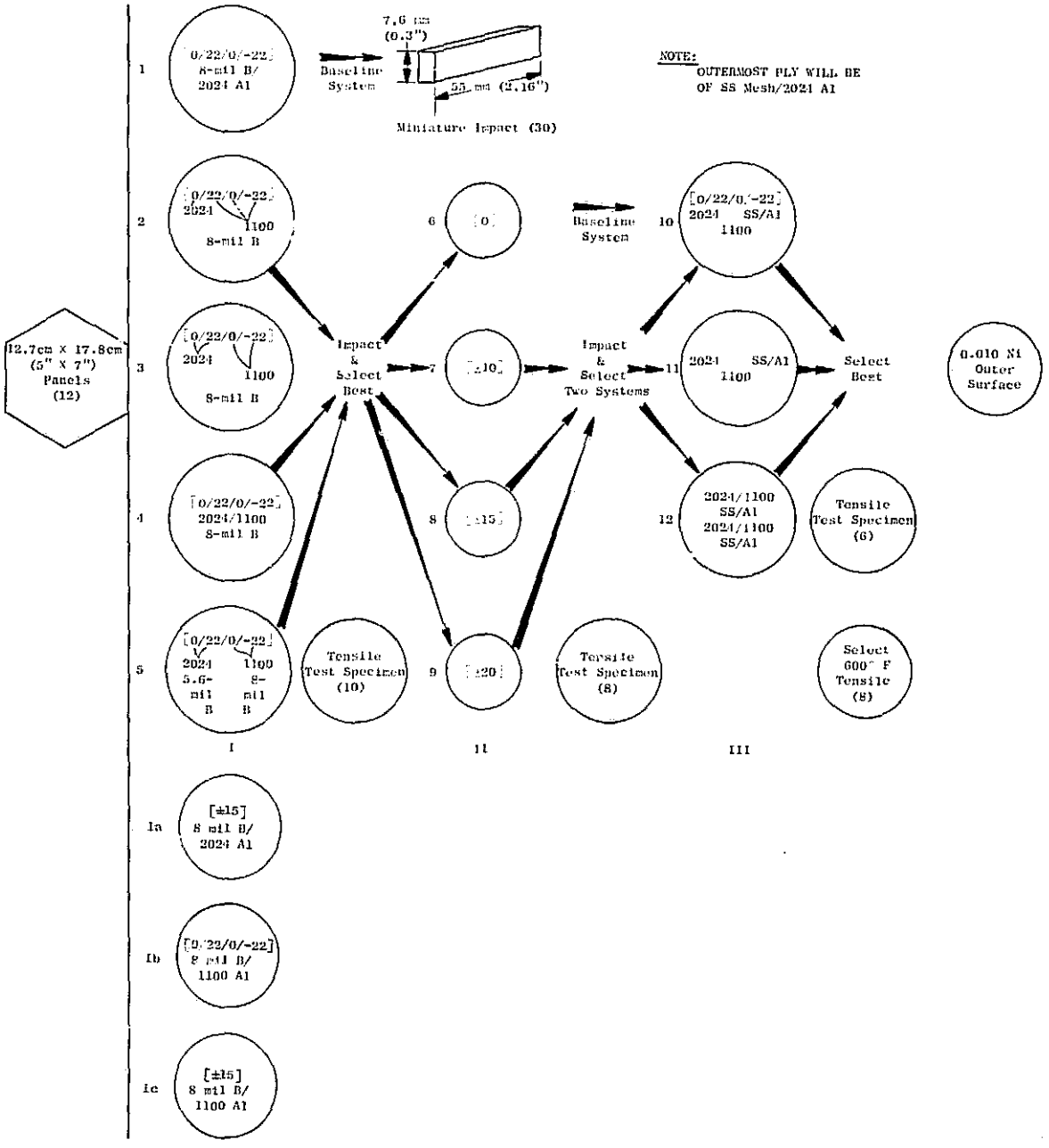

Figure 1. Program Flow Diagram for the 8-Ply Panels.

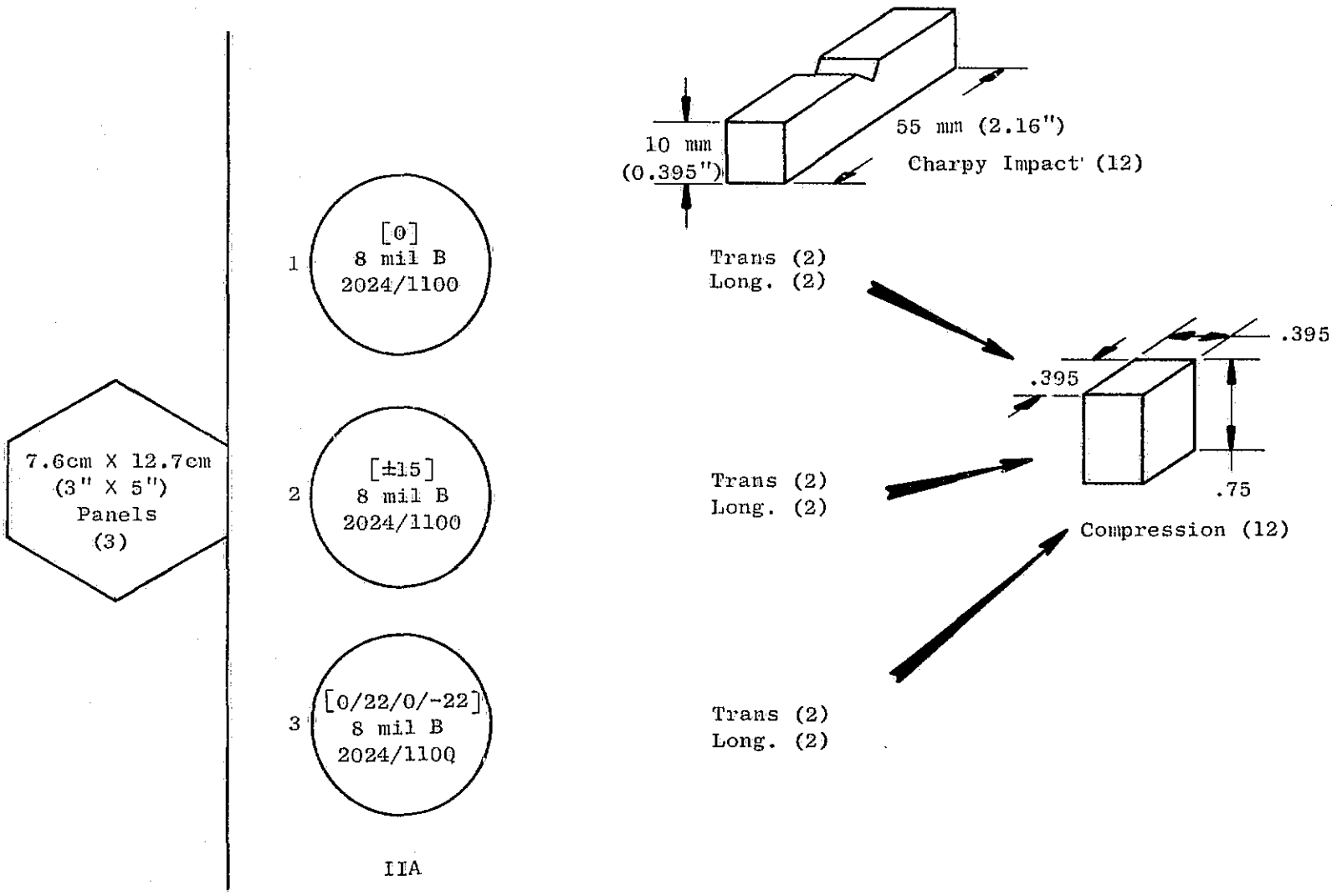

Figure 2. Program Flow Diagram for the 7.6 cm X 12.7 cm (3" X 5") 46-Ply Panels.

Eight-Ply Panels

The eight-ply panels were screened for impact behavior by use of pendulum impact testing and tensile tests.

Pendulum Impact Testing - The general requirements for the impact testing machine are that it shall be a pendulum type of rigid construction and have a capacity more than sufficient to break the specimen in one blow. The impact machine is inaccurate to the extent that some energy is used in deformation or movement of its component parts or of the machine as a whole; this energy will be registered as used in fracturing the specimen. The machine should not be used for values above 80 percent of the scale range.

Tests may be made at various velocities, but these shall not be less than 3 or more than 6 m/sec (not be less than 10 nor more than 20 ft/sec). Velocity shall always be stated as the maximum tangential velocity of the striking member at the center of strike. The impact value is taken as the energy absorbed in breaking the specimen. The machine is furnished with scales graduated in foot-pounds (ft-lbs) on which the reading can be estimated in increments of 0.25 percent of energy range. Means are provided to locate and support the test specimen against two anvil blocks in such a position that the center of the notch can be located within 0.25 mm (0.010 inch) of the midpoint between the anvils. Dimensions of the pendulum and supports should be such that interference is minimized between the pendulum and the broken specimens.

The center line of the striking edge advances in a plane that is 0.40 mm (0.010 inch) of the midpoint between the supporting edges of the specimen anvils. The striking edge must be perpendicular to the longitudinal axis of the specimens.

Impact velocity, v, of the pendulum (neglecting friction) can be determined through the use of the following equation:

$$v = \sqrt{2gh}$$

where:

v = striking velocity in meters (or feet) per second

g = acceleration of gravity in meters (or feet) per second

h = initial height of the striking edge in meters (or feet)

To ensure the accuracy of the Charpy machine, it is periodically checked against standardized specimens which are available from the U.S. Army Materials Research Agency. A set consists of fifteen 10 mm × 0.394 inch) V-notched specimens of known energy values, five at each of the three energy levels (see Table I). The average value at each energy level as

Table I. Composite Systems, Panel Numbers, Dimensions, and Corrected Impact Energies of Miniature Specimens.

	Composite System	Panel No.	Thickness mm	Width mm	Area mm^2	Corrected Impact Energy		Impact Strength		Comment
						joules	ft-lb	kJ/m^2	$ft\text{-}lb/in.^2$	
	2024 Al Alloy	---	2.03	6.22	12.65	35.0	25.8	2767	1316	---
1	55% [0/22/0/-22], 8-mil 2024	5282-C	1.91	7.52	14.36	7.7	5.7	536	257	---
1A	55% [±15], 8-mil 2024	5582-D	1.85	8.31	15.37	11.4	8.4	742	351	---
1B	55% [0/22/0-22], 8-mil, 1100	5281-E	1.88	9.88	18.57	35.8	26.4	1928	917	Shingled
1C	55% [±15], 8-mil, 1100	5581-F	1.93	10.34	19.96	31.7	23.4	1588	757	Shingled
2	55% [0/-22/0/-22], 8-mil, 2024/1100	5282/1-G	1.91	7.39	14.11	26.0 (14.0)	19.2 (10.4)*	1843 (992)	914 (495)	---
3	55% [0/22/0/-22], 8-mil, 2024/1100/1100/1100	5282(1)-H	1.98	5.97	11.82	15.3	11.3	1294	509	Shingled
4	55% [0/22/0/-22], 8-mil, 2024/2024/1100/1100	5282(1)-I	1.98	6.81	13.48	12.2	9.0	905	431	---
5	55% [0/22/0/-22], 5.6-mil and 8-mil, 2024/2024/1100/1100	526/82(1)-J	1.52	7.14	10.95	21.4	15.8	1954	935	---

*Specimens impacted on 1100 Al outer ply.

determined in the proof tests will correspond to the nominal values of the standard specimens within 1.0 ft-lb or 5.0 percent, whichever is greater.

Unnotched specimens also are extensively used. They tend to indicate the notch sensitivity of a material and serve as a direct comparison against different material properties. Through this comparison, the effect of crack propagation from unnotched areas may be evaluated.

For the purpose of a specimen configuration more nearly matching a blade thickness-to-chord (tm/c) ratio, as well as a cost reduction, miniature impact tests on boron/aluminum 8-ply panels have been conducted using a Charpy Physmet miniature impact tester, Model CIM-24, seen in Figure 3. The dimensions of such specimens are 55 mm × 10 mm (2.16 inch × 0.4 inch) × the thickness. The miniature impact specimens are unnotched. An estimated full-size Charpy impact value may be found by using the following relationship:

$$E = \frac{161.3\ (E_{impact})}{A}$$

where:

E = estimated full-size Charpy impact energy in joules or ft-lbs.

E_{impact} = energy absorbed by the miniature impact specimen in joules or ft-lbs

A = cross-sectional area of the full-size specimen in mm^2. For the cross-sectional area in $inch^2$, the constant is 0.25 $inch^2$.

In this screening phase, twelve 8-ply panels were consolidated.

The test results on the B/Al specimens for part I are presented in Table I, along with the specimens from a 2 mm (0.080 inch) thick 2024 Al sheet after a simulated press cycle treatment of 495° C (920° F) for 20 minutes. Each test result is an average of data from at least two tests. Specimens derived from the all-1100 Al exhibited extensive delaminations during machining. Impact testing on this 1100 Al material system, however, produced the highest impact strength of 35.8 joules (26.4 ft-lbs), but the specimens were severely shingled, indicating poor bonding. The B/Al system which indicated the greatest potential as a viable blade material was the ATAC (2024/1100 Al); when impacted against the 2024 Al side, it attained an impact strength of nearly 27.1 joules (20 ft-lbs). The ATAC composite configuration was selected for incorporation in the part II effort on evaluation of filament orientation. These test results, recorded Table II, along with duplicate specimens impacted on the 1100 Al side reveal the anisotropic nature of this ATAC system.

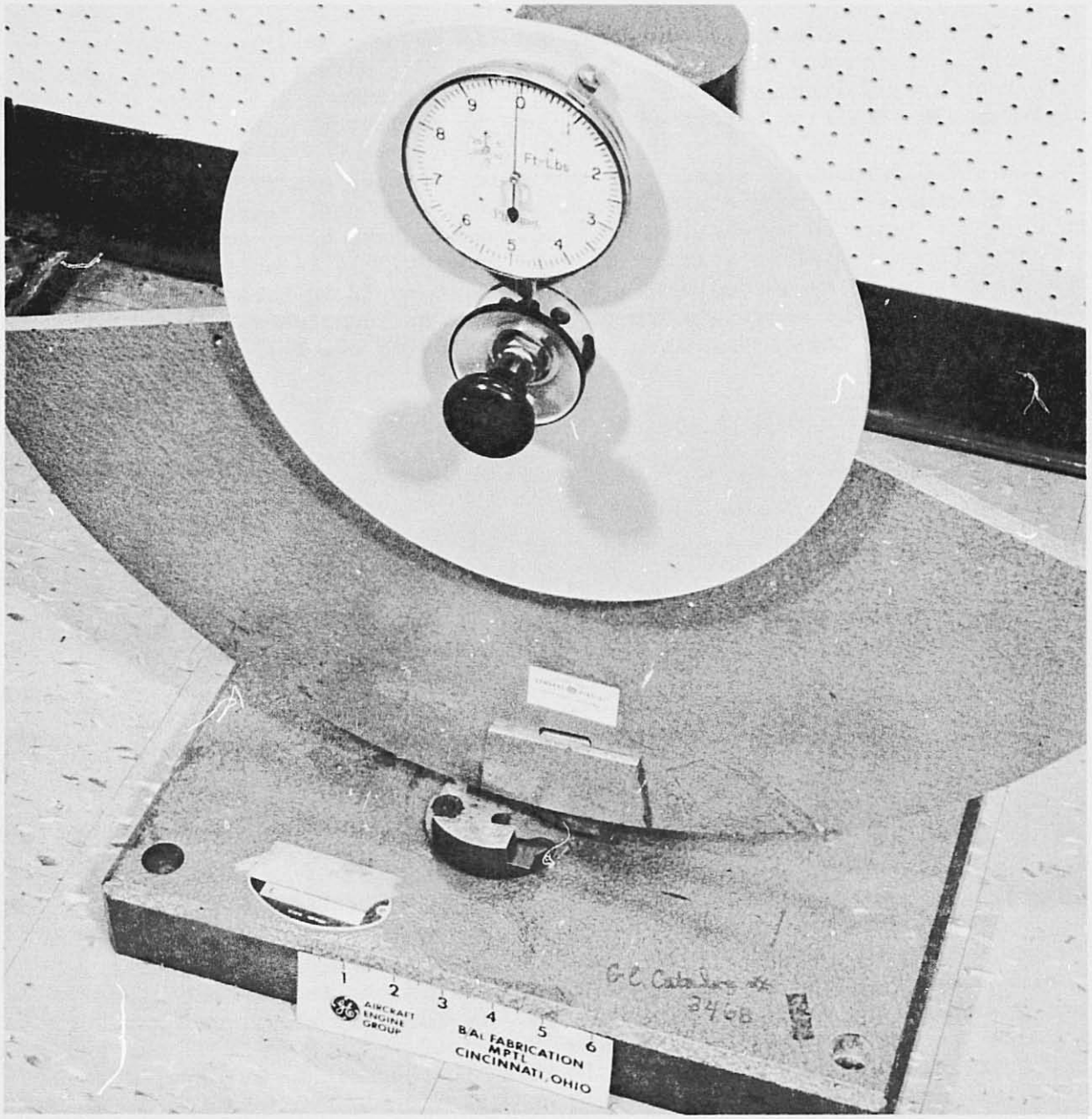

Figure 3. Physmet Impact Testing Machine, Model CIM-24.

Table II. Composite Systems, Panel Numbers, Dimensions, and Corrected Impact Energies of Miniature Specimens.

	Composite System	Panel No.	Thickness mm	Width mm	Area mm	Corrected Impact Energy		Impact Strength	
						joules	ft-lb	kJ/m^2	$ft\text{-}lb/m^2$
6	55% [0], 8-mil, 2024/1100	5082/1-O	1.98 (1.98)	7.24 (7.47)	14.33 (14.79)	17.34 (10.70)	12.8 (7.9)*	1210 (723)	577 (345)
7	55% [±10], 8-mil, 2024/1100	5182/1-P	1.98 (1.98)	7.95 (7.62)	15.74 (14.71)	16.12 (10.16)	11.9 (7.5)*	1024 (691)	488 (320)
8	55% [±15], 8-mil, 2024/1100	5582/1-Q	1.93 (1.93)	7.62 (7.37)	14.70 (14.22)	20.32 (10.03)	15.0 (7.4)*	1382 (705)	658 (336)
9	55% [±20], 8-mil, 2024/1100	5282/1-R	1.08 (1.98)	7.98 (7.59)	15.80 (15.03)	20.87 (10.57)	15.4 (7.8)*	1321 (703)	629 (335)

*Specimens impacted on 1100 Al outer ply.

Matrix Enhancement - As part III of the planned effort to evaluate enhancement, specimens from the three remaining B/Al composite panels containing stainless steel mesh were miniature impact tested. In addition, two other panels were consolidated and similarly tested to determine the material combination influence on these material systems.

The stackup sequence and ply orientations for the five fabricated panels are presented in Table III. These panels were prepared from the Continuous Roll Bonded (CRB) tapes. The designation of 2024/1100-B indicates a single ply containing 55 v/o boron with the 2024 Al on one side and the 1100 Al on the other, while the designation of 2024-B or 1100-B indicates the ply contained the designated alloy on both surfaces. In the case of panel N5282/1-G4, the 0.2 mm (8-mil) boron filament was wound on one mil 1100 Al with a cover layer of one mil 1100 Al. Between each of the ply layers, a 2 mil layer of 2024 Al was inserted and pressed. Finally, panel N5282/1-G5 contained the ATAC system, but with the sequence reversing itself at the center to provide for 2024 alloy on the outer layer. As before, these panels were all pressed at 920° F at a pressure of 8 ksi for 20 minutes.

Two longitudinal and transverse specimens were impact tested from each of these five, eight-ply panels. Again, the miniature impact specimens were 10 mm × 55 mm (0.4" × 2.16") by the thickness. Figures 4 and 5 show both the longitudinal and transverse impact specimen of the five panel specimens after impact. Only a slight amount of delamination was evident and only on a longitudinal G2 panel specimen. The delamination on this specimen was not too surprising since it contained plies consisting of all-1100 Al. The results given in Tables IV and V indicated that panel number N5282/1-G4 had an average impact strength of 23.4 joules (17.3 ft-lbs). This impact strength is not as high as the 26.0 joules (19.2 ft-lbs) determined on the previous ATAC impact specimen, and it is felt that the material was probably more extensively bonded, thereby limiting the filament movement in the matrix and decreasing the material's impact energy absorption capabilities. However, it was believed that if the boron filament were surrounded by the 1100 Al, higher impact strengths would be achievable; this was not the case. It also appears that the stainless steel mesh plies in panels G1, G2 and G3 do not provide further enhancement.

After examining the failure modes on specimens from these three panels, it was noted that fracture occurred without delamination. This would indicate that the panels were overbonded when pressed at 8 ksi, and suggests that higher impact strength could be obtained by pressing at lower pressures. Metallographic observations (as seen in Figure 6), on a transverse veiw of specimens G1 and G3 reveal the well bonded characteristic with no visible indication of interlayer separation. The results recorded here indicate that the G1 configuration causes the least impact strength loss. However, both G1 and G3 were selected for nickel plating and subsequent impact testing. One additional observation is that the reversal of the stacking sequence at the center so as to provide for the 2024 Al on the outward layer does decrease the impact strength, but only by about 25 percent of that for the all-ATAC system impacted on the 2024 Al side.

Table III. Fabricated 12.7 cm x 17.8 cm (5" x 7") Panel Configuration.

Panel No.	Ply Configuration	
	Ply Orientation	Stackup Sequence
N5282/1-G1	0°	2024/1100-B
	22°	2024/1100-B
		SS MESH/Al
		SS MESH/Al
	0°	2024/1100-B
		SS MESH/Al
		SS MESH/Al
	22°	2024/1100-B
	0°	2024/1100-B
N5282/1-G2	0°	2024 -B
		SS MESH/Al
	22°	1100 -B
		SS MESH/Al
	0°	2024 -B
		SS MESH/Al
	22°	1100 -B
		SS MESH/Al
	0°	2024 -B
N5282/1-G3	0°	2024/1100-B
		SS MESH/Al
	22°	2024/1100-B
		SS MESH/Al
	0°	2024/1100-B
		SS MESH/Al
	22°	2024/1100-B
		SS MESH/Al
	0°	2024/1100-B
N5282/1-G4		2024
	0°	1100-B
		2024
	+22°	1100-B
		2024
	0°	1100-B
		2024
	-22°	1100-B
		2024
	0°	1100-B
		2024
	+22°	1100-B
		2024
	0°	1100-B
		2024
N5282/1-G5	0°	2024/1100-B
	+22°	2024/1100-B
	0°	2024/1100-B
	-22°	2024/1100-B
		2024
	-22°	1100/2024-B
	0°	1100/2024-B
	+22°	1100/2024-B
	0°	1100/2024-B

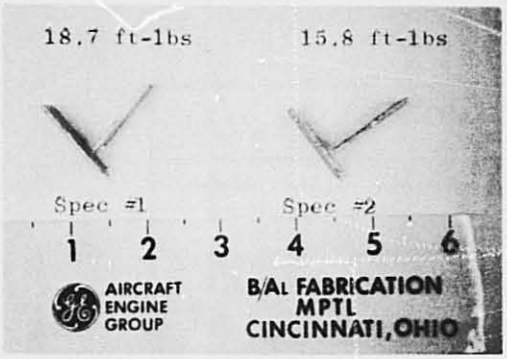

Longitudinal

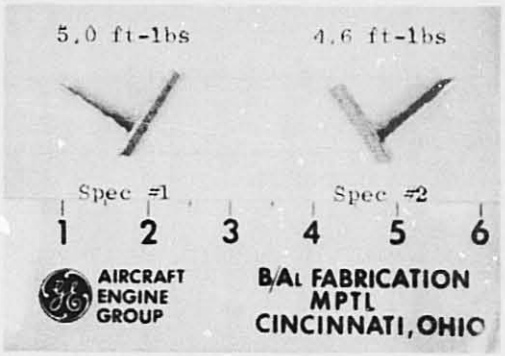

Transverse

Panel N5282/1-G1 0/22/0/-22 v/o 40%

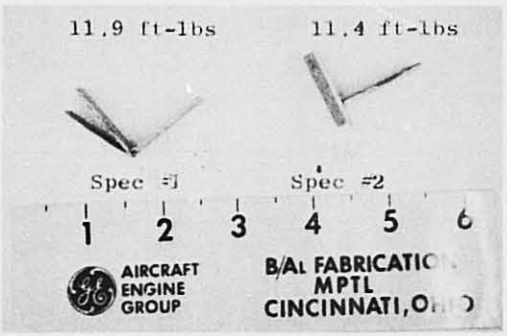

Longitudinal

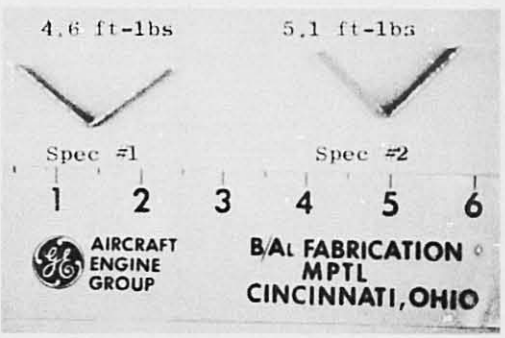

Transverse

Panel N5282/1-G2 0/22/0/-22 v/o 38%

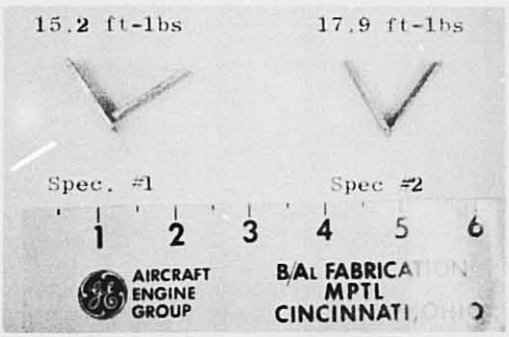

Longitudinal

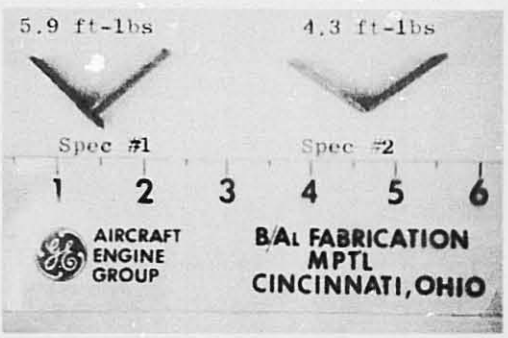

Transverse

Panel N5282/1-G3 0/22/0/-22 v/o 40%

Figure 4. Longitudinal and Transverse Miniature Impact Specimens Pressed at 920° F/8 ksi.

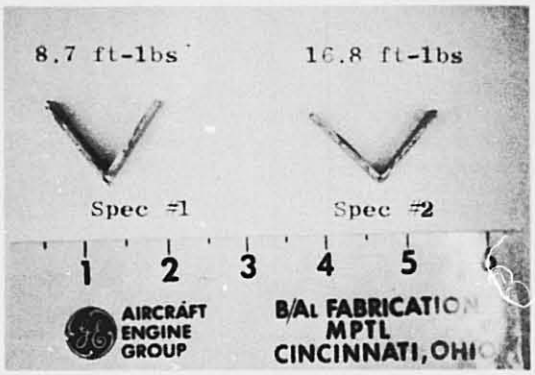

Longitudinal

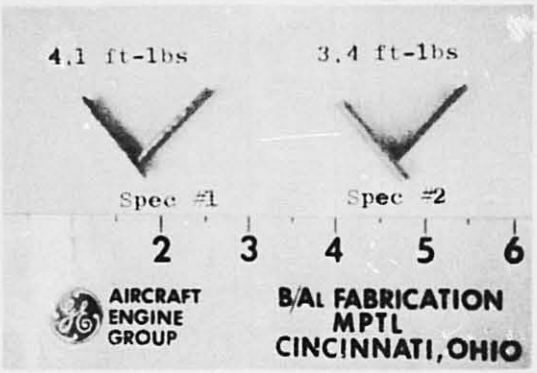

Transverse

Panel N5282/1-G4 0/22/0/-22 v/o 58%

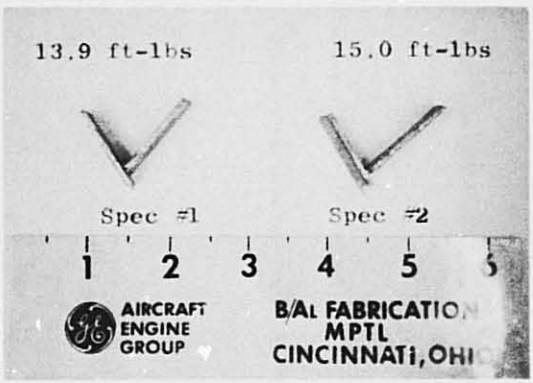

Longitudinal

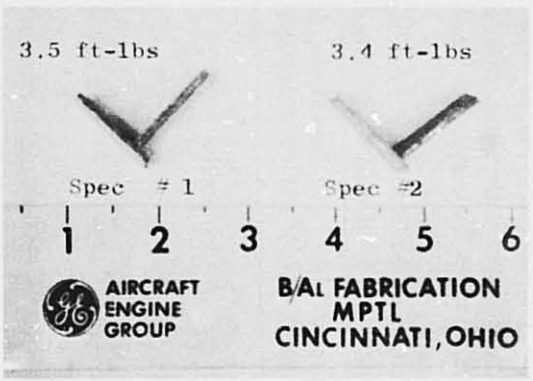

Transverse

Panel N5282/1-G5 0/22/0/-22 v/o 53%

Figure 5. Longitudinal and Transverse Miniature Impact Specimens Pressed at 920° F/8 ksi.

Table IV. Composite Systems, Panel Numbers, and Corrected Charpy Impact Strength for Longitudinal Specimens Pressed at 920° F/8 ksi/20 Minutes.

Composite System	Panel Number	Corrected Impact Strength		Impact Energy		Impact Strength	
		Specimen No. 1 (ft/lb)	Specimen No. 2 (ft/lb)	joules	ft/lb	kJ/mm^2	$ft\text{-}lb/in.^2$
40% [0/22/0/-22] 8-mil, 2024/1100	N5282/1-G1	18.7	15.7	23.3	17.2	1383	659
40% [0/22/0/-22 8-mil, 2024/1100	N5282/1-G2	11.9	11.4	15.9	11.7	896	427
40% [0/22/0/-22] 8-mil, 2024/1100	N5282/1-G3	15.2	17.9	22.4	16.5	1228	585
55% [0/22/0/-22] 8-mil, 2024/1100 (1100 Al against B)	N5282/1-G4	16.8	17.8	23.4	17.3	1220	581
55% [0/22/0/-22] 8-mil, 2024/1100 (Inverted @ Center)	N5282/1-G5	13.9	15.0	19.5	14.4	1020	486

Table V. Composite Systems, Panel Numbers, and Corrected Impact Energies of Miniature Tansverse Specimens.

Composite System	Panel No.	Specimen No. 1 Corrected Impact Energy (joules)	Specimen No. 2 Corrected Impact Energy (joules)	Corrected Impact Energy (joules)	Corrected Impact Strength	
					kJ/mm^2	$ft\text{-}lb/in.^2$
40% [0/22/0-22] 8-mil, 2024/1100	N4282/1-G1	6.8	6.2	6.5	336	160
40% [0/22/0/-22] 8-mil, 2024/1100	N3282/1-G2	6.2	6.9	6.5	319	152
40% [0/22/0/-22] 8-mil, 2024/1100	N3282/1-G3	8.0	5.8	6.9	339	19C
55% [0/22/0/-22] 8-mil, 2024/1100 (1100 Al against B)	N5282/1-G4	5.6	4.6	5.1	237	113
55% [0/22/0/-22] 8-mil, 2024/1100 (Inverted @ Center)	N5282/1-G5	4.7	4.6	4.7	235	112

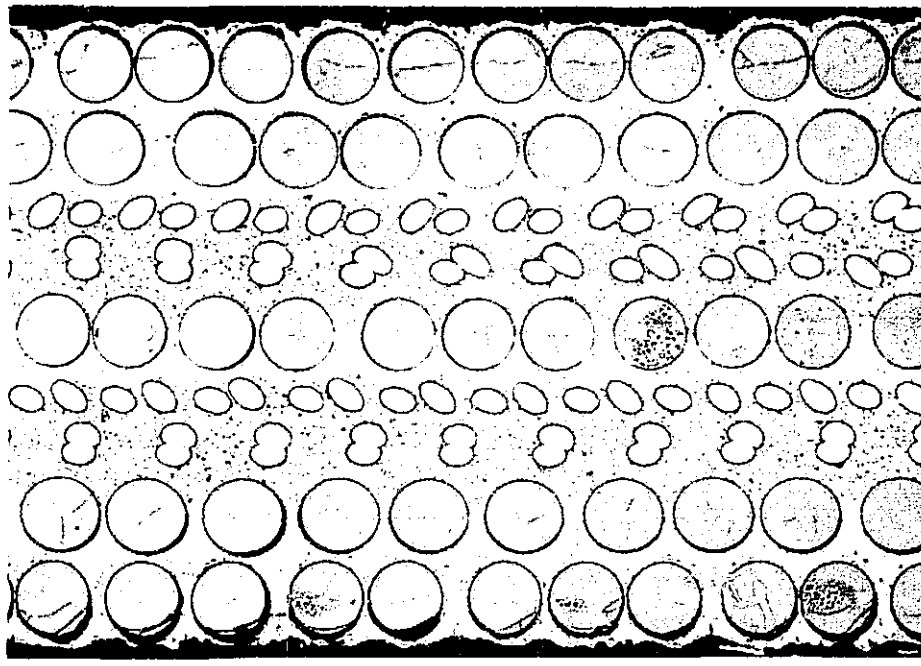

Specimen N5282/1-G1

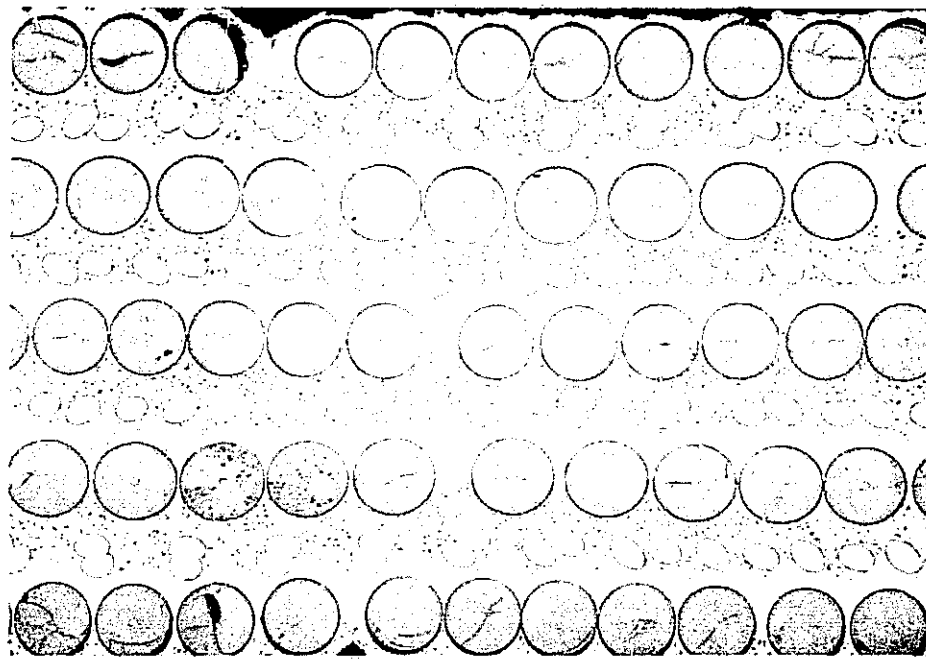

Specimen N5282/1-G3

Figure 6. Transverse Metallographic Observations of the Two Matrix Enhancement Panels, N5282/1-G1 and N5282/1-G3.

Miniature impact specimens from the two select systems, G1 and G3, were nickel plated and impact tested. The average nickel plate thickness was 4 mils per side. In general, the eight specimens after impact testing indicate a smaller degree of bend that their uncoated counterparts. A series of specimens were subjected to a heat treat and then tested. The impact test results given in Table VI reveal that the average longitudinal impact strengths for the nickel plated G1 and G3 specimens were, respectively, 11.7 joules (8.6 ft-lbs) and 16.7 joules (12.3 ft-lbs) before heat treatment and 15.6 joules (11.5 ft-lbs) and 13.6 joules (10.0 ft-lbs) after heat treatment. Although the impact data are scattered, they present a general trend of a loss of impact strength with nickel plating.

Tensile Testing

Tensile tests were performed on the 8-ply panels from parts I and II. The room temperature tensile tests were conducted on a Tinius-Olsen testing machine in both longitudinal and transverse fiber directions. Only single specimens were obtained from longitudinal and transverse direction from each panel. Nine two standard 2024 aluminum specimens and nine composite panels were tested (a total of eighteen composite specimens). The results presented in Table VII reveal that panel number 5082/1-0, with zero degree ply orientation and a 2024/1100 AT/AC matrix system, gave the highest ultimate tensile strength and yield strength (in the longitudinal direction) of, respectively, 211.3 ksi and 173.1 ksi. The somewhat lower strength for the [±10] orientation can be attributed to a premature grip failure.

It was determined that panel 5282-C, [0/22/0-22] ply orientation and an all-2024 matrix system displayed longitudinal and transverse tensile strenghs of 166.8 ksi and 22.0 ksi, respectively. Also noted was the composite system 5282/1-G which exhibited the highest longitudinal strength of 194.3 ksi for the angle ply systems and was one of the select candidate materials. This 5282/1-G system exhibited a transverse strength of 20.8 ksi.

Attempts made to fabricate tensile specimens from the all-1100 aluminum panels were unsuccessful as the material delaminated excessively during sectioning.

Forty-Six-Ply Panels

The planned approach to evaluate the Ab-ply panels included the preparation and evaluation of Charpy specimens machined to the standard test configuration as well as compression specimens derived from the panels.

Charpy Testing - Charpy specimens were employed to obtain standard impact energy data as well as additional impact fracture information from load-time recordings. This summary contains a description of the instru-

Table VI. Ni Plated Composite System, Panel Numbers and Corrected Impact Energies of Miniature Longitudinal and Transverse Specimens.

	Before Ni Plate Average Corrected Impact		With Ni Plate		With Ni Plate and Heat Treat	
Panel No.	Joules	ft-lbs	Joules	ft-lbs	Joules	ft-lbs
N4282/1-G1	18.7	(13.8)	11.7	(8.6)	15.6	(11.5)
N4282/1-G1 Trans.	6.5	(4.8)	6.7	(5.0)	7.9	(5.8)
N3282/1-G3	17.5	(12.9)	16.7	(12.3)	13.6	(10.0)
N3282/1-G3	6.1	(4.5)	6.6	(4.9)	5.7	(4.2)

Table VII. Composite Systems, Panel Numbers, Corrected Ultimate Tensile Stress and 0.2% Yield Strength.

Composite System	Panel No.	UTS (Ksi)		0.2% YS (Ksi)	
		Longitudinal	Transverse	Longitudinal	Transverse
2024 Al Alloy	---	36.9	---	14.8	---
55% [0/22/0/22], 8-mil 2024	5282-C	166.8	22.0	122.9	19.7
55% [±15], 8-mil, 2024	5282-D	147.1	19.2	109.5	17.3
55% [0/22/0/-22], 8-mil, 1100	5281-E	---	---	---	---
55% [±15], 8-mil, 1100	5581-F	---	---	---	---
55% [0/-22/0/-22],8-mil, 2024/1100	5282/1-G	194.3	20.8	121.5	19.8
55% [0/22/0/-22],8-mil, 2024/ 1100/1100/1100	5282(1)-H	---	---	---	---
55% [0/22/0/-22],8-mil, 2024/ 2024/1100/1100	5282(1)-I	130.1	14.2	85.8	13.6
55% [0/22/0/-22], 5.6-mil and 8-mil, 2024/2024/1100/1100	526/83(1)-J	156.8	15.9	92.5	12.3
55% [0], 8-mil, 2024/1100	5282/1-O	211.3	10.9	173.1	10.3
55% [±10], 8-mil, 2024/1100	5182/1-P	136.1	---	114.9	---
55% [±15], 8-mil, 2024/1100	5582/1-Q	150.2	12.9	102.5	11.0
55% [±20], 8-mil, 2024/1100	5282/1-R	152.4	17.6	81.6	12.1

mented impact test technique, results from calibration tests, and results from tests on the B/Al composite specimens.

Specimens - Calibration specimens were standard notched Charpy impact specimens per ASTM E23. The specimens were nominally 10 mm × 10 mm in cross section and 55 mm in length (0.395 inches × 0.395 inches and 2.16 inches in length). Calibration specimens were in two groups: (1) aluminum specimens supplied by the manufacturer of the instrumented striking tup used in this program and (2) steel specimens obtained from the Army Materials and Mechanics Research Center (AMMRC) at Watertown Arsenal. This latter group of specimens consisted of three lots of five specimens each. AMMRC had previously determined the impact energies of each lot and had found that the variation in impact energy from specimen to specimen was less than either ±1.36 joules (±1 ft-lb) or ±15 percent of the known average value. These AMMRC specimens are widely used as referee standards for qualification of impact test facilities and are referenced in ASTM E23.

The B/Al specimens consisted of both standard size (10 mm × 10 mm × 55 mm) notched and unnotched Charpy specimens. Transverse as well as longitudinal fiber orientations were employed. A few B/Al specimens were shorter than the standard length; however, these were long enough for proper support in the test fixture and presented no problem in testing.

Test Apparatus - All testing was performed on a Tinius-Olsen Model 64 universal impact tester. The machine was set up per requirements of ASTM E23 and is certified to do testing per the ASME Boiler and Pressure Vessel Code.

Instrumented impact testing was made possible by the substitution of a specially instrumented tup for the standard tup within the machine hammer assembly. The instrumented tup was procured from Effects Technology, Inc. through the Tinius-Olsen Company and had the same geometry as the standard tup except for the installation of strain gauges in recesses on the sides of the tup back from the tapered nose.

With appropriate instrumentation, these strain gauges permitted recording of the instanteous load-time tup response resulting from impact with specimens during testing. A block diagram of the instrumentation is shown in Figure 7. A Vishay strain gauge potentiometer was employed to provide the excitation voltage and the shunt resistance for balancing the strain gauge Wheatstone bridge circuit on the tup. The Vishay device also served as an amplifier for the strain gauge output to permit display on the Tektronix oscilloscope screen.

Testing involved placing a specimen in the impact test machine and releasing the hammer-pendulum to swing down and fracture the specimen on impact. The load-time response of the instrumented tup as displayed on the oscilloscope screen was photographed to provide a permanent record.

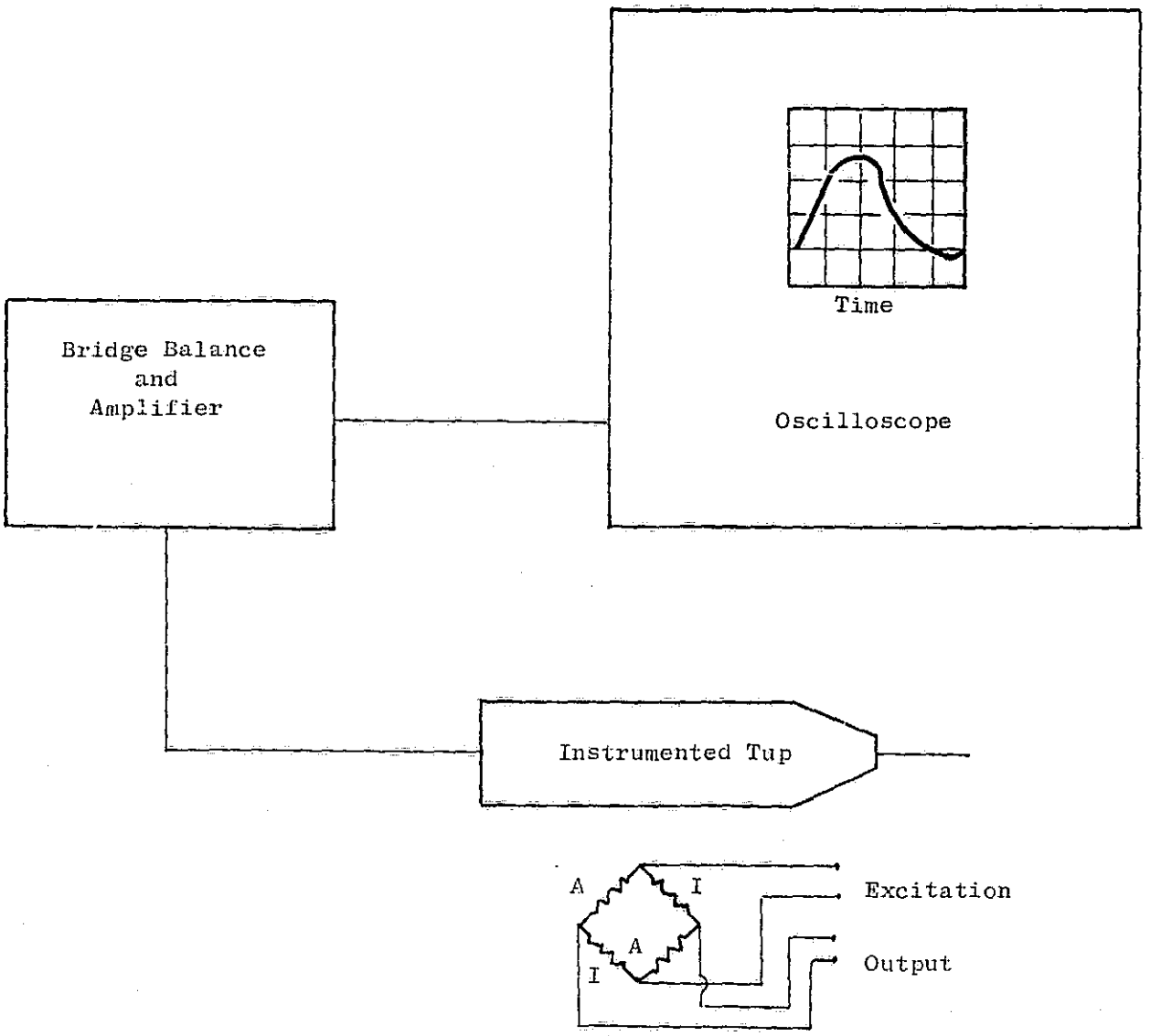

Figure 7. Instrumentation Block Diagram.

Test Results - Impact energy data for the fifteen steel Charpy specimens procured from AMMRC are presented in Table VIII. The average impact energy obtained from each group of five specimens was within the range of consistency of the referee data obtained previously by AMMRC. In fact, only one individual result (S/N S8-3) was greater than 5 percent different from its corresponding referee value. It was concluded that the testing machine was in calibration per ASTM E23 and was thereby suitable for subsequent testing of B/Al specimens in this program.

Copies of the load-time oscilloscope traces obtained from the AMMRC steel specimens in general all appear to display similar appearance, being slightly skewed symmetrically about a vertical line through the maximum. The absence of a small portion of the left side of each trace resulted from the fact that the impulse of the signal itself was used to trigger the oscilloscope sweep.

Impact energy data were also obtained from aluminum alloy "calibration" specimens supplied by the instrumented tup manufacturer, Effects Technology, Inc. These data are also presented in Table VIII. Information received from the load-time traces of these specimens indicated that maximum load values to be obtained from impact fracturing of the specimens would be 1550 ± 50 pounds. As the data in Table VIII show, neither the measured impact energy nor the maximum height of the load-time trace (proportional to max. load) was consistent from specimen to specimen. Since immediately prior testing of the AMMRC steel specimens gave consistent results and demonstrated the propriety of the test machine, these aluminum specimens were rejected for calibration purposes. The results, however, are reported here as a matter of record.

Impact energy data obtained from sixteen B/Al composite specimens and two 2024-T3 aluminum alloy specimens are presented in Table IX. The 2024-T3 specimens were tested to provide reference information. In the case of the B/Al material, both notched and unnotched specimens with both transverse and longitudinal fiber orientations were tested. In all cases, longitudinal specimens exhibited greater impact energy than corresponding transverse specimens. Unnotched longitudinal specimens generally had higher impact energies than notched longitudinal specimens within each group. Notched and unnotched results from transverse specimens in each group differed only slightly.

Copies of the load-time traces for the [0/22/0-22] and [±15] (T and V) series of B/Al specimens are shown in Figures 8 and 9. These traces exhibit the same shape characteristics as those traces for the AMMRC steel and Effects Technology, Inc., aluminum specimens.

Analysis - It is important to note that the oscilloscope load-time traces are truly voltage-time traces where the voltage is directly proportional to load. The AMMRC steel specimens, thus, were tested not only to ensure the calibration of the testing machine, but also to provide data for determination of the proportionality constant between voltage and load.

Table VIII. Calibration Specimen Results.

Specimen Number	Measured Impact Energy, W_T (joules)	(ft/lbs)	AMMRC Std. Impact[1] Energy (joules)	(ft/lbs)	Indicated Impact[2] "Energy", $\bar{V}A$ (m/sec-cm^2)	(ft/sec-in.^{2})	Max Height[2] of Load-Time Trace (cm)	(in)
AMMRC Steel Specimens								
P6-1	17.6	13.0	16.8	12.4	No Photo	No Photo	No Photo	No Photo
P6-2	17.6	13.0	16.8	12.4	27.5	14.0	1.57	0.62
P6-3	16.3	12.0	16.8	12.4	No Photo	No Photo	No Photo	No Photo
P6-4	16.9	12.5	16.8	12.4	No Photo	No Photo	No Photo	No Photo
P6-5	16.9	12.5	16.8	12.4	17.9	9.1	0.84	0.33
R7-1	69.1	51.0	71.7	52.9		No Photo	No Photo	No Photo
R7-2	69.1	51.0	71.7	52.9	156.0	79.3	8.13	3.20
R7-3	71.8	53.0	71.7	52.9	155.4	79.0	7.85	3.09
R7-4	74.5	55.0	71.7	52.9	150.1	76.3	7.72	3.04
R7-5	69.1	51.0	71.7	52.9	146.7	74.6	7.85	3.09
S8-1	94.8	70.0	92.8	68.4	213.2	108.4	11.13	4.38
S8-2	92.1	68.0	92.8	68.4	206.5	105.0	10.54	4.15
S8-3	99.6	73.5	92.8	68.4	223.6	113.7	11.28	4.44
S8-4	94.8	68.0	92.8	68.4	183.1	93.1	9.50	3.74
S8-5	93.5	69.0	92.8	68.4	196.3	99.8	10.24	4.03
Effects Technology Aluminum Specimens								
4A1	10.2	7.5	--	--	49.8	25.3	2.69	1.06
5A1	13.6	10.0	--	--	65.3	33.2	3.51	1.38
6A1	12.9	9.5	--	--	60.0	30.5	3.23	1.27
8A1	12.9	9.5	--	--	69.6	35.4	3.66	1.44
9A1	10.2	7.5	--	--	64.1	32.6	3.40	1.34
10A1	9.5	7.0	--	--	46.6	23.7	2.39	0.94

(1) Average determined in previous AMMRC tests
(2) Adjusted for electronic amplification and photo magnification

Table IX. B/Al Test Results ATAC Material.

Spec. No.		Notched/ Unnotched	Fiber Orient	Measured Impact Energy (joules)	Measured Impact Energy (ft/lbs)	Indicated "Energy"(1) VA (m/sec-cm^2)	Indicated "Energy"(1) VA (ft/sec/in.^{2})	Max. Height (cm)	Max. Height (in.)
U1	[0]	Notched	Long.	47.4	35.0	141.4	71.9	7.45	2.93
U2	"	Notched	Long.	46.1	34.0	152.2	77.4	7.77	3.06
U5	"	Unnotched	Trans.	1.4	1.0	No Photo	No Photo(2)	No Photo(2)	
U6	"	Unnotched	Trans.	2.0	1.5	No Photo	No Photo(2)	No Photo(2)	
V1	[0/22/0/22]	Notched	Long.	27.8	20.5	103.7	52.7	5.56	2.19
V3	"	Unnotched	Long.	27.8	20.5	89.3	45.4	4.75	1.87
V5	"	Notched	Trans.	7.5	5.5	66.9	34.0	3.46	1.36
V6	"	Unnotched	Trans.	5.5	4.0	38.9	19.8	2.11	0.83
T1	[±15]	Notched	Long.	12.9	9.5	57.6	29.3	3.13	1.23
T3	"	Unnotched	Long.	19.6	14.5	65.1	33.1	3.53	1.39
T5	"	Unnotched	Trans.	4.7	3.5	48.4	24.6	1.91	0.75
T7	"	Notched	Trans.	4.1	3.0	44.8	22.8	2.44	0.96
1(3)	Unreinforced	Notched	--	23.0	17.5	152.0	77.3	7.64	3.01
7(3)	Unreinforced	Unnotched	--	153.1	113.0	440.2	223.8	16.94	6.67

(1) Adjusted for electronic amplification and photographic magnification
(2) Low impact energy; tup response was not sufficient to trigger oscilloscope sweep
(3) 2024-T3 aluminum specimens supplied with B/Al specimens
(4) U, V and T are designated specimen types

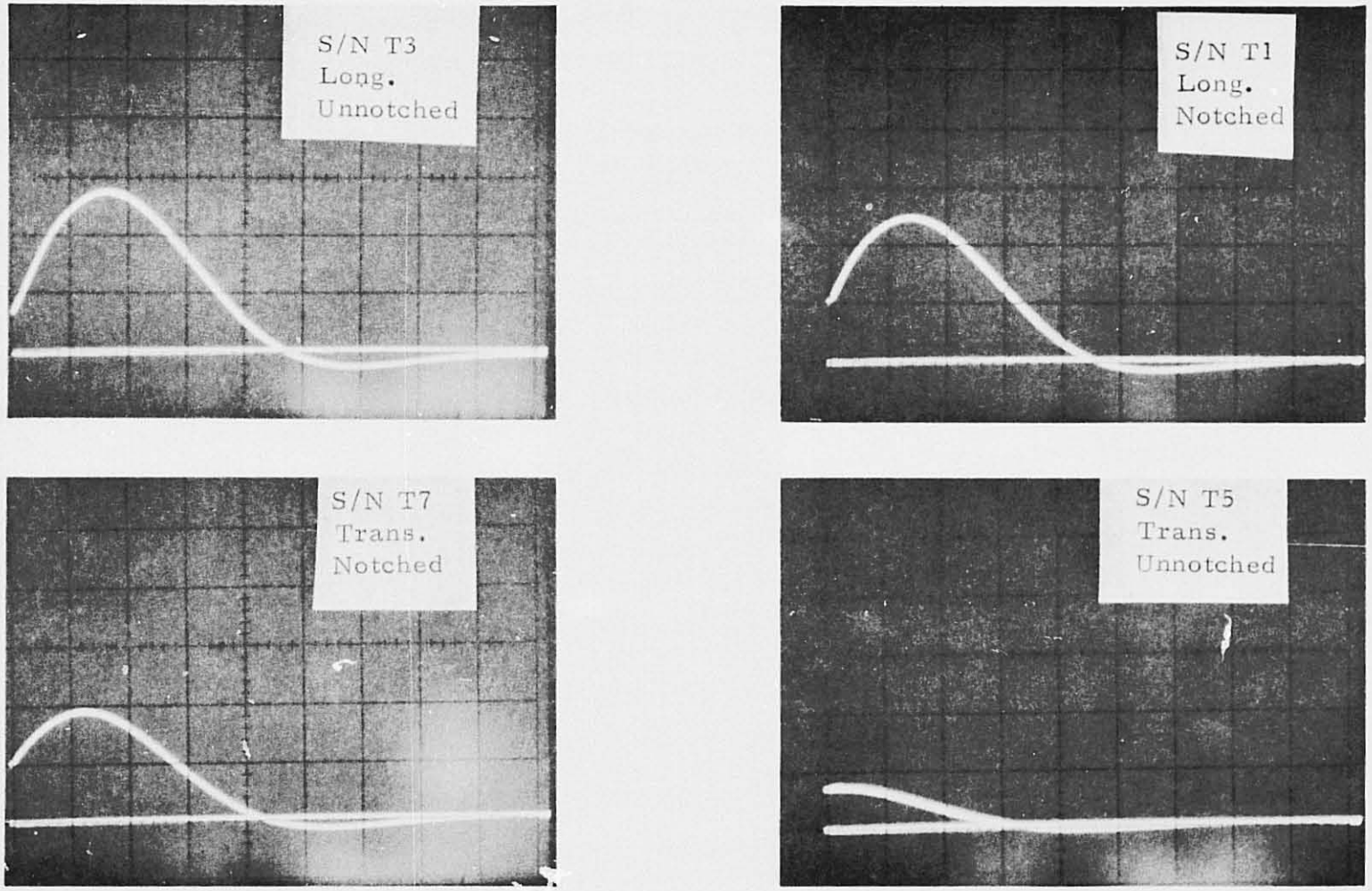

Y = 50 mv/div. (except T5; Y = 100 mv/div.)
X = 1 msec/div.
1 div. = 0.50 in.

Figure 8. T-Series B/Al Composite Specimen Load-Time Traces.

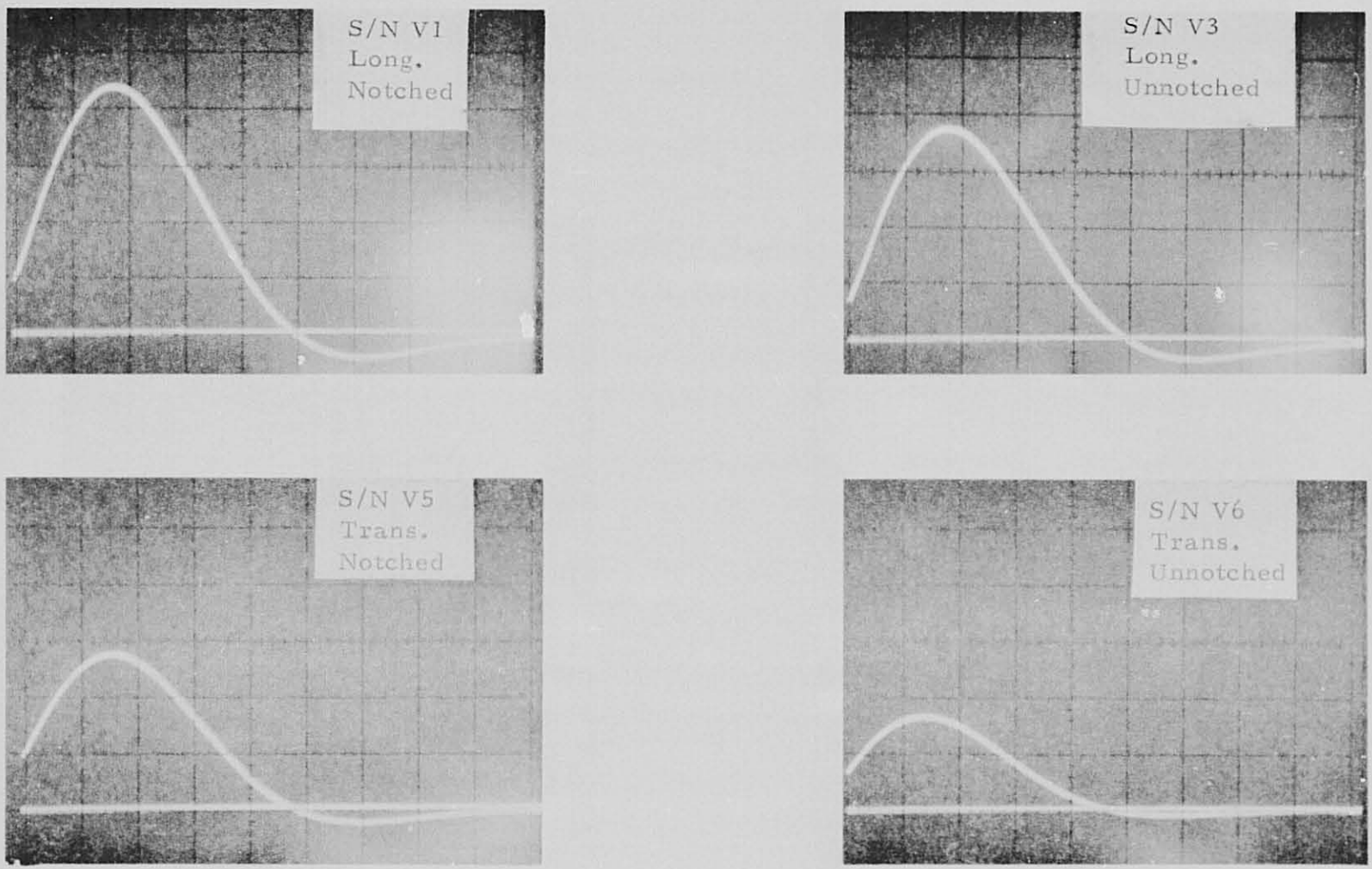

Y = 50 mv/div.
X = 1 msec/div.
1 = 0.50 in.

Figure 9. V-Series B/A1 Composite Specimen Load-Time Traces.

The calibration procedure employed in this program was developed previously by Server and Tetelman[1]. The procedure involved comparison of the Charpy impact energy (W_T) as recorded by the swing of the hammer to the area (A) under the oscilloscope voltage-time trace. This procedure is expressed mathematically as follows:

$$W_T = A\ C_x C_y P_d \bar{V} / C_a \qquad (1)$$

where:

W_T = measured Charpy impact energy (ft-lbs)

A = area (in.^{2}) under oscilloscope load-time trace as measured by a planimeter

C_x = X-axis scale factor (1 msec/division in this program)

C_y = Y-axis scale factor (20, 50 or 100 mv/division in this program)

P_d = Y-axis conversion factor (lb/volt output)

$\bar{V}$ = "effective" tup velocity during impact loading

C_a = area (in.^{2}) of one square division of the oscilloscope screen (C_a = 0.25 in.^{2} in this study)

The "effective" tup velocity ($\bar{V}$) from Equation (1) can be determined from

$$\bar{V} = 1/2\ (V_o + V_f) \qquad (2)$$

where:

$V_o = \sqrt{(2\ gh_o)}$ = velocity immediately prior to impact

$V_f = \sqrt{(2\ gh_o - 2/m\ W_T)}$ = velocity immediately after impact

g = gravitational constant (32.2 ft/sec^2)

h_o = initial height of hammer (4.38 ft)

m = mass of hammer (1.87 slugs)

---

[1]The Use of Pre-cracked Charpy Specimens to Determine Fracture Toughness," Dynatup reprint of UCLA Report ENG-7153, September 1971.

Since all quantities in Equation (1) above were known or measured, P_d can be calculated. Prior to the indicated calculation, a plot was made of W_T (ft-lbs) versus $\bar{V}$ A (ft/sec-in.^{2}) which, by Equation (1) should have resulted in a linear relationship. This plot for all specimens including the AMMRC steel calibration specimens is shown in Figure 10. As can be seen, a very good linear correlation with little scatter was obtained between W_T and $\bar{V}$ A for the AMMRC steel specimens. Similarly, a linear correlation with somewhat more scatter is indicated for the B/Al and aluminum specimens. The disturbing feature of Figure 10 is that the B/Al and aluminum specimen data do not scatter about the AMMRC steel specimen trend line. The reason for this behavior is not known since the trend line is merely indicative of the instrumentation proportionality constants represented in Equation (1). It is important to note that all of the tests were run in succession on the same day. The instrumentation was not disturbed or altered for the duration.

The experimental results were also plotted in terms of W_T versus the maximum height of the oscilloscope "load"-time traces. This height (in units of output voltage per division) is proportional to the maximum fracture load in the test. In Figure 11, the same trends as in Figure 10 are evident. The AMMRC steel specimen results indicated a definite linear correlation with little scatter. The B/Al and Al specimen results also indicated a linear correlation; however, the results did not scatter about the AMMRC steel trend line.

No additional analysis of the data was done for two reasons:

1. In light of the above, a load calibration constant obtainable from the well-behaved AMMRC steel calibration specimens would not adequately represent the B/Al test specimens.

2. The smooth, regular shape of the B/Al oscilloscope traces did not reveal any discrete fracture events such as crack initiation, delamination or fiber pull-out.

Both of the above are somewhat disappointing findings; however, it may be fairly concluded that proper experiments have been conducted and that the instrumentation did yield proportional measures of energy absorbed in fracture.

In summary, the impact strengths of the ATAC Charpy specimens oriented at [0], [0/22/0-22] and [±15] were found to be approximately 47, 27.8 and 16 joules (35, 20 and 12 ft-lbs), respectively.

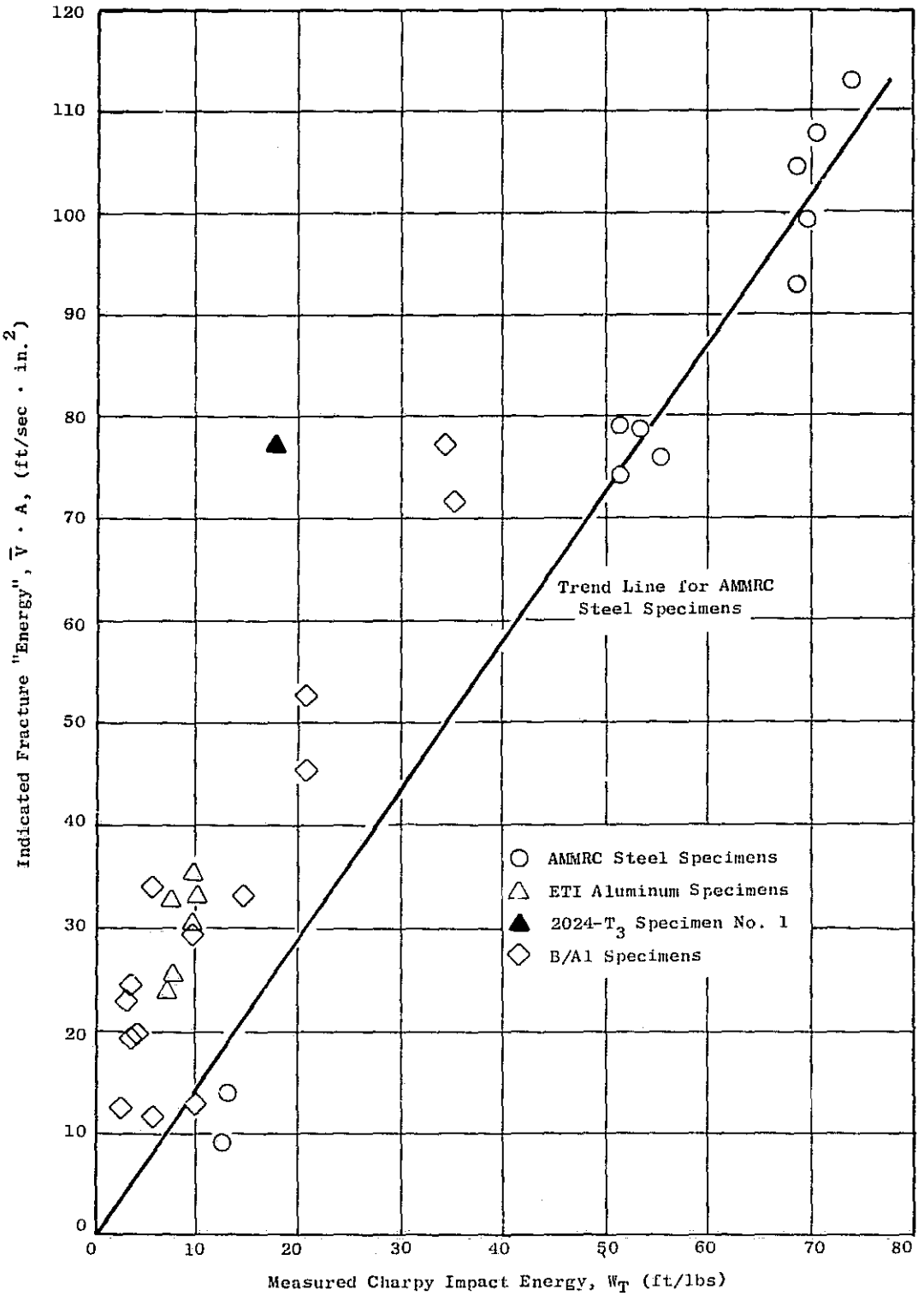

Figure 10. Correlation of Measured Charpy Impact Energy Data with Instrument Indicated Absorbed Energy.

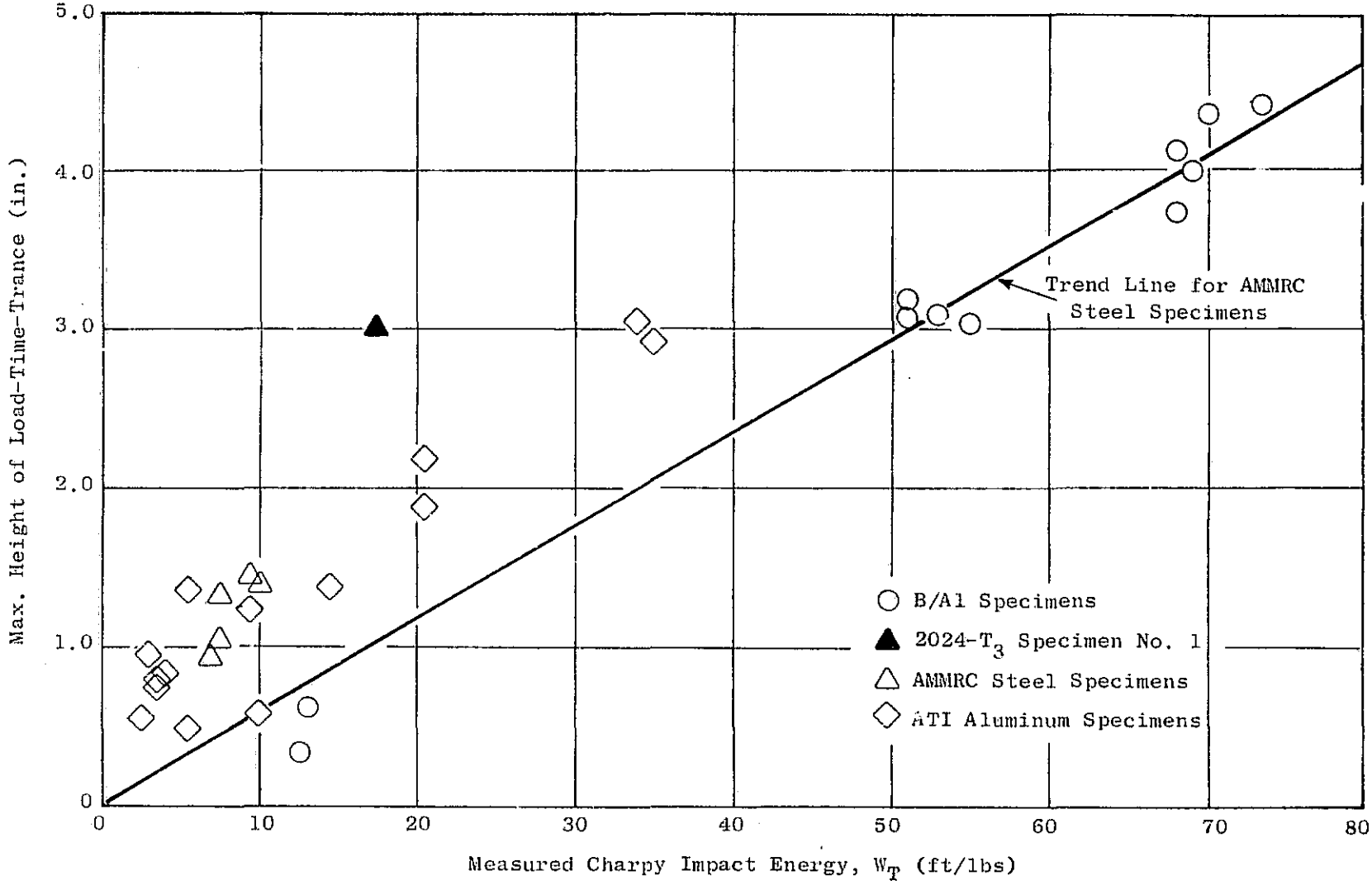

Figure 11. Correlation of Measured Charpy Impact Energy Data with Maximum Height Load-Time Traces.

3.1.2 Compression Testing

Compression Tests

Compression testing was performed in a Baldwin Testing machine at room temperature on specimens machined from Charpy impact specimens. These specimens were nominally 10 mm × 10 mm by 19.1 mm in length (0.395 inches × 0.395 inches by 0.75 inches). The test results recorded in Table X show a longitudinal compression strength of nearly 180 ksi and a transverse compression strength of about 40 ksi. The ultimate compression strength of the unreinforced 2024 Al alloy is only about 15 ksi.

The failure modes of these specimens can be seen in Figures 12 and 13. The typical shear mode of failure can be noted on all specimens. It can be seen that on the [0/22/0/-22] specimen more extensive delamination is prevalent due to the 0° plies aligned in the compression direction.

3.2 FABRICATION

Throughout the preceding efforts, only a single processing parameter of 920/6 ksi/20 minutes was employed. This was done to minimize the processing variables on the outcome of the planned testings. However, it was recognized that processing parameters could greatly alter the composite behavior. To evaluate the effect of pressure on impact strength, six additional 8 ply panels were fabricated at both the ATAC and all-1100 Aluminum matrix with the 8 mil diameter boron filament oriented at [0/20]. Design studies had indicated that this layup, which is a [±10] layup with a 10° bias, could increase the bird impact resistance in advanced fan blades. Consequently, two panels of each material were pressed at pressures of 6 ksi, 7 ksi, and 8 ksi. The impact data, shown in Figure 14, contained considerable scatter and, therefore, complicate a definitive interpretation. For example, considering data from flat panel specimens consolidated at the same condition (920° F/6 ksi), longitudinal impact strengths for ATAC composites ranged from 42 ft-lbs to 13 ft-lbs, whereas similar data for 1100 Al composites ranged from 30 ft-lbs to 21 ft-lbs. Average impact energy values as a function of consolidation pressure, as seen in Figure 14, reveal the general trend of the results. In addition, inspection of the specimens revealed extensive and somewhat inconsistent delaminations.

From these studies, it was decided to further evaluate the impact characteristics of the all-1100 Al composites at three other orientations of [±10], [±15], [0/22/0/-22] after pressing at pressures of 6 ksi, 8 ksi, and 10 ksi. In addition, three panels of the [0/22/0/-22] orientation were pressed at 900° F/10 minutes at pressures of 6 ksi, 8 ksi and 10 ksi. These data are presented in Table XI. As before, for the [0/20] all-1100 Al panel, considerable difficulty of delamination was encountered during specimen preparation. An important factor, as a consequence of this effort, is the limited bond integrity of the boron to 1100 Al as well as the 1100 Al to the 1100 Al. As a consequence, an internal program effort was initiated toward solving the bonding deficiencies of the 1100 Al matrix.

Table X. Room Temperature Compression Test Results on Longitudinal and Transverse Specimens.

Composite System	Panel No.	Spec. No.	Trans. Compression Strength (ksi) Ult.	Trans. Compression Strength (ksi) 0.2 Yield	Spec. No.	Long. Compression Strength (ksi) Ult.	Long. Compression Strength (ksi) 0.2 Yield
2024 Al Alloy	---	---	---	---	---	15.9 13.9 14.9 Avg	---
55 v/o, [0], 8-mil, 2024/1100	5082/1-U	U5 U6	36.5 35.7 36.1 Avg	29.1 32.9 31.0 Avg	--- ---	--- ---	--- ---
55 v/o [±15], 8-mil, 2024/1100	5582/1-T	T8A T8B	43.0 41.7 42.4 Avg	32.7 33.3 34.0 Avg	T4A T4B	183.0 179.4 181.2 Avg	182.0 179.0 180.5 Avg
55 v/o [0/22/0-22], 8-mil, 2024/1100	5582/1-V	V5 V6	36.9 38.1 37.5 Avg	28.1 26.8 27.5 Avg	V4A V4B	165.1 183.4 174.5 Avg	164.1 180.8 172.5 Avg

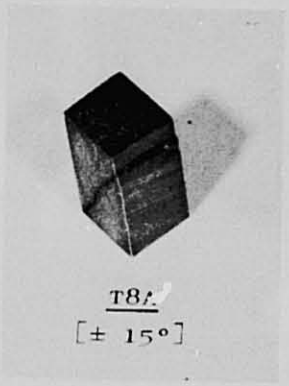

T8A
[± 15°]

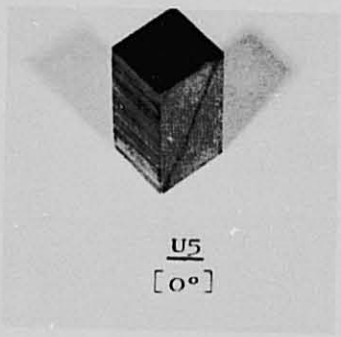

U5
[0°]

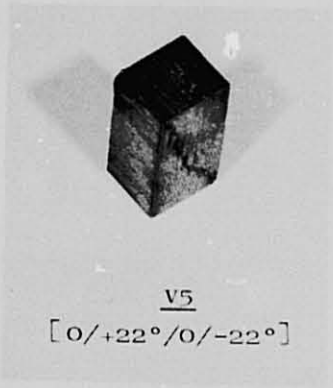

V5
[0/+22°/0/-22°]

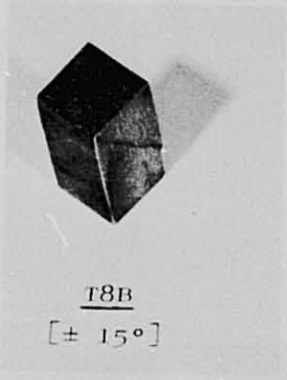

T8B
[± 15°]

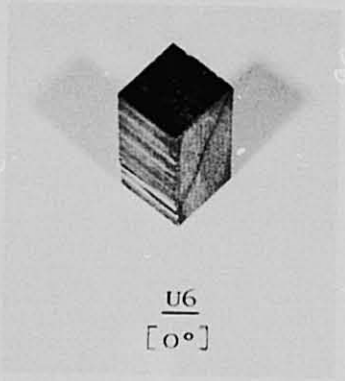

U6
[0°]

V6
[0/+22°/0/-22°]

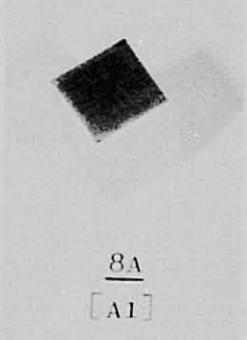

8A
[A1]

8B
[A1]

Figure 12. Photographs of Compression Specimens.

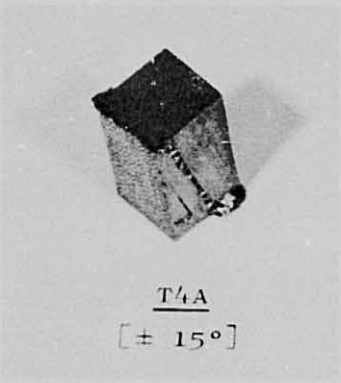

T4A
[± 15°]

V4A
[0/+22°/0/-22°]

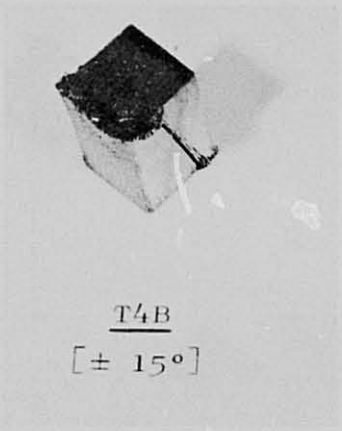

T4B
[± 15°]

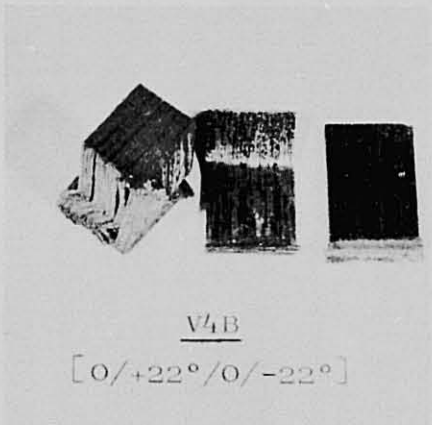

V4B
[0/+22°/0/-22°]

Figure 13. Photographs of Compression Specimens Longitudinal Compression.

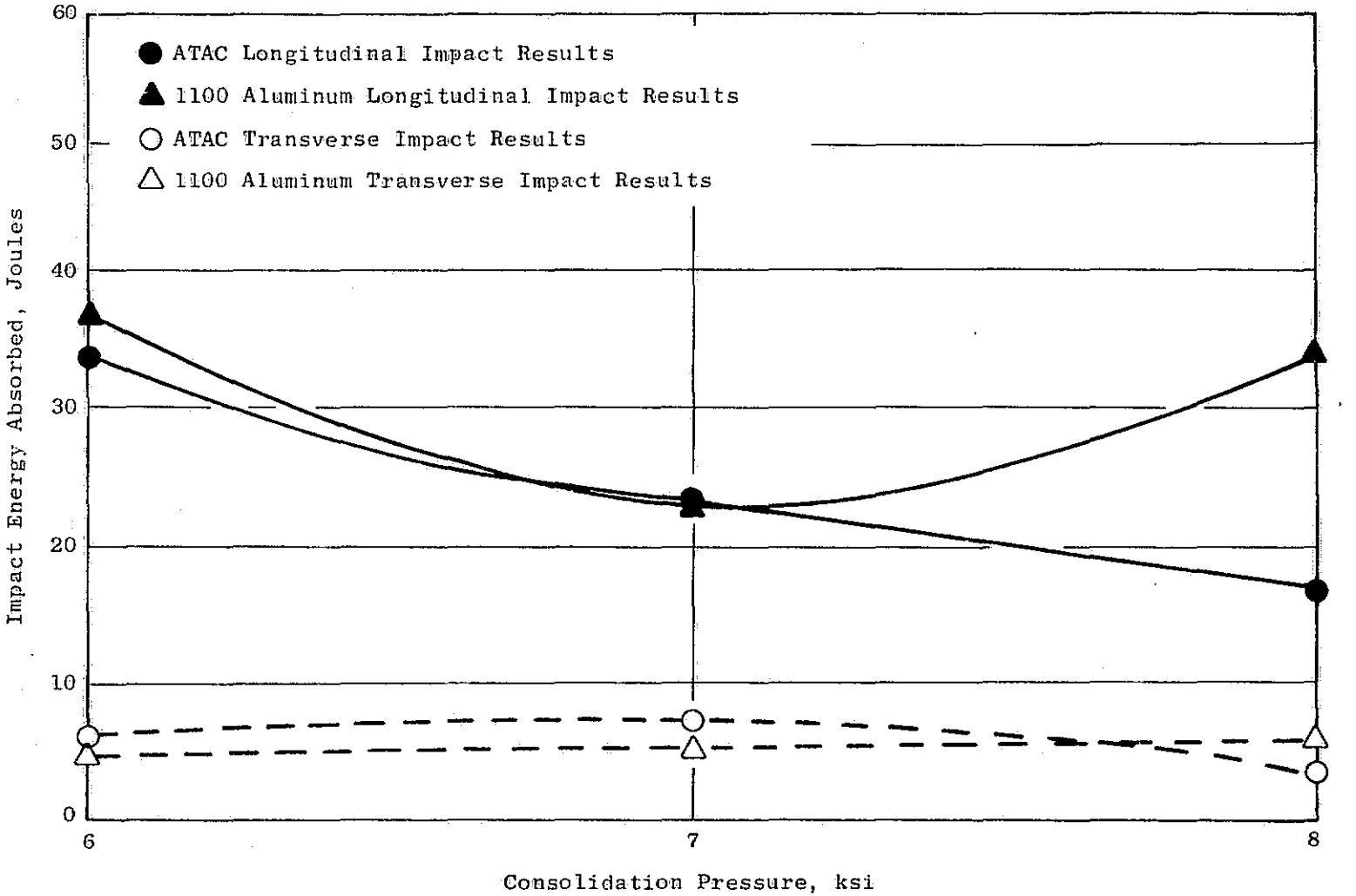

Figure 14. Task I Part IIIA Average Impact Energy Vs. Consolidation Pressure for ATAC and 1100 Aluminum Composites (Pressed at 920° F Temperature).

Table XI. Part III B Longitudinal Impact Test Results Miniature Impact Specimens.

Panel No.	Orientation	Press Parameter	Specimen No. 1L-I Joules	1L-I Ft-lbs	2L-I Joules	2L-I Ft-lbs	Average Joules	Average Ft-lbs
N5231-A	[0/22/0/-22]	920F/6 ksi	Delaminated; could not be tested		17.8	13.1	17.8	13.1
N5(0/2)81-B	[0/-20]	920F/6 ksi	16.7	12.3	21.3	15.7	19.0	14.0
N5581-C	[±15]	920F/6 ksi	-	-	-	-	-	-
N5181-D	[0/22/0/-22]	920F/6 ksi	47.3	34.9	55.5	40.9	57.4	37.9
N5281-A1	[0/22/0/-22]	920F/8 ksi	-	-	-	-	-	-
N5(0/2)81-B1	[0/-20]	920F/8 ksi	19.5	14.4	17.5	12.9	18.4	13.6
N5581-C1	[±15]	920F/8 ksi	28.7	21.2	40.1	29.6	34.4	25.4
N5181-D1	[±10]	920F/8 ksi	-	-	-	-	-	-
N5281-A2	[0/22/0/-22]	920F/10 ksi	-	-	-	-	-	-
N5(0/2)81-B2	[0/-20]	920F/10 ksi	34.7	25.6	43.5	32.1	38.2	28.2
N5581-C2	[±15]	920F/10 ksi	31.7	23.4	35.4	26.1	33.5	24.7
N5181-D2	[±10]	920F/10 ksi	12.6	9.3	23.2	17.1	17.9	13.2
N5281-A3	[0/22/0/-22]	920F/6 ksi	33.2	24.5	13.8	10.2	23.5	17.3
N5281-A4	[0/22/0/-22]	920F/8 ksi	12.9	9.5	15.2	11.2	14.0	10.3
N5281-A5	[0/22/0/-22]	920F/10 ksi	53.0	39.1	34.2	25.2	43.5	32.1

As a result of the insufficient and unreliable bond strength at both the interply (aluminum to aluminum) and the intraply (boron to aluminum) interfaces, the program efforts were curtailed and an internally funded program was initiated. This internally funded program effort is detailed in the following paragraphs.

The relatively straightforward approach taken in this work involved the investigation of chemical/mechanical surface preparation techniques to produce good bonding. At the outset, a large variety of different chemical, electrochemical and mechanical surface treatments were reviewed, as described in the literature.[1,2,3] From this review and other consultations, this program evaluated four mechanical surface preparation methods, as follows:

- 3M Scotch Brite
- Grit blast
- "Silly Putty" containing abrasive

Four chemical treatment procedures, given the letter designation of the person(s) responsible for their development, were also evaluated, as follows:

- S/F (Stillman/Farmer)
- L (Losekamp)
- K/H (Kirtchik/Heat Bath)
- K/A (Kirtchik/Amchem)

All treatments contained a cleaning operation; i.e., cleaning in a proprietary solution of Ridoline Number 72. Also evaluated was the deoxidizer and its concentration, along with, in some cases, an etchant. Finally, a fixant to uniformly oxidize the aluminum surface and prevent an excessive oxide buildup upon air exposure was evaluated.

Two types of 1100 Al alloy sheets, one in the "O" condition (annealed) and the other in the fully hardened condition, H-18, were surface treated and then bonded at temperatures between 800° and 900° F. In forming monotape sandwiches, selected regions of the sheets' mating surfaces contained a release agent to allow for post-bond cycle separation. At the start of the investigation, a graphite spray, designated T-50, was used as the surface release agent; later, a chemical conversion coating of the amorphous chromate type was found to be more effective. The individual monotapes were then sectioned and evaluated by a bond integrity test (BIT), a modified peel test shown in Figure 15. Each BIT value reported represents an average of three individual tests. Scanning electron microscopy (SEM) techniques were also used to evaluate the bond characteristics. As a reference, 2024 Al sheet specimens were prepared with minimal surface preparation (uniformly abrading the surface with Scotch Brite-3M), acetone cleaned, bonded

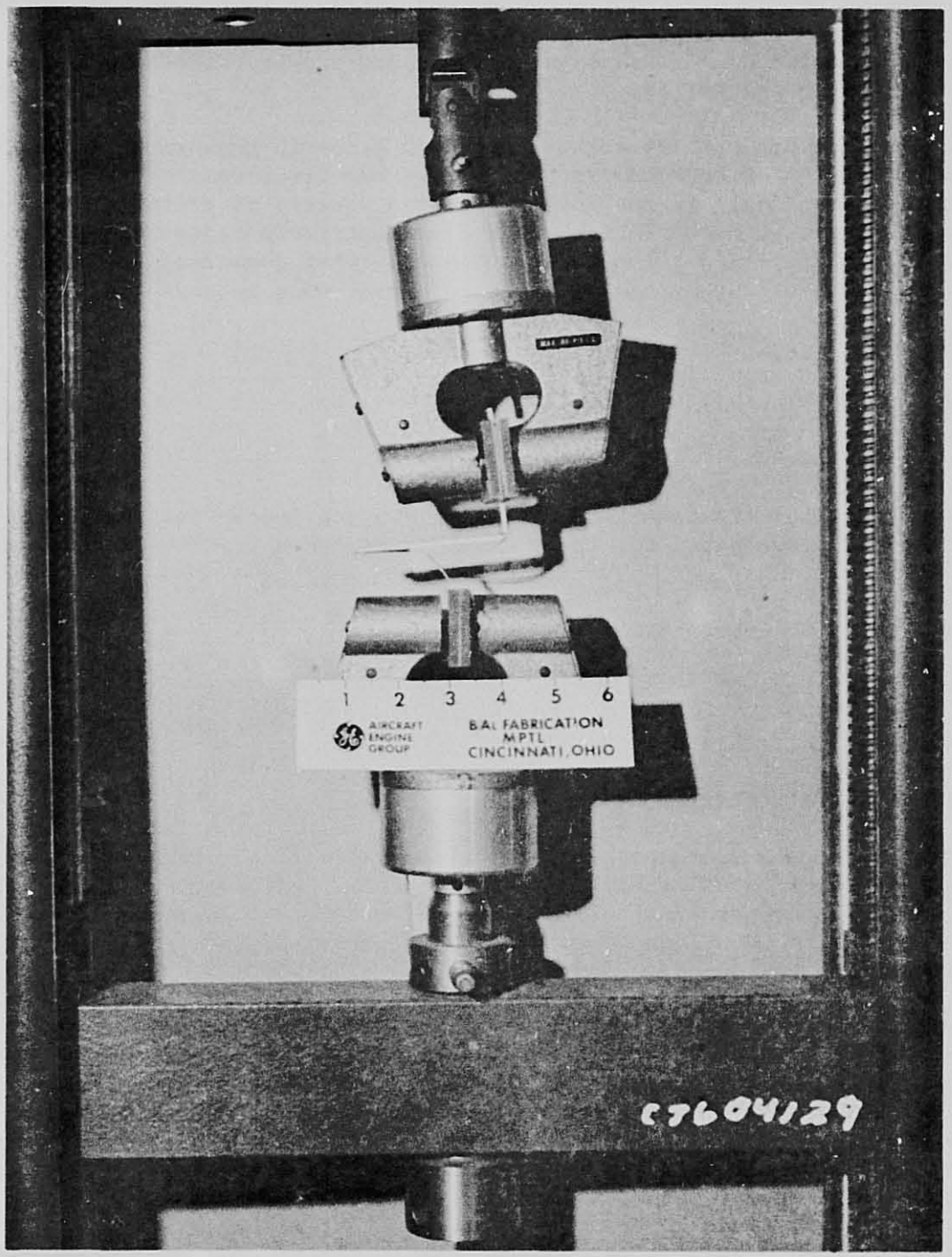

Figure 15. Peel Test Facility.

at 930° F/6 ksi/ 30 minutes (the previous standard procedure), and again peel tested.

Under selected conditions, both acrylic and polystyrene fugitive binders were used to determine their effects on 1100 Al/1100 Al bonding.

As an integral part of the effort, 0.008 inch diameter boron filaments were composited with both the 1100 Al and 2024 Al matrices to form monotape panel specimens. These monotapes consisted of a sandwich of aluminum foil on each side of the collimated boron filaments, spaced at 0.0093 inch, to produce a 57% v/o in the aluminum matrix, with an average ply thickness of 0.0093 inch. In a previous program, the 0.008 inch boron filaments were spaced at 0.0088 inch to achieve 60% v/o, as seen schematically in Figure 16. The decision to increase the lateral spacing of the filaments was based on the microscopic examination of failures of the original material. These failures were observed to occur at the boron/aluminum interface, indicating that this intraply surface was the weaker bonded region and, by increasing the land regions, better bonding could be achieved. The selection of the monotape thickness was based on the desire to maintain a square array in the consolidated tape. As with the Al/Al bond evaluation, both BIT and SEM techniques were employed to rank the monotape bond behavior.

After establishing both Al/Al and B/Al bond behavior, monotape plies were initially formed and then consolidated into 8-ply panels. Evaluation was accomplished by cutting panels into miniature impact specimens. Following Charpy impact testing of these specimens, light metallographic evaluations yielded the filament arrangement and volume fraction, while SEM aided in discerning the modes of failure.

Peel Strength Testing

1100 Al/1100 Al Bond (Interply Bond) - Peel strengths on specimens given the S/F surface preparations are shown on the bar chart in Figure 17. Both the S/F 9 and S/F 15 were found to exhibit high peel strengths.

Two further variables were included in the specimens prepared with S/F 13-19. One of these is the shelf life; it can be noted that the storage effect of from one day to one week reduces the bond strengths by greater than 50% on S/F 13, 14, and 16, while only a 15% decrease is evident for S/F 15. The other is a bond strength comparison between the annealed (O) and the hardened (H) 1100 Al; in all cases, the annealed (O) material evokes a higher bond strength, probably because of the greater inherent ductility of the softer aluminum.

Comparisons of the 1100 Al/1100 Al peel strengths generated with the mechanical surface treatments and the L1, L2 etches are illustrated in Figure 18. The 3M excoriation treatment had been used as the previous standard surface preparation and yields a relatively low peel strength. The grit blast treatment produces the highest bonding of the four considered

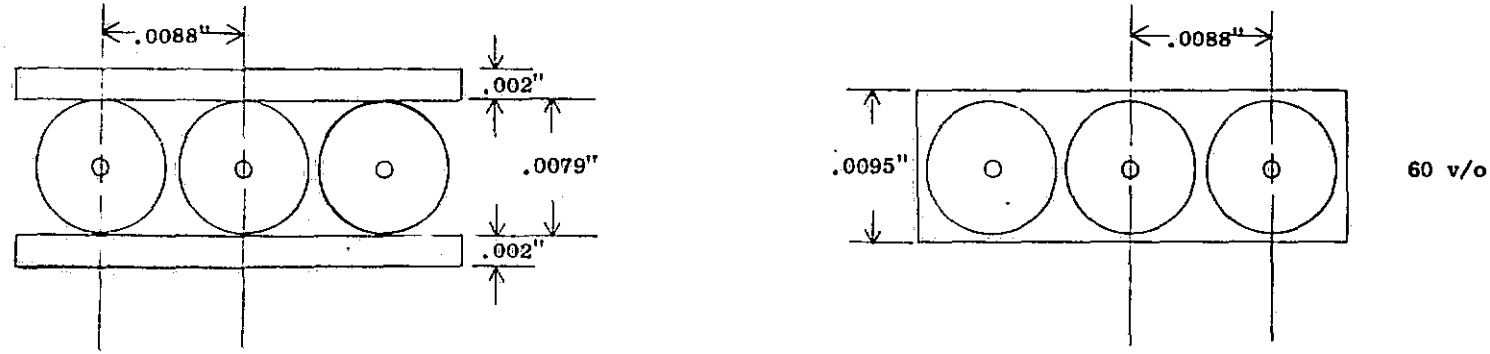

PREVIOUS B FILAMENT/MATRIX ARRAY

AS WOUND

CONSOLIDATED

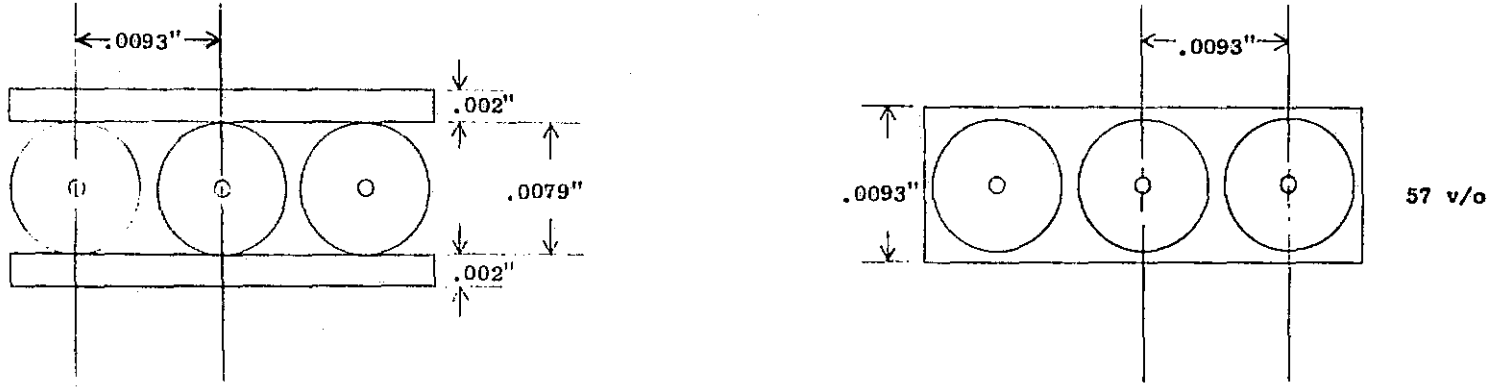

CURRENT B FILAMENT/MATRIX ARRAY

Figure 16. B/Al Composite Ply Spacing in As-Wound and After Consolidation Condition.

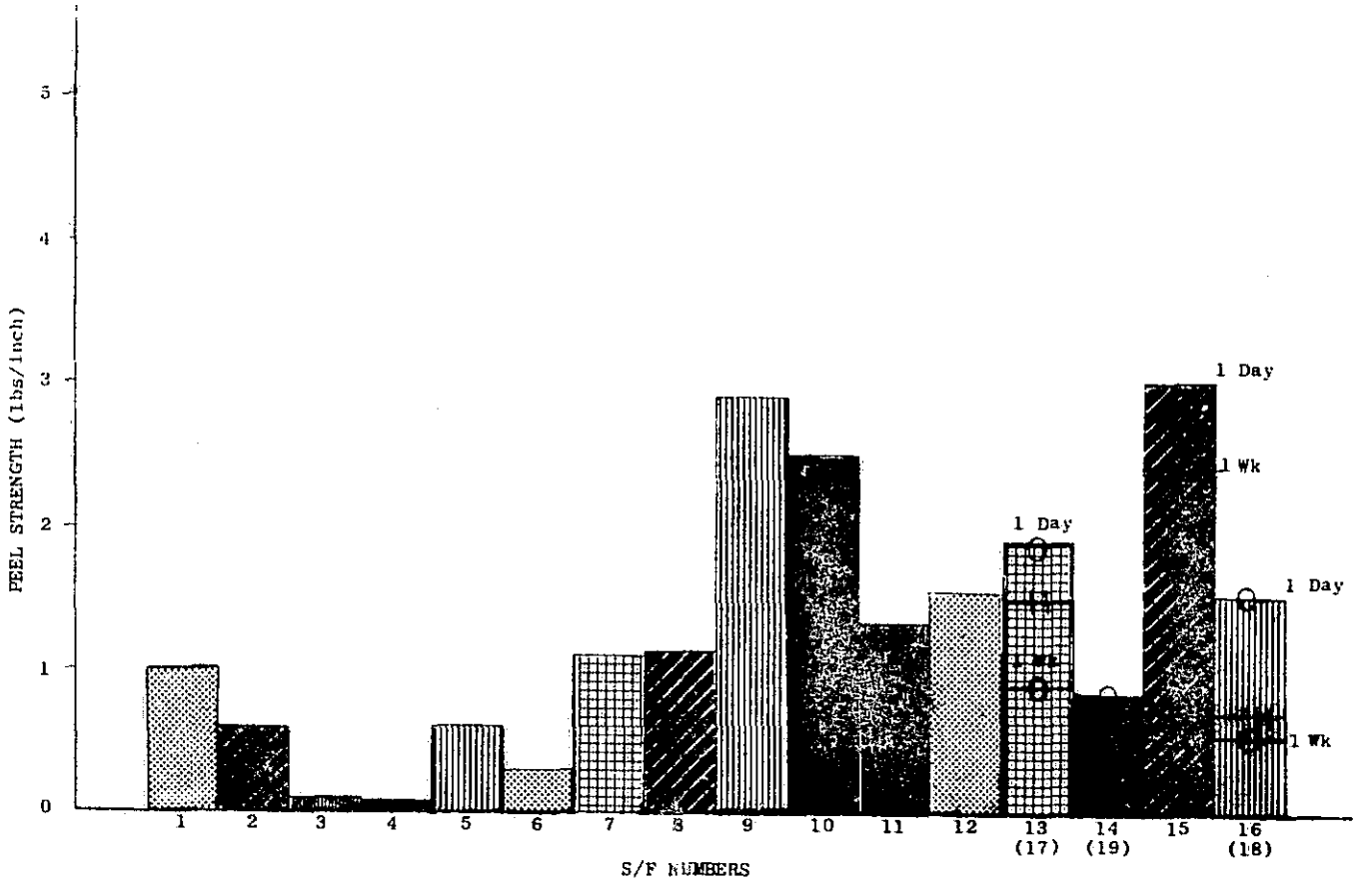

Figure 17. Peel Strengths of 1100 Al/1100 Al with Chemical Surface Preparation - S/F Series Pressed at 900° F/8 ksi/10 minutes.

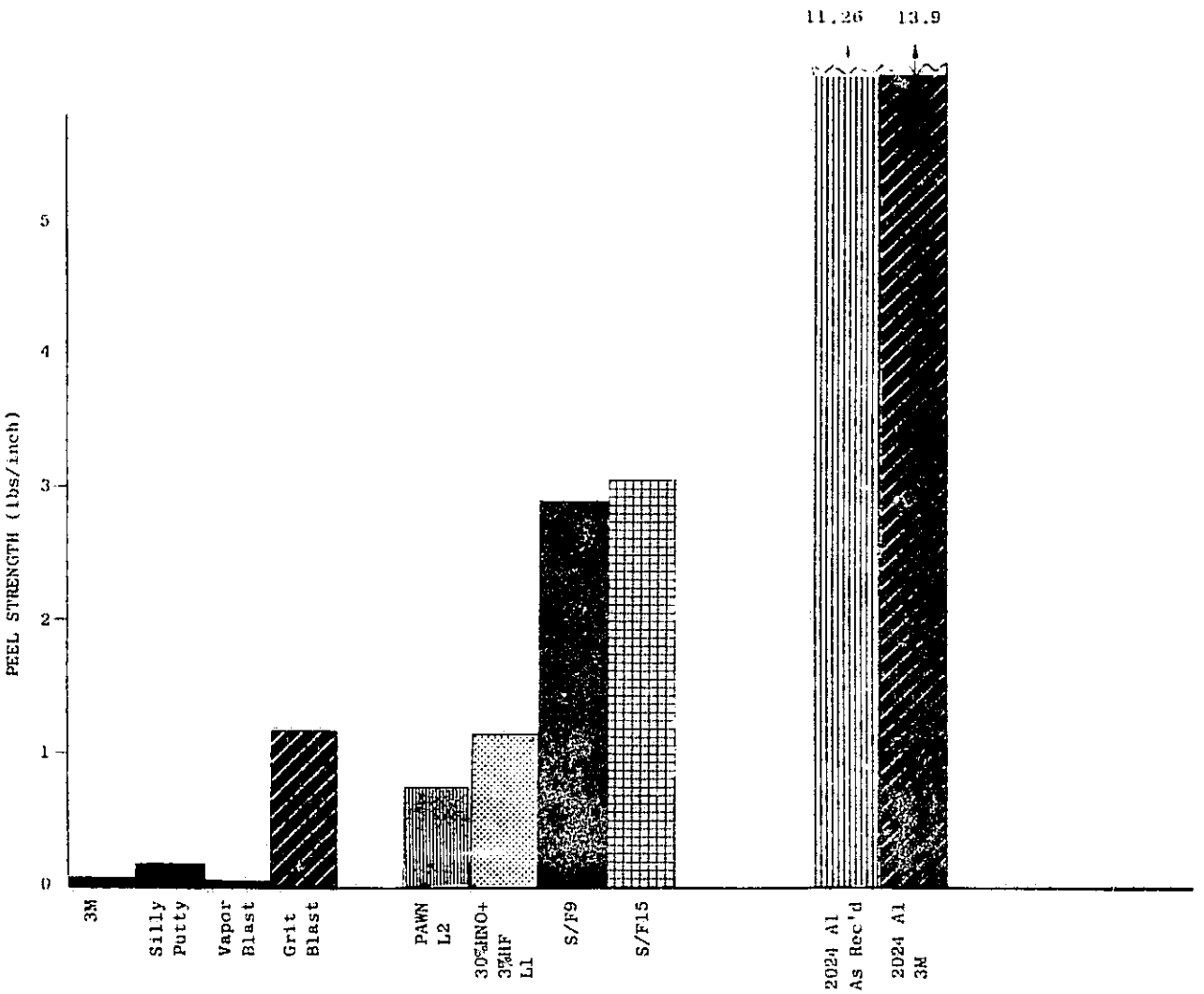

Figure 18. Peel Strengths of 1100 Al/1100 Al and 2024 Al/2024 Al Specimens Pressure at 900° F/8 ksi/10 minutes.

mechanical surface treatments. Both the L1 and L2 surface preparations yield intermediate bond strengths, with the L1 the higher of the two. The other surface treatments, K/A and K/H, led to unbonded specimens for the K/A 2, 3, and 4 and the K/H 2. Specimen K/A 1 had a low peel strength of 0.4 lb/inch, while both K/H 1 and 3 had even lower bond strengths of about 0.2 lb/inch.

As a reference, 2024 Al sheets were prepared in one case by merely cleaning the surface with an acetone wipe and, in the other case, by cleaning with the previous standard 3M procedure. The results, also shown in Figure 18, reveal 2024 Al bond strengths 3 to 4 times higher than those obtained with the best surface preparation procedures for the 1100 Al. An understanding of why the 2024 Al generates higher bond strength is of basic concern.

Boron/Aluminum Monolayer Bond (Intraply Bond) - All B/Al single ply layers of tape, referred to as a monolayer tape or monotape, in the first series of tests were consolidated at 900° F/8 ksi/10 minutes. In the preparation of the initial three (A, B, and C) monotapes, an overlap insert technique was employed to provide an unbonded area. Due to unwanted bonding of the sacrifical aluminum sheet and the inordinate amount of time required to prepare these specimens, another pressing technique, designated the localized pressure technique (shown in Figure 19, was developed). This localized pressure technique produced uniformly bonded monotapes.

Figure 20 summarizes the peel strengths on specimens containing a sacrificial aluminum sheet covered with a T-50 release agent. As a reference, two boron/2024 Al monotapes (H & I) were similarly prepared, but at the previous standard condition of 930° F/6 ksi/30 minutes. Again, it can be noted that these boron/2024 Al monotapes bonded exceptionally well with peel strengths of about 15 lbs/inch. One additional observation, higher peel strengths were consistently achieved with the monotapes containing the polystyrene fugitive binder as compared with those containing the acrylic cement. It is important to note that the B/Al monotapes with the L1, 3M, and the S/F 9 surface preparations with the polystyrene fugitive binder had high and nearly equal peel strengths of about 7 lbs/inch.

Additional tapes were bonded with a stripable sacrificial layer of 0.004 inch aluminum sheet on one side and a nonbonding layer of 0.005 inch stainless steel on the other side. As a result, the bonded monotape appeared corrugated on the side against the sacrificial sheet, but was smooth in appearance on the surface against the stainless steel sheet. The peel test results on specimens cut from these monotapes are shown in Figure 21. The lines across the bars represent the peel strength of the smooth side of the monotape and, in all cases, are lower. This greater bond on the corrugated side undoubtedly can be attributed to the ability of the sacrificial sheet forcing the aluminum more closely in proximity with the boron filament, as well as better filling of the interstitial positions between the filaments.

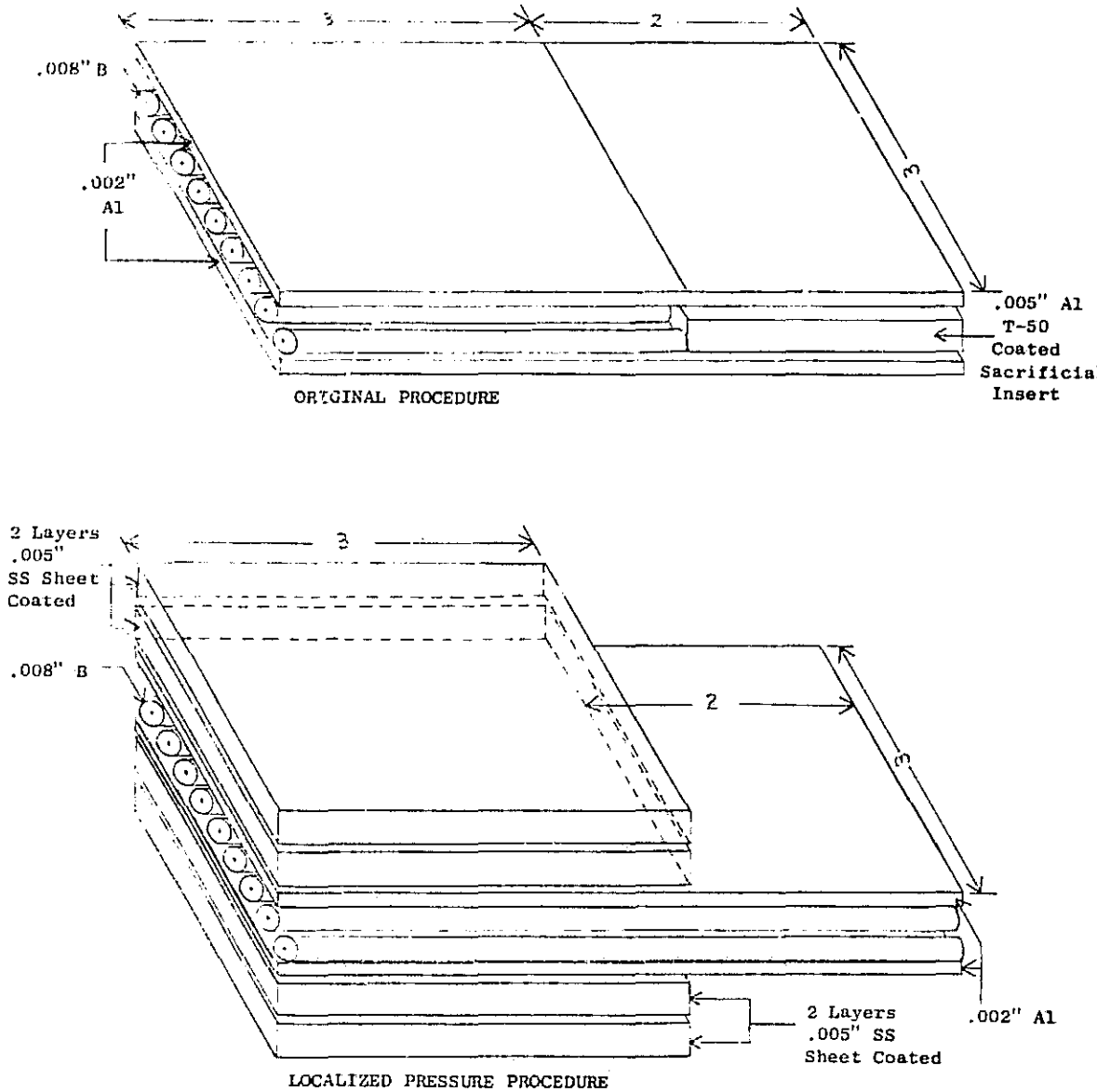

Figure 19. Schematic Illustrations of Techniques for Generating Unbond Regions for BIT Peel Test Specimens.

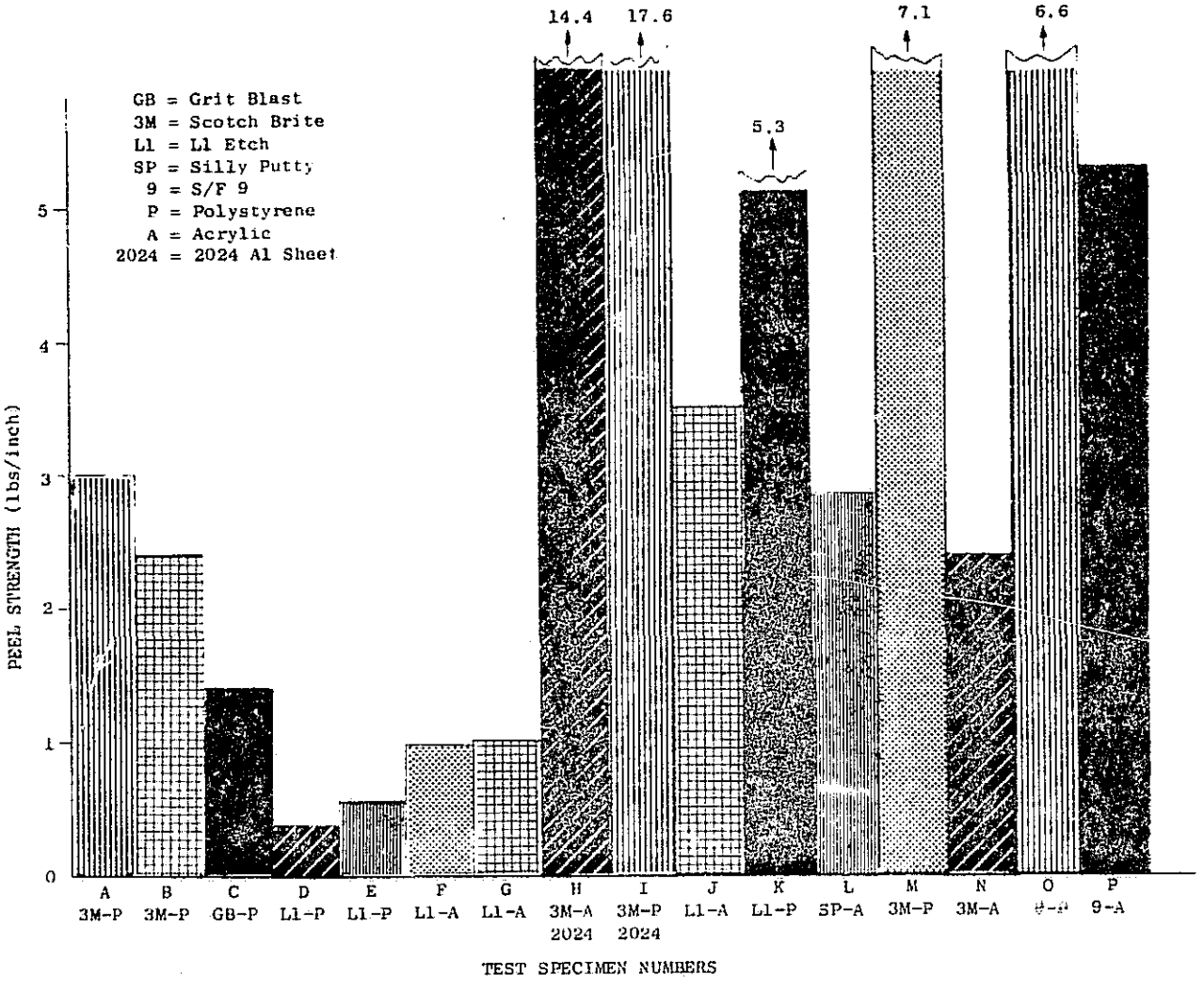

Figure 20. Peel Strengths of B/Al Monotapes Prepared from 1100-0 and 2024 Al Sheet.

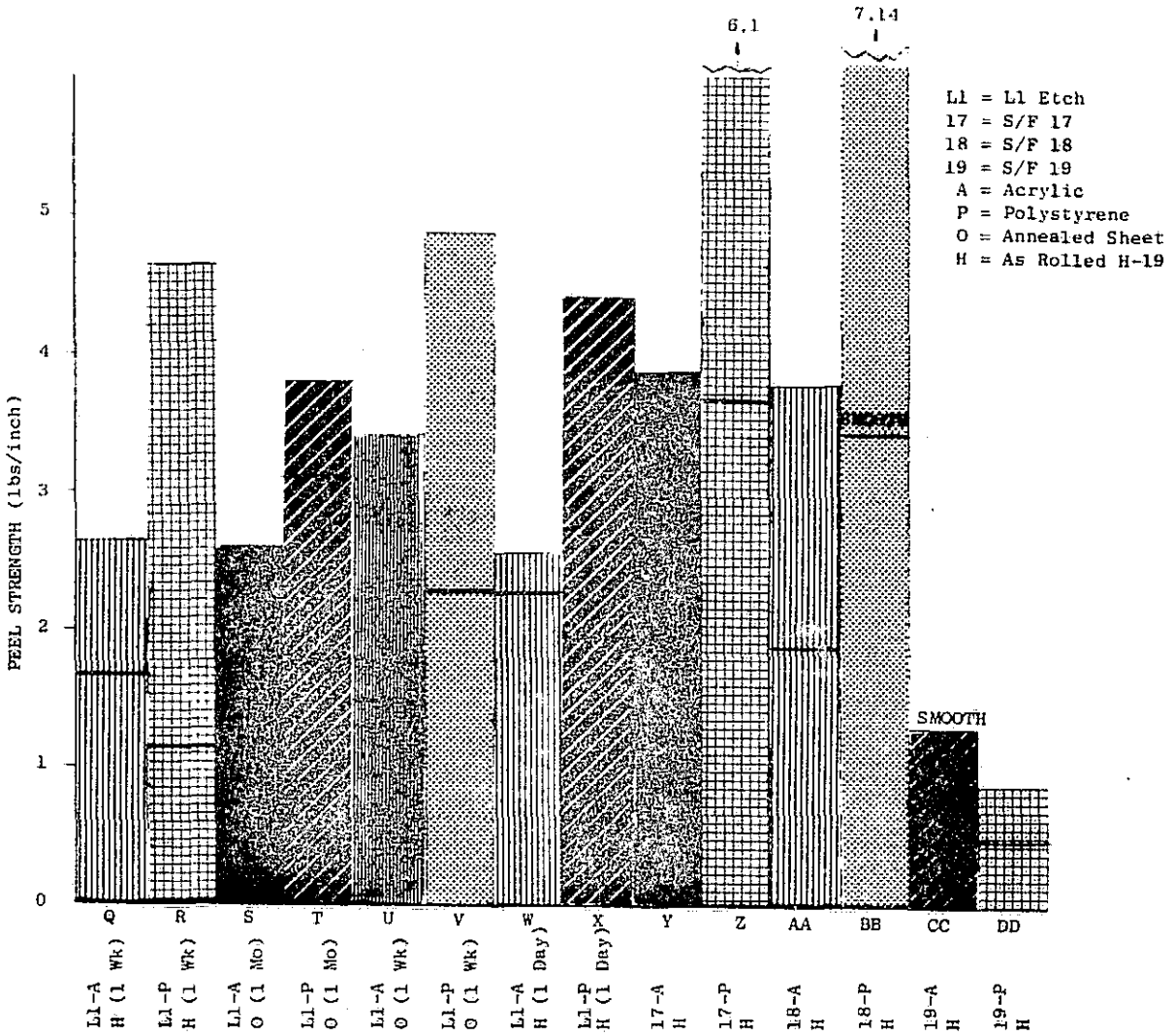

Figure 21. Peel Strengths of B/Al Monotapes Prepared from 1100 Al Both in Annealed (O) and Rolled (H) Conditions, Top of Bar Represents Peel Strengths when Pressed with Sacrificial Al Sheet while Intermediate Line Represents Peel Strength when Pressed Against Smooth Stainless Steel Sheet.

As before, the monotapes prepared with the polystyrene binder (P) were better bonded than the monotapes prepared with the acrylic binder (A). For example, the surface treatments S/F 17 and S/F 18 produced high intraply bond strength with the polystyrene cement (about 7 lbs/inch), but noticeably lower (less than 4 lbs/inch) for the acrylic cement. Another observation, again in agreement with the Al/Al bond peel tests, was the lower strength with the as-rolled or hardened (H) aluminum sheets compared with the annealed (O) sheets.

The loss of bond strength due to "shelf-life" of the L1 surface preparation on "O" sheets was evident. In general, bond strength deteriorated about 20% with storage time extending from one day to one week (see specimens J & K on Figure 20 and specimens U & V on Figure 21) and an additional bond strength loss of nearly 25% occurred with times extending from one week to one month (specimens U & V versus S & T).

Bonding at lower temperatures and pressures were also evaluated. Monotapes were prepared at temperatures of 800, 850, 865, and 900° F. Although a peel strength of one lb/inch could be achieved at 800° F, peel strengths of nearly two lbs/inch were obtained at 850° F. Bond pressures below 2.5 ksi at 850° F produced peel strengths of only 0.1 lb/inch, while pressures of 4 ksi at 850° F produced a peel strength of 1.7 lbs/inch. Based on these studies, a near optimized pressing condition of about 850° F/3.5 ksi/10 minutes was selected for fabrication of B/Al monotapes.

An integral part of forming single ply monotapes involves coating the inner foil surfaces with the fugitive adhesive binder, outgassing the binder, and press bonding the monotape layers. To more uniformly bond the aluminum foil, a plastically deformable stripable outer layer placed on the outside of the monotapes during consolidation aided in forcing the elements of the monotape in proximity with each other. One earlier method, designated CRB, employed the heat shrinkable polyethylene tetraphthalate (Mylar). In a separate press roll bond cycle, the deformable Mylar partially deformed the outer aluminum foils around the boron filaments. However, in the CRB method, the fugitive binder remained behind and had to be removed in a separate outgassing step.

An extension of this process employed an aluminum sacrificial sheet with a chemical conversion coating to prevent bonding. The designation of this procedure was PROS, standing for Protective Reproducible Outer Surface. After the bond cycle, the covered monotapes (MT) were stored and then were readily cut to size with the sacrificial sheet remaining on the outer surface. Immediately before panel fabrication, the outer layer (of a distinct greenish-yellow color) was easily removed.

In summary, these peel tests identified the higher peel strength with the 2024 Al alloy compared to the 1100 Al alloy, two surface preparations (3M and S/F 9) which evoked a well bonded condition for 1100 Al, the desirability of using a polystyrene fugitive binder over the acrylic, and better bond characteristics of the monotapes prepared with the deformable outer layer.

Scanning Electron Microscopy Observatons

Scanning electron microscopy techniques discerned the surface characteristics of both the filament and the aluminum (see Figure 22). As part of this study, a cursory examination was made on the as-received boron filament. It revealed that the magnified surface characteristics of the 0.004 inch diameter boron filament is the coarsest of the three boron filament surfaces as evidenced by the larger nodules, while the surface of the 0.008 inch diameter boron filament is the smoothest. This smooth surface, in part, may permit the 0.008 inch diameter boron filament to more readily debond and pull away from the restraining matrix. One approach to generate a smoother surface is to precoat the filament surface with, say, a vapor deposited unalloyed aluminum surface.

The surface topography of the as-rolled 0.002 inch thick 1100 Al sheet, as shown in Figure 23, exhibits the typical striations aligned in the rolling direction, and undoubtedly replicated by the machined grooves on the mill rolls. These striations carry over from the different surface preparations and are obliterated only by severe surface etchings or abrasions.

Scanning electron metallography reveals surface characteristics of specimens in the as-prepared condition, in the after peel testing, and from select B/Al monotapes. Select SEM's show these characteristics.

As-Prepared Condition - The scouring effect of the 3M-Scotch Brite preparation is evident in Figure 24. Here the abraded lines depict the rather superficial nature of this preparation procedure and indicate that less than 10% of the area was affected. It would be desirable to relate the percent of abraded surface with the bond characteristics.

Extensive SEM observations were made on all chemically prepared surfaces. Surface etching characteristics with the S/F 9 and S/F 15 etchings shown in Figures 25 and 26 illustrate the distinctive difference between the milder HNO_3 etch, S/F 9, and the more select area-attacking $FeCl_3/HCl$ etch, S/F 15. For the S/F 15 etch, there was some indication of a preferential grain boundary attack along with forming of a block-like surface, typical of face centered cubic metal. The surface morphology of the S/F 9 is believed to be typical of that type of surface which affords good metallurgical bonding behavior between the 1100 Al sheets.

Boron/Aluminum Processing for Panel Preparation

The successful employment of composite materials in component form requires a thorough understanding of the bonding behavior, along with careful selection of suitable matrix, filament size, volume fraction and spacing. From previous work, certain techniques have been identified for monotape fabrication, including the 0.008 inch diameter boron filament at about 55% v/o arranged in a square array. Next, it is necessary to define processing conditions for fabricating B/Al panels.

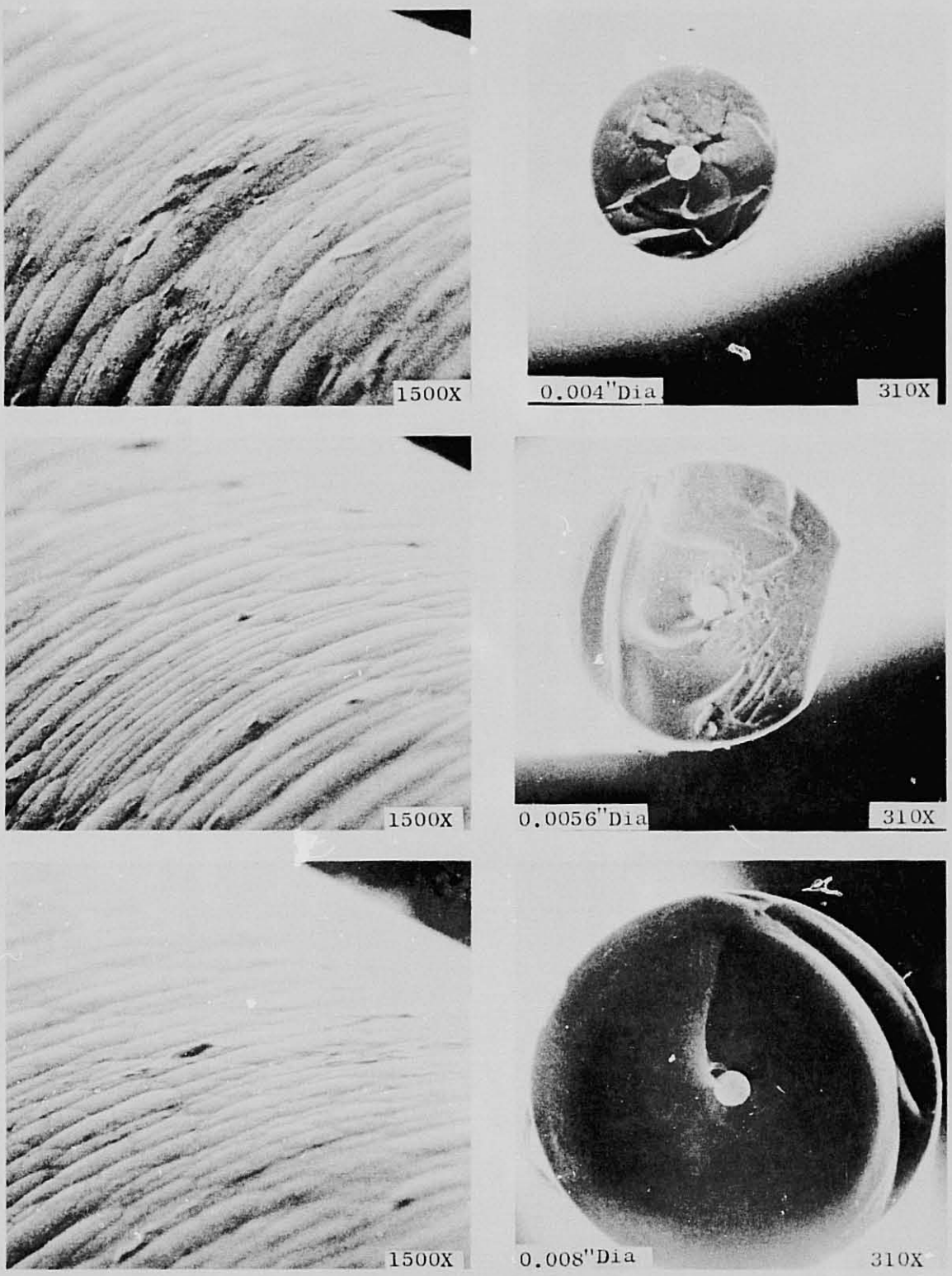

Figure 22. SEM Photos of Boron Surfaces.

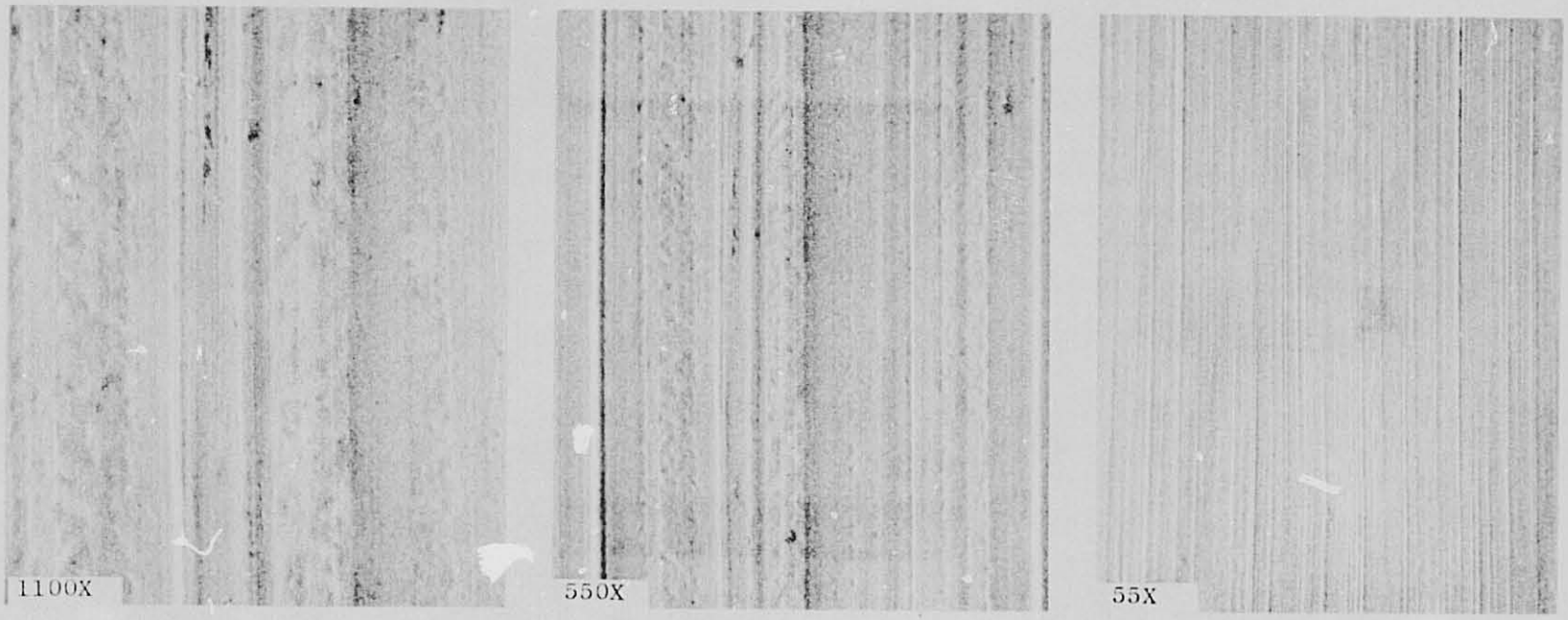

Figure 23. Surface Features of As-Received, 0.002 inch 1100 Al Sheet. Striations Generated from Mill Roll Grooves. SEM at 45°.

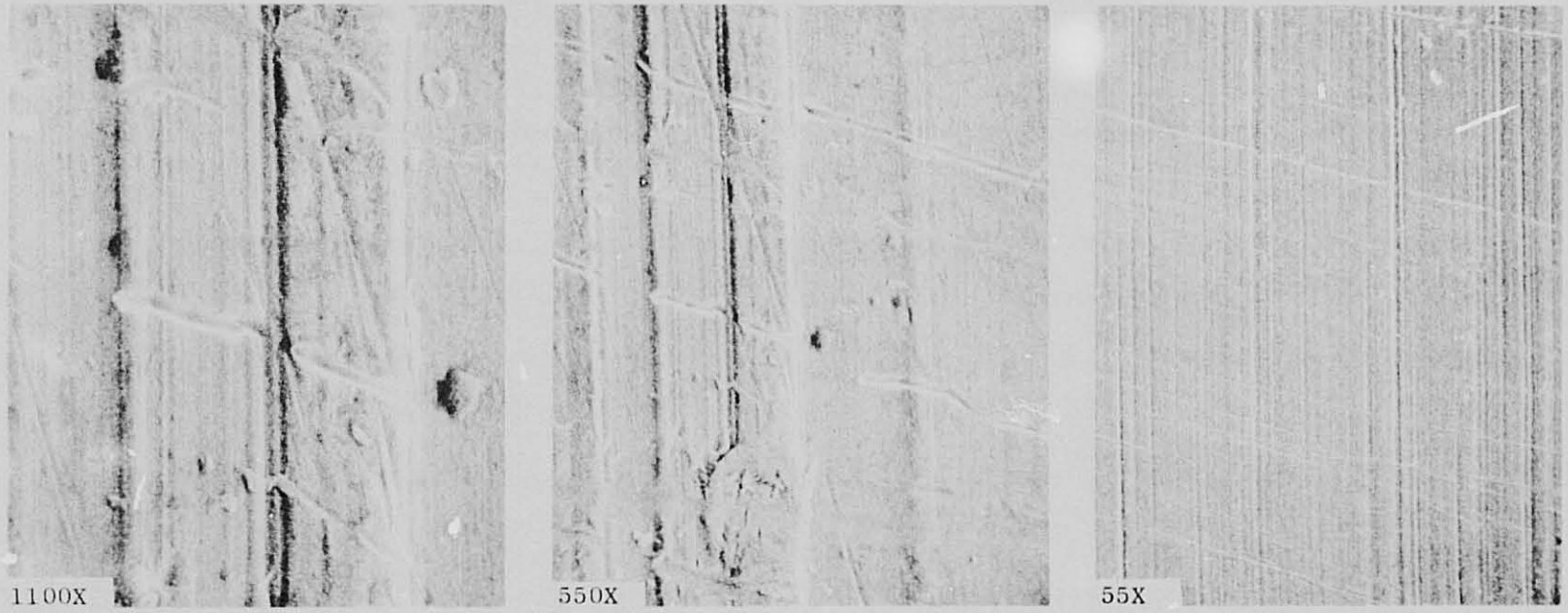

Figure 24. Surface Features of 0.002 inch 1100 Al Sheet After 3M-Scotch Brite Surface Preparation. SEM at 45°.

Figure 25. Extent of 0.002 inch 1100 Al Surface Attack with S/F 9 Preparation. SEM at 45°.

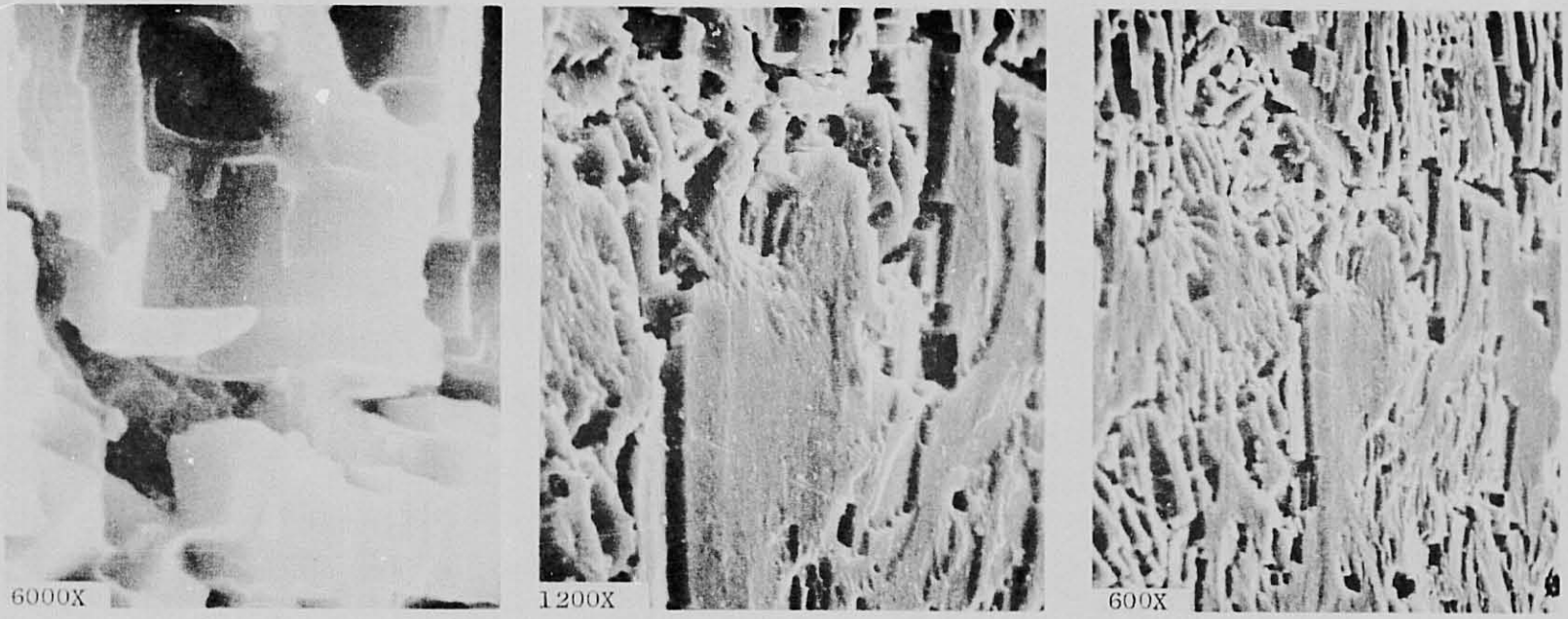

Figure 26. Extent of 0.002 inch 1100 Al Surface Attack with S/F 15 Preparation. SEM at 45°.

To evaluate the monotape press parameter, five-inch by three-inch, 8 ply, 0° orientation panels were consolidated and tested. A summary of the results are given in Table XII. In the initial series, the monotapes were prepared at 875° F/5 ksi/10 minutes. The monoplies used on the first panel (C-5081-A) had the S/F 9 surface treatment on both sides and, in monotape preparation, were pressed with smooth stainless steel sacrificial sheets. The second panel (C-5081-B) was identically consolidated and also contained monotapes with the S/F 9 surface treatment, but, in this instance, the monotapes were pressed with the protective reproducible outer surface (PROS) sacrificial sheets. The third panel was identically consolidated from monotapes prepared from tapes with the S/F 15 treatment by the PROS procedure. These 8-ply panels were all consolidated by the newly developed Rapid Bond Cycle (RBC) process. The average thickness of these consolidated panels was 0.075 inch or an average consolidated ply thickness of 0.00937 inch. The test results, presented in Table XIII, show the relatively low impact strengths of panels prepared from the smooth monotapes. Further, it was noted that panel C-5081-B, formed from the S/F 9 PROS monotape, exhibited the highest impact strength of the three. Post-test inspection of the impacted panels showed that considerable interply delamination occurred. To achieve better bonding, it was reasoned that lower monotape bond temperature and pressure and a higher panel pressing temperature and pressure were needed. The next three panels were pressed from monotapes prepared at a lower temperature of 850° F and three pressures of 2.5, 5 and 6 ksi. The panel bond time was increased from 10 minutes to 20 minutes. The impact results show that the panel fabricated from tapes prepared at the lowest pressure of 2.5 ksi had the highest impact strengths. However, the monotapes bonded at 2.5 ksi showed some indication of delamination during monotape ply cutting. Consequently, the monotape press pressure was increased to 3 ksi on the next series of panels. The next panel, C-5081-C, was formed from monotape prepared at 850°F/3 ksi/10 minutes with the 3M abrasive nylon surface treatment at the intraply layer. The corrected impact strength for a single panel thickness (0.075 inch) is approximately 40 ft-lbs, about 43 ft-lbs for a two-panel thickness, and 55 ft-lbs for a triple panel thickness. This phenomena of increased impact strength with increasing panel thickness is probably unique to composite structures and suggests another insight into impact behavior.

As a result of the panel evaluation, it was concluded that the protective reproducible outer surface (PROS) sheet was a significant aid in improving the impact strength of the monotape. Further, the highest impact results were obtained when two different surface preparations were used; i.e., abrasive nylon (3M) at the matrix-boron (intraply) interface and S/F 9 at the matrix-matrix (interply) interface. In addition, it was found that a potential synergistic gain in impact strength could be realized by proper selection of the monotape and panel press cycle conditions.

Table XII. Effect of Monotape and Specimen Press Parameters on Strength.

Panel No.	Process Parameters			Corrected Impact Strengths (ft-lbs)		
		Monotape	Press Condition	Single Panel Thickness	Double Panel Thickness	Triple Panel Thickness
C-5081-A	S/F 9*	875F/5 ksi/10 min.	900F/8 ksi/10 min.	6.1, 5.5		
C-5081-B	S/F 9	875F/5 ksi/10 min.	900F/8 ksi/10 min.	23.8, 16.5		
C-5081-C	S/F 15	875F/5 ksi/10 min.	900F/8 ksi/10 min.	18.9, 17.5		
C-5081-D	S/F 9	850F/2.5 ksi/10 min.	900F/8 ksi/20 min.	21.7, 23.7	34.3	
C-5081-E	S/F 9	850F/4 ksi/10 min.	900F/8 ksi/20 min.	22.6, 21.7	28.0	
C-5081-F	S/F 9	850/4 ksi/10 min.	900F/8 ksi/20 min.	Peel Test Specimen		
C-5081-G	S/F 9	850F/6 ksi/10 min.	900F/8 ksi/20 min.	20.3, 19.0	26.3	
C-5081-H	S/F 9	850/3 ksi/10 min.	900F/8 ksi/20 min.	Tensile Specimens		
C-5081-I	S/F 9	850F/3 ksi/10 min.	900F/8 ksi/20 min.	Tensile Specimens		
C-5081-J	3M	850F/3 ksi/10 min.	900F/8 ksi/20 min.	40.7, 39.0	41.8, 45.1	55.0

*Outer monotape (MT) surface pressed against smooth stainless steel sheets. All others were pressed with a protective, reproducible outer sheet (PROS).

Table XIII. Pendulum Impact Characteristics of B/Al J79 Blades.

S/N	Intraply Treatment	Type Failure	Boron Filament Diameter	Impact Value (ft-lb)	Remarks
12A	Abrasive Nylon	Airfoil	5.6	40	Failed at 30% Span
1	S/F 9	None	8.0	94	Slight Tip Damage
2	Abrasive Nylon	Dovetail	8.0	46	Root Type Failure
3	S/F 9 Preparation	None	8.0	105	Tip Damage
4	Abrasive Nylon	Lower Span	8.0	83	Root Type Failure

3.3 TRANSLATION OF PROCESS DEVELOPMENT

An integral aspect of the process development activity is the technology translation to blade fabrication. As a result of the high potential resistance of the 1100 aluminum with the S/F 9 surface treatment, the General Electric Company continued with their internally funded program into the fabrication of J79 B/Al blades. With this developed surface treatment technology, four blades were consolidated.

All four contained the abrasive nylon (3M) intraply surface treatments, while two contained the abrasive nylon and two the S/F 9 interply surface treatment. Visual observation revealed that one blade surface treated with the abrasive nylon interply surface treatment exhibited some dovetail delamination (S/N 2). However, both blades with the S/F 9 interply treatment exhibited excellent airfoil, as well as dovetail, bond quality (S/N 1 and S/N 3). Ultrasonic examinations corroborate these findings.

To evaluate blade impact behavior, five B/Al blades were pendulum impacted in a special fixture mounted on a Charpy impact testing maching. One blade (S/N 12A) with the 5.6 mil diameter boron filament in the 1100 aluminum matrix tip and 2024 aluminum matrix root, processed in an earlier program at 920° F/6 ksi/30 minutes, exhibited measured Pendulum impact values of about 40 ft-lbs. The other four all-1100 aluminum matrix blades were processed at 900° F/8 ksi/20 minutes by the RBC process. These impact values are summarized in Table XIV. Three impacted blades are shown in Figure 27.

To investigate the significance of surface treatment on this improved impact resistance, two blades (S/N 2 and 4) were fabricated from 8 mil boron using the RBC process, but with only the abrasive nylon (3M) interply surface treatment. Comparing the impact results of these blades with those of blades S/N 1 and 3 (processed identically except for the S/F 9 surface treatment) leads to the conclusion that the surface preparation has a significant influence on impact strength.

It is important to note that blade S/N 12A, fabricated using the previous vacuum bond process and the abrasive nylon (3M) surface treatment, failed at 30% span with an energy absorption of only 40 ft-lbs. The RBC process in combination with the S/F 9 surface treatment yielded energy absorption capabilities nearly three times greater without a detectable failure. This improvement results principally from the developed surface preparation along with a combination of increased boron filament diameter, improved filament spacing, better fugitive binder and, the RBC process.

On the basis of these results, it was concluded that this surface preparation processing technology could be successfully translated into panel and blade fabrication for the SCAR blade program among others.

Table XIV. Blade Summary, J101 Stage 1 Fan Blade.

Parameter	Present Metal Blade	Composite Blade
N_b	32	32
Materials	6-4 Ti	B/Al
Temperature, ° F	175	175
C_o	3.52	3.52
C_t	3.60	3.60
T_M/C_o	0.068	0.068
T_M/C_T	0.025	0.025
$Solidity_o$	2.62	2.62
$Solidity_t$	1.40	1.40
R_t (Inlet)	13.16	13.16
R/R (Inlet)	0.45	0.45
β_o*	18.72	18.72
β_t*	60.89	60.89
ϕ	1.094	1.50
θ_o	99.7	99.7
θ_t	2.93	2.93
Mid-Span Location	50%	No Mid-Span

C_o = Chord at root, inches
T_M/C_T = Airfoil maximum thickness/chord at tip, dimensionless
R_t = Radius at tip, inches
R/R = Airfoil root radius/tip radius, dimensionless
β* = Airfoil stagger angle from tangential, degrees
ϕ = Tip untwist, degrees
θ = Airfoil camber, degrees

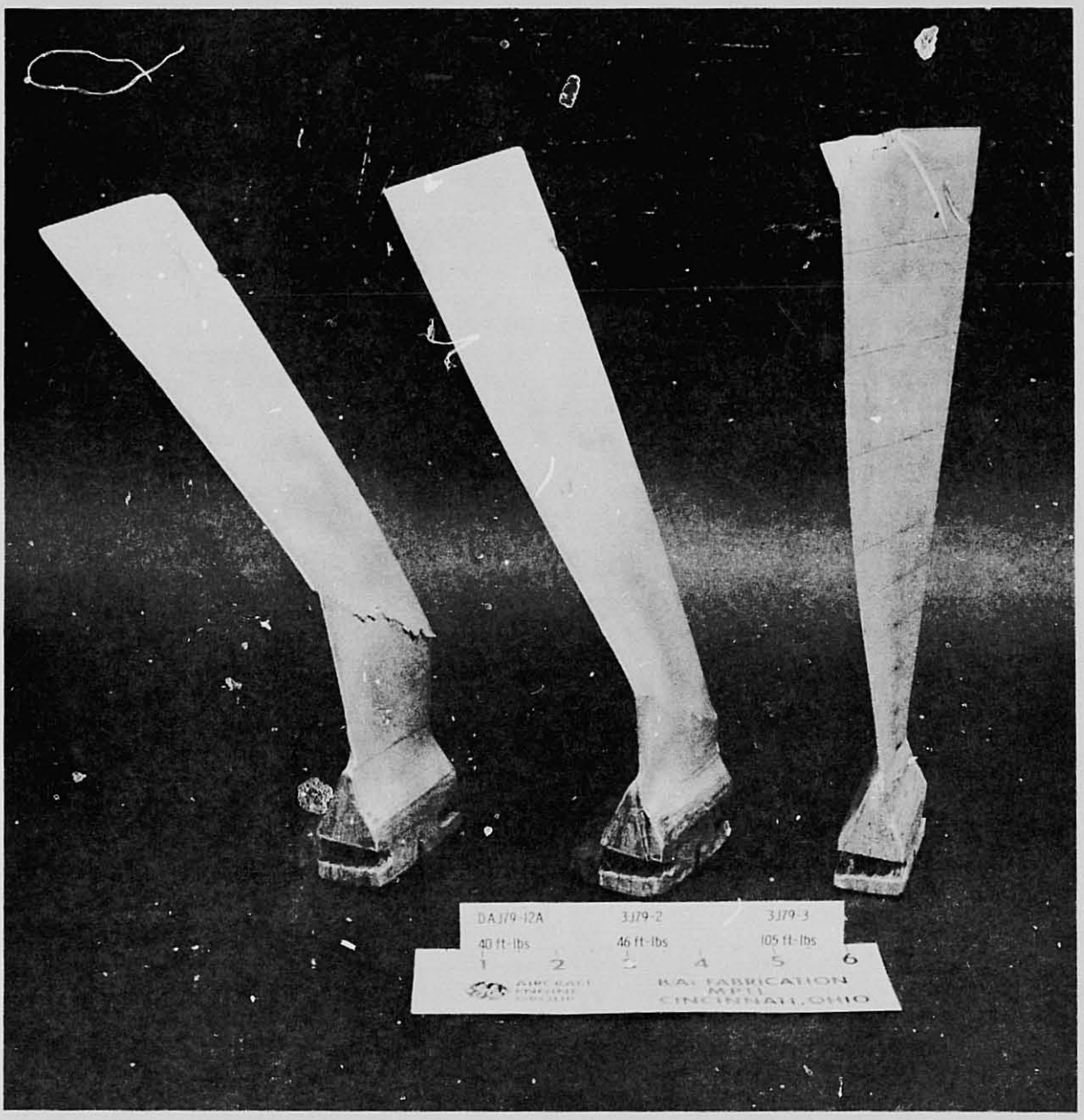

Figure 27. Three Pendulum Impacted Blades. Both Blades S/N 12A and S/N 2 Failed During Impact, While S/N 3, Other than Tip Fracture, Suffered No Visible Damage.

3.4 DESIGN

3.4.1 Summary

The J101 fan was selected for demonstration in this program due to its similarity to the preliminary SCAR fan. Further, the first stage blade was selected for maximum cost and weight benefit and to concentrate on the improvement of impact resistance.

The blade airfoil configuration of the existing titanium blade was maintained throughout this program. Analysis indicated that the established aeromechanical stability requirements could be met by a cantilevered B/Al blade (the mid-span shroud required on the titanium blade could be removed on the B/Al blade). The aeromechanical characteristics of several material systems were investigated analytically. Maintaining a first flexural frequency above the 2/rev excitation with sufficient margin was the limiting criteria. Either a 5.6 mil or 8 mil diameter boron fiber can be used; however, a 57% volume fraction of boron is required. A (±10) layup is most desirable to obtain the desired blade frequencies followed, in decreasing order of desirability, by (0/20), (±15), and (0/22/01-22) layups. The blade stress analysis was limited to determination of surface stresses for steady state operation. A more extensive analysis, beyond the scope of this program, is required to determine the stress components (particularly shear and short transverse) to establish the material strength requirements.

An impact study was conducted to determine the bird ingestion requirements of the J101 stage 1 fan blade. These studies were extrapolated to provide comparisons to the SCAR fan. The blade impact capability was not determined analytically. Material selections to achieve the best impact resistance was based on the materials screening and evaluation in Task I.

3.4.2 Blade Configuration

The J101 fan flowpath, shown in Figure 28, includes an 18 strut front frame with 18 variable pitch inlet guide vane flaps immediately aft of the frame struts. The existing fan has 32 first stage titanium blades which run at a tip tangential velocity of 1504 ft/sec (sea-level-static, standard day). The J101 engine specifications were used to define the design point operating conditions, which are summarized below.

Condition	Rotor Speed° RPM	Max First STG. Blade Temp° F
Hot Day Takeoff	13,266	175
Max. Steady State Operation	13,935	350
Max. Design Overspeed	14,215	350
Burst Speed	16,345	Room Temperature

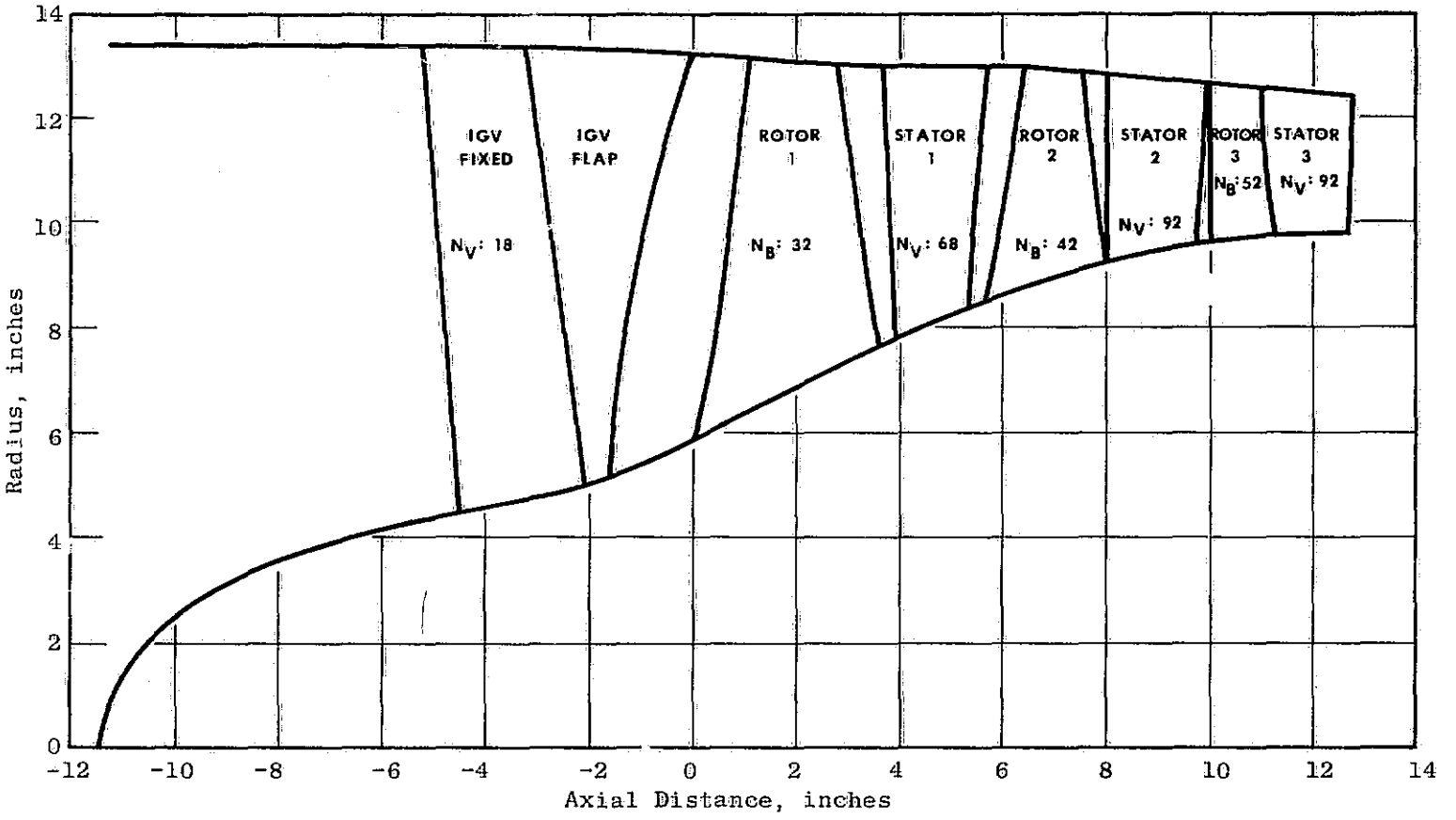

Figure 28. LP Compressor Aerodynamic Flowpath.

The first stage titanium fan blade shown in Figure 29, requires a mid-span shroud to obtain a first flexural frequency above the 2/REV excitation line (hence, it is referred to as a "high flex" blade). The mid-span shroud is elliptically shaped, located at 50% span from the airfoil root and at 60% chord from the airfoil leading edge. The titanium blade includes a flow path platform machined integrally with the blade and a rectangular shank for transition from the airfoil to a conventional dovetail attachment oriented tangentially 20° from the rotor centerline.

The J101 first stage B/Al fan blade is a cantilevered design with an airfoil identical to the titanium airfoil, except for the modifications required to remove the mid-span shroud. Table XIV summarizes and compares the J101 first stage B/Al fan blade geometric characteristics with those of its titanium counterpart. All parameters are identical except for the removal of the mid-span and the difference in material properties.

The camber and orientation angles distributions along the airfoil height are identical for the B/Al and titanium blade as shown in Figures 30 and 31. Note in Figure 32 that the cantilevered B/Al airfoil is slightly thinner than the titanium airfoil in the mid-span shroud area. This material, added around the mid-span shroud on the titanium blade to reduce the local stresses, is not required for the B/Al blade design.

This program did not require a B/Al blade flowpath platform design as the contribution of this component to the blade impact resistance and structural integrity were not considered to be of significance.

The abrupt cross sectional change between the airfoil and rectangular shank of the titanium blade causes excessive stress concentrations and processing difficulties in the B/Al blade. To rectify this situation, the B/Al shank length was increased 0.170 inches relative to the titanium blade and the radius to the dovetail was decreased correspondingly. The B/Al blade shank was tapered from the airfoil root section of the dovetail. The 20° dovetail tangential orientation was maintained to minimize the shank radial curvature, as shown in Figure 33.

The blade attachment incorporated a conventional dovetail with a flank angle of 65° and a keyhole outsert fabricated from SAE 4140 steel. The outsert has an internal slot to fit the B/Al dovetail and an outside diameter of 0.75 inches to fit the circular disk slot. As shown in Figure 34, the disk slot neck was designed to permit 15° of blade rotation in the direction of a foreign object impulse, or opposite the direction of the rotor rotation. Based on impact test results of the J79 B/Al keyhole attachment, the disk was designed to provide a 5° recovery beyond the blade normal radial position.

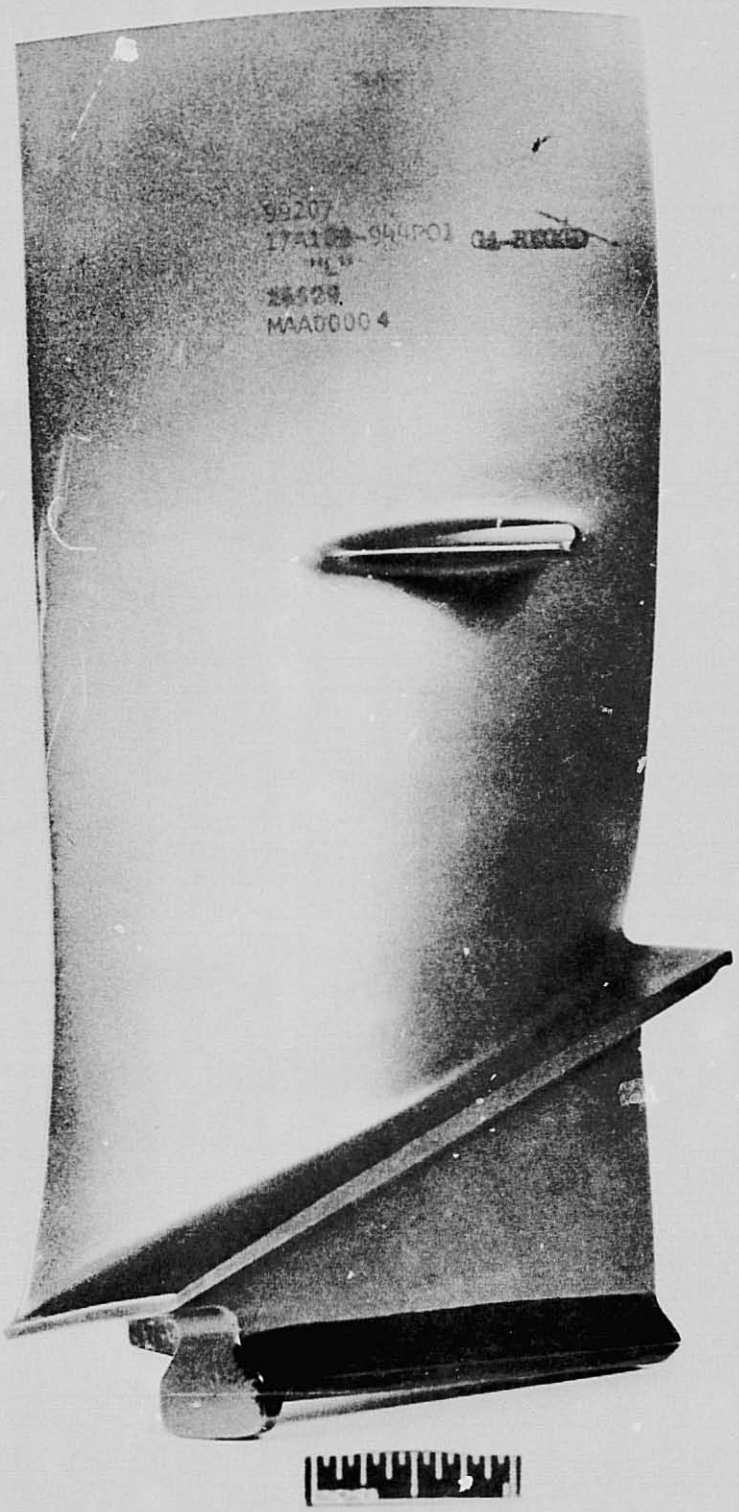

Figure 29. J101 First Stage Titanium Fan Blade.

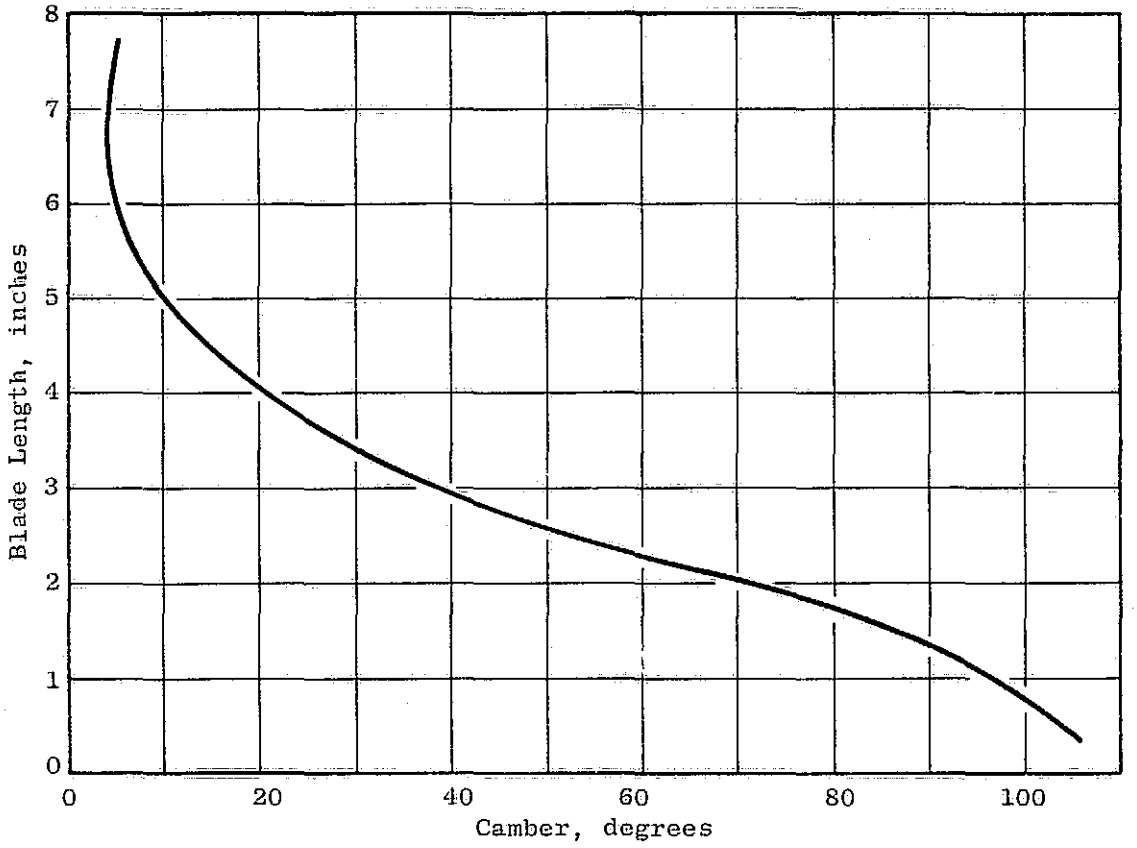

Figure 31. J101 Boron/Aluminum Blade, Camber.

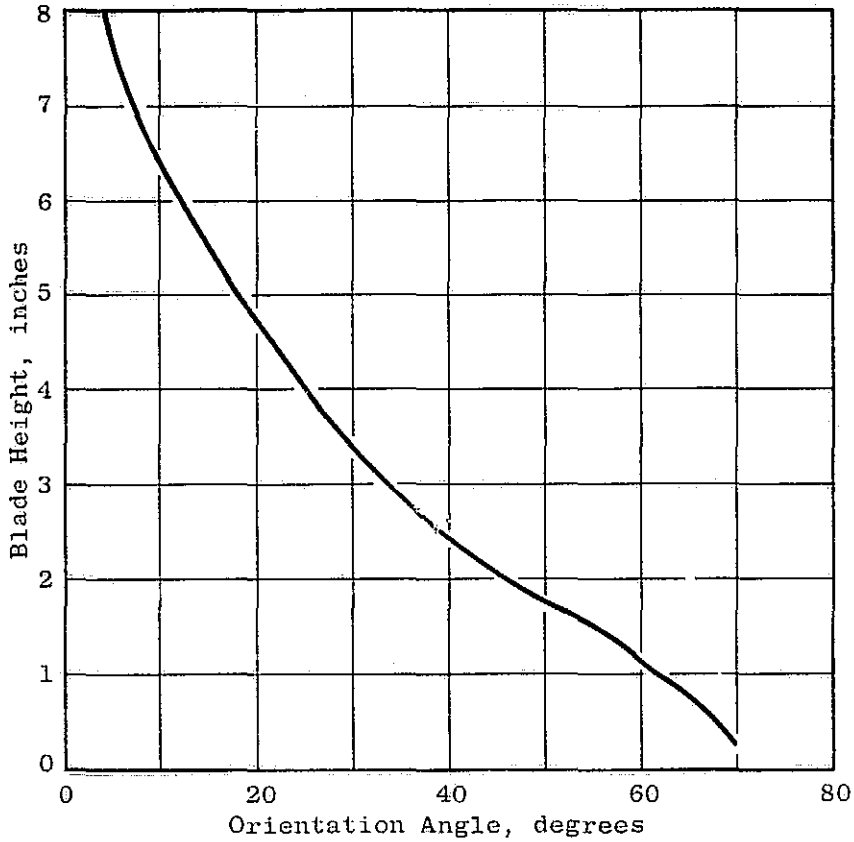

Figure 31. J101 Boron/Aluminum Blade Orientation Angle.

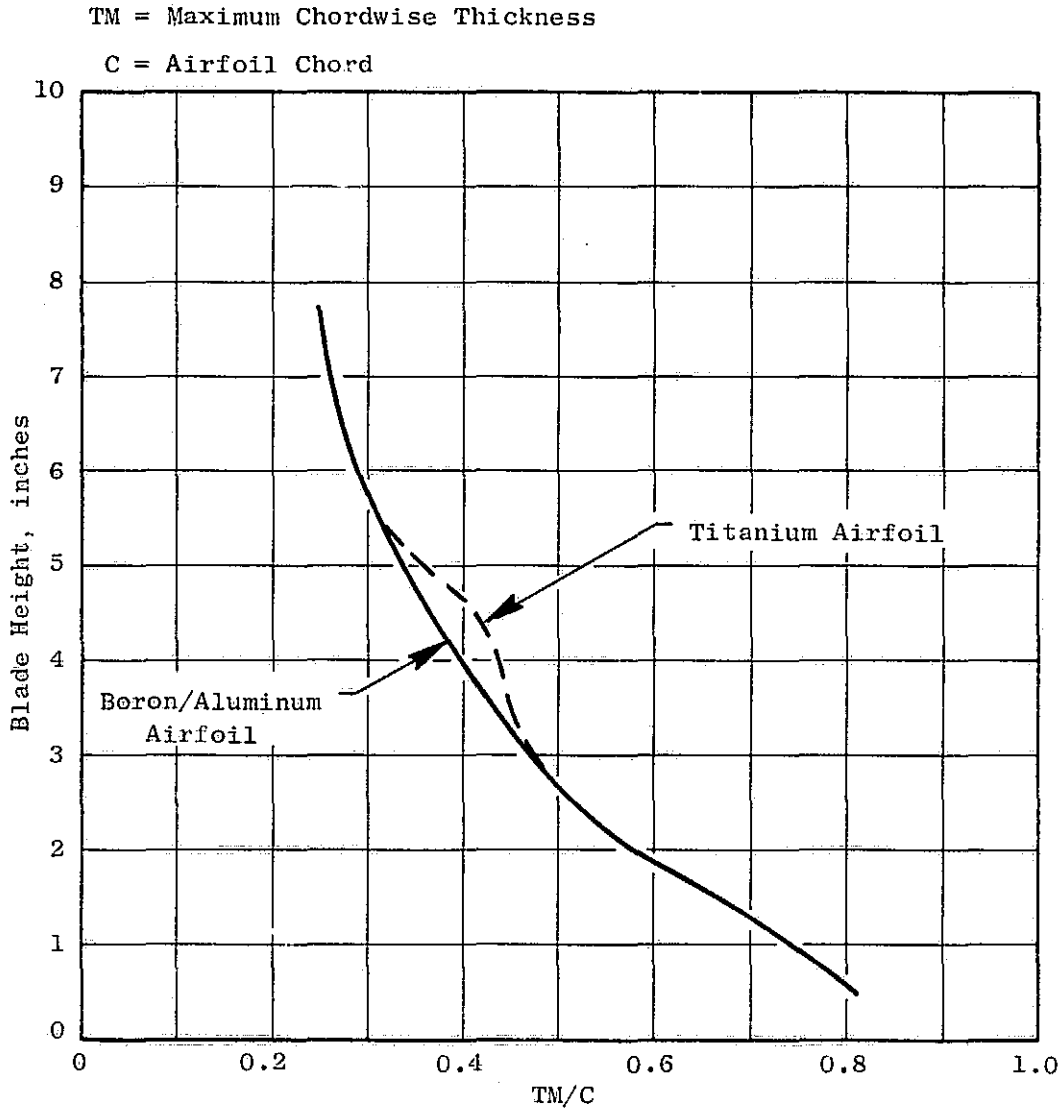

Figure 32. J101 Boron/Aluminum Blade, TM/C.

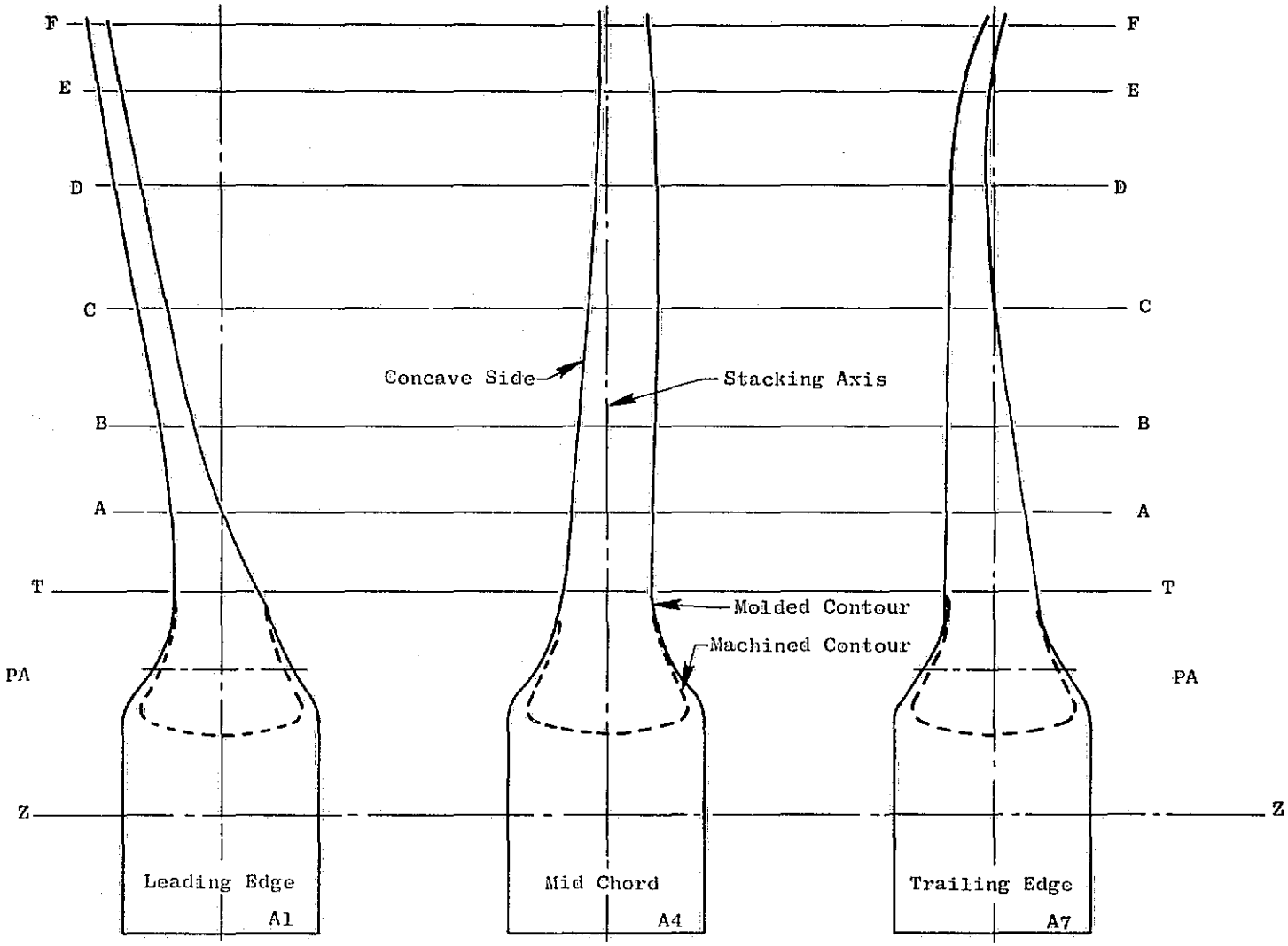

Figure 33. Molded Blade Contour

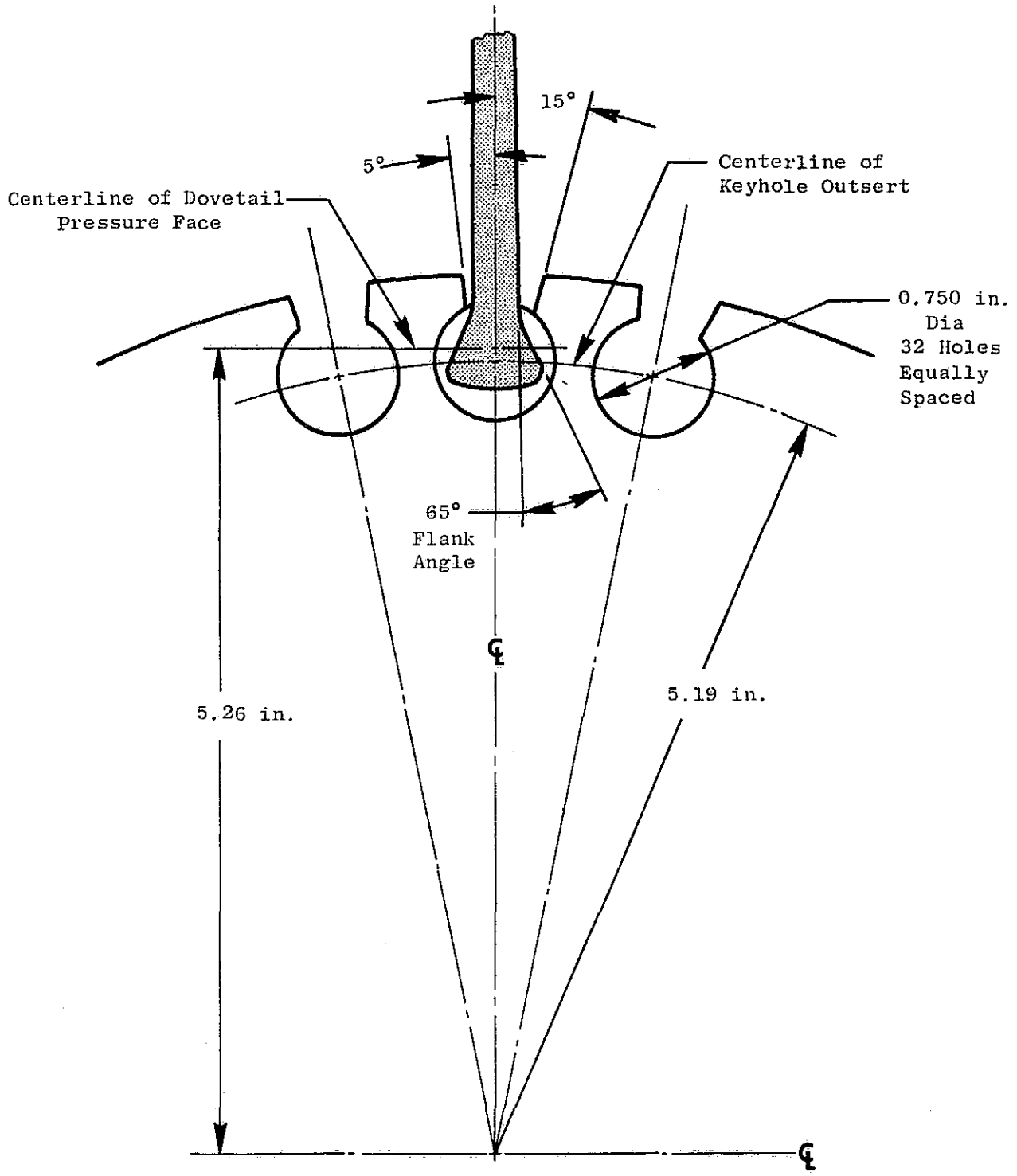

Figure 34. J101 B/A1 Blade Swingroot Attachment

3.4.3 Blade Preliminary Design

A detailed drawing of the J101 Blade is shown in Figure 35. The B/Al blade internal design relative to the boron fiber diameter, aluminum matrix material and fiber orientation within this program was to be based primarily on the material screening and evaluation studies of Task I. The design analysis effort was related to preliminary studies of the structural integrity of the selected material systems. These design analyses included investigation of 5.6 mil and 8.0 mil diameter boron with (±10), (±15), (0/22/0/-22) and (0/20) fiber orientations. The various aluminum matrix materials were not studied analytically as the material properties of both 1100 and 2024 aluminum required for the analysis are nearly identical.

Initially, a B/Al hybrid configuration, Figure 36, was studied which included 8.0 mil boron/1100 aluminum in the core plies and 5.6 mil boron/2024 aluminum in the outer shell. The 5.6 mil boron outer plies (50% volume fraction boron) were selected because of concern in ability to form the 8.0 mil boron without excessive fiber fracture during pressing. The 2024 aluminum was used in the high stressed outer shell because of the low shear strength of 1100 aluminum based on the initial impact results in Phase I, a (±15°) layup was selected. The design included nickel-plating and a single ply of wire mesh impact protection on the leading edge. A plot of the blade volume material distribution of 8.0 mil boron/1100 aluminum, 5.6 mil boron/2024 aluminum and leading edge protection materials is shown in Figure 37.

A computer analysis based on the above airfoil coordinates and materials was completed. The resultant Campbell Diagram (blade frequency and excitation lines versus rotor speed) is shown in Figure 38. The first torsional frequency is 1515 cps at 100% rotor speed and well-spaced between the 6/rev and 8/rev excitation lines. The reduced velocity, a dimensionless parameter indicating blade stability, is 1.05 at 100% rotor speed. This is low enough to provide good blade stability margin even at the fan aerodynamic stall line. The second flexural frequency is below the first torsional with sufficient separation to avoid any coupled modes. The first flexural frequency is only 10% above the 2/rev excitation line at 100% rotor speed. The 101 design criteria specifies a minimum of 15% separation at 110% rotor speed.

As fabrication of the 8.0 mil boron fibers did not appear to present any problems, and the impact and tensile strengths of the fibers was appreciably higher than the 5.6 mil boron, a decision to build the entire blade from 8.0 mil boron was made. The increased modulus of elasticity provided nearly 15% separation of the first flexural frequency and the 2/rev excitation line. Further increase of the first flexural frequency was achieved by placing spanwise fibers on the outer surface plies of the blade. The higher Charpy impact strength was obtained with unidirectional fiber orientation. Some (0/22/0/-22) cross ply was still required in the core to maintain the first torsional frequency.

FOLDOUT FRAME

SECTION	AIRFOIL SECT NOT ALONG STACKING AXIS	CHORD OVERALL	TWIST ANGLE	DEEP LEADING EDGE	DEEP TRAILING EDGE	UNDIMENSIONED DRAWING NO 40151T9-415
A-A	.410	.064	———	———	———	———	SHT NO. 1
B-B	.041	.076	———	———	———	———	2
C-C	1.401	.075	———	———	———	———	3
D-D	1.877	.077	———	———	———	———	4
E-E	2.247	.075	3.424	9°34'	———	———	5
F-F	2.55	.074	3.469	10°35'	———	———	6
G-G	3.25	.068	3.527	17°26'	———	———	7
H-H	3.745	.064	3.553	22°30'	———	———	8
J-J	4.521	.059	3.59	28°35'	———	———	9
K-K	4.671	.058	3.600	31°28'	———	———	10
L-L	5.470	.055	3.602	36°56'	———	———	11
M-M	6.244	.052	3.598	40°04'	.013	.011	12
N-N	6.867	.051	3.574	43°12'	.016	.011	13
P-P	7.451	.050	3.555	45°38'	.015	.012	14
R-R	7.681	.045	3.557	47°0'	.016	.012	15

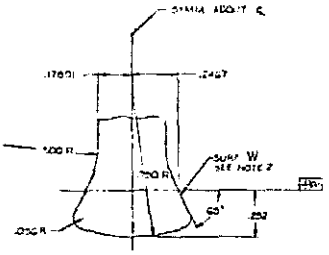

BASIC DOVETAIL DIM
SCALE 5/1

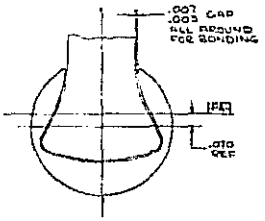

VIEW S (20)
SCALE 5/1

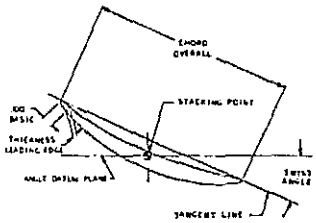

SECT A-A THRU L-L
SCALE NONE
SEE TABLE (16)

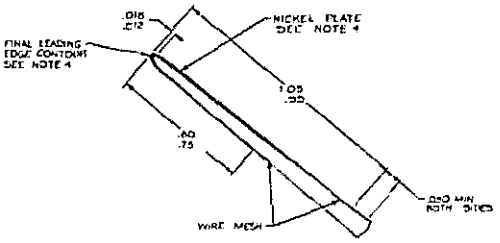

SECT T-T
SCALE 10/1

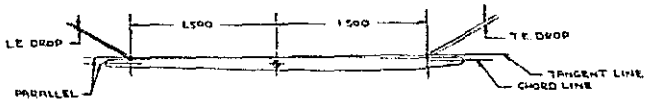

SECT M-M THRU R-R
DEFINITION OF TANGENT LINE OTHERWISE SAME AS SECT A-A THRU L-L

Figure 35. J101 Finish

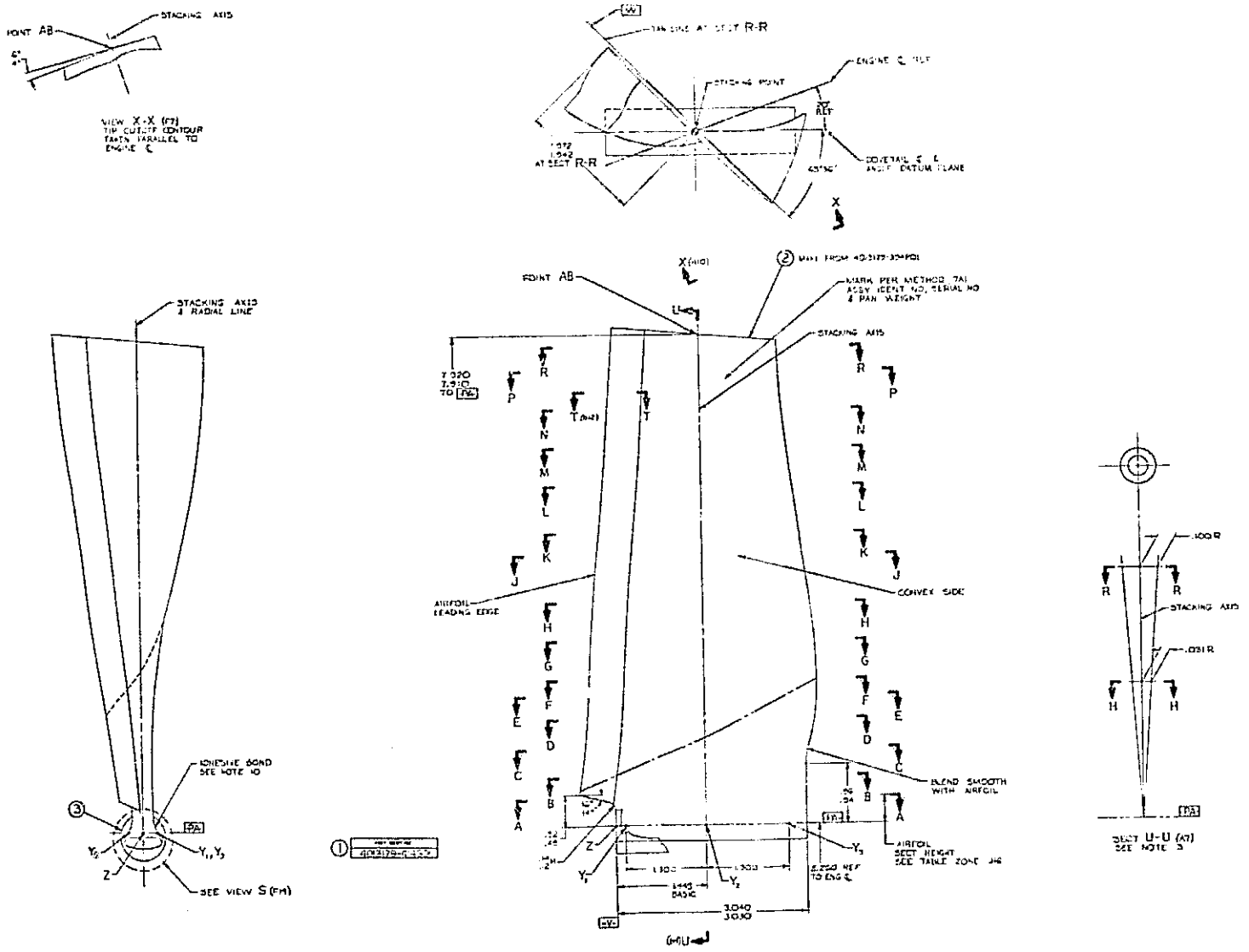

e 35. J101 Finished Detail Drawing.

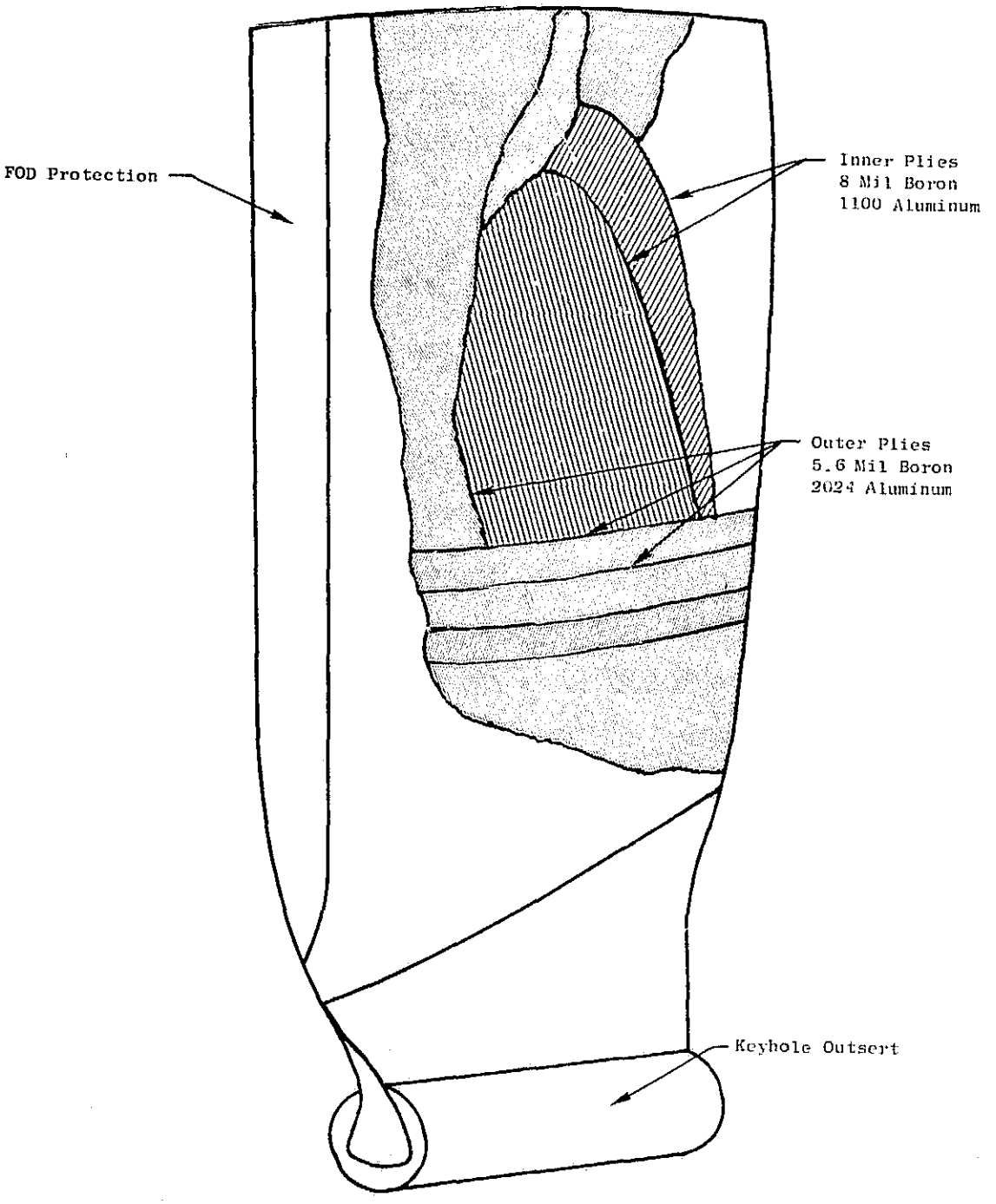

Blade	Chord, in.	Length, in.	Weight, lb
Ti	3.6	8.0	0.8
B/Al	3.6	8.0	0.5

Figure 36. J101 Hybrid B/Al Blade Design.

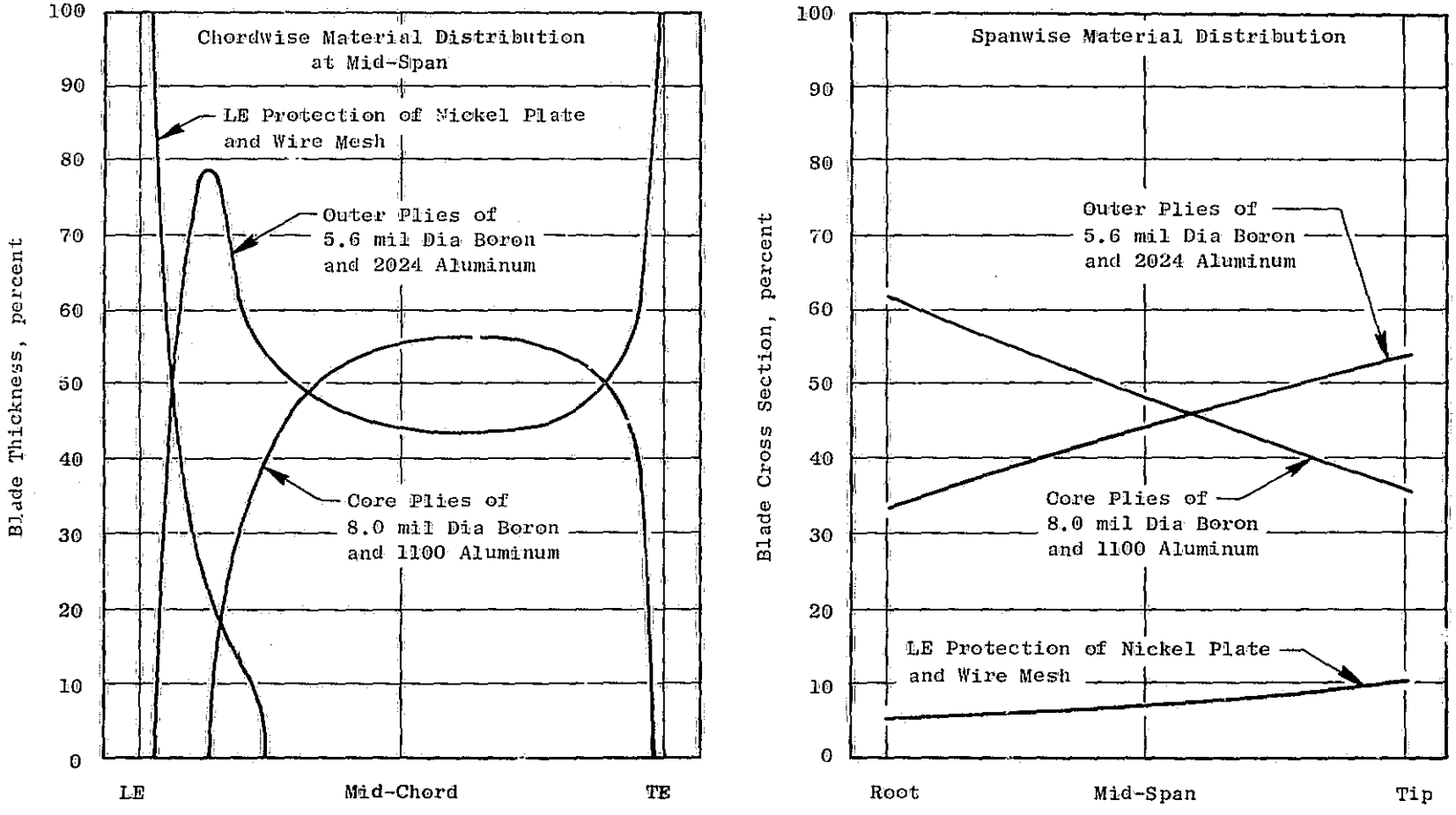

Figure 37. Hybrid B/Al Blade Volume Material Distribution.

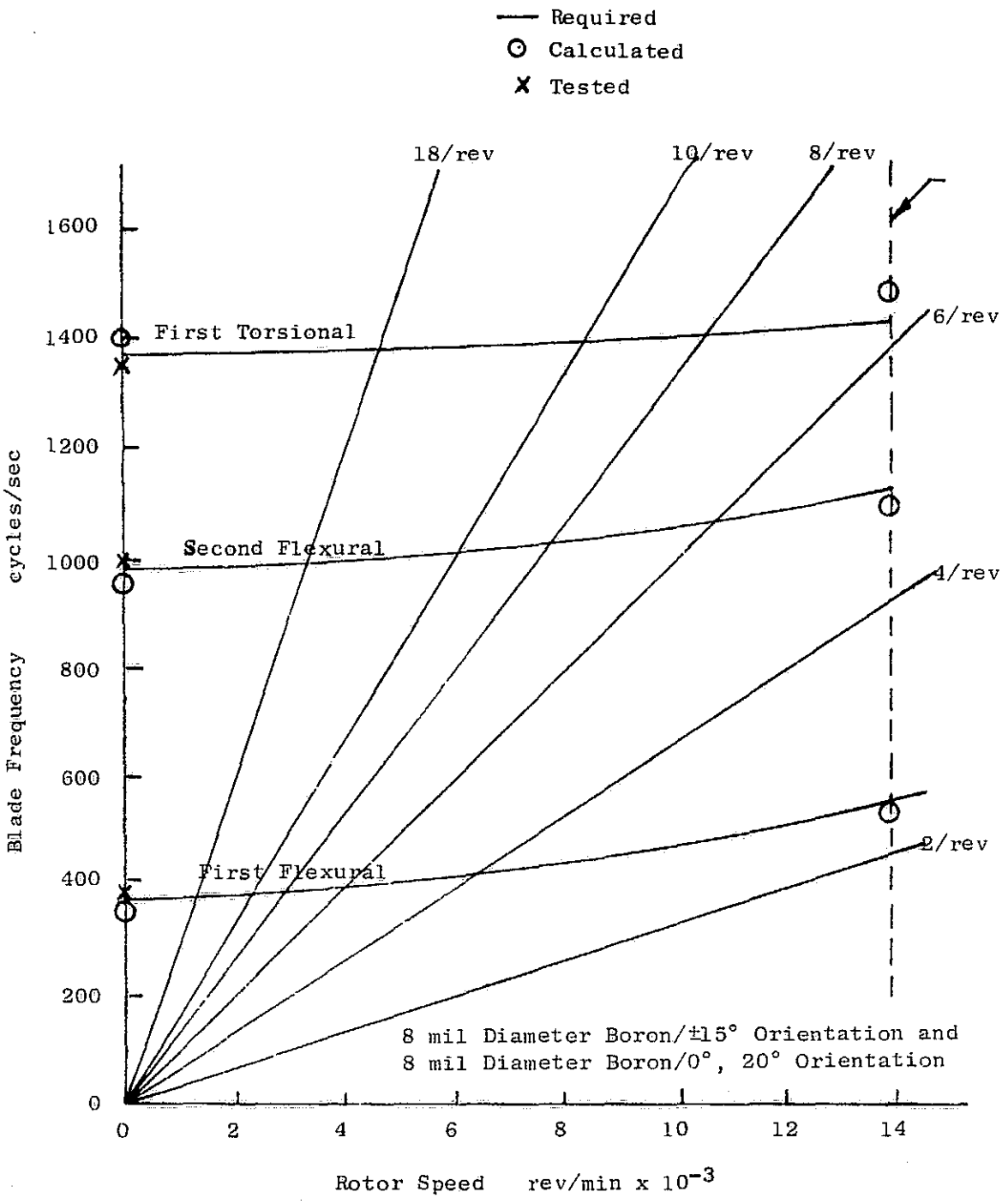

Figure 38. Campbell Diagram, J101 Stage 1 B/Al Fan Blade.

Ply lofting of the blade was completed using all 8.0 mil boron. The plies were lofted to fit the nominal airfoil contour sections and included nickel plating and a single-ply of wire mesh in the leading edge region only. The resulting blade ply stack-up is shown in Figure 39.

After the external geometry of the blade was established and the 8.0 mil boron was selected, analysis was conducted to insure that a B/Al material system was available to satisfy the following major design requirements:

(1) A first torsional frequency not less than the titanium blade, 1625 Hz, to maintain a reduced velocity stability parameter equal to the titanium blade at 100% rotor speed.

(2) A first flexural frequency of 560 Hz to obtain a 15% margin over the 2/rev excitation at 110% rotor speed.

(3) Avoid coincidence of second flexural resonance and per rev excitation at 100% rotor speed.

(4) Most severe combination of maximum effective steady state stress and vibratory stress (assume vibratory stress equal to uncorrected bending stress) within the appropriate Goodman Diagram.

(5) Obtain maximum bird impact resistance with objective of one pound ingestion without airfoil root failure or significant loss of blade material.

The B/Al blade analysis used the twisted blade computer program with anticipated adjustments between calculated and test results based on the APSI (Advanced Propulsion System Integrater) B/Al blade, which was geometrically similar to the J101 blade. Based on the APSI blade experience, the calculated first flexural frequency was increased 4% and the first torsional frequency was decreased 11%.

Initially, both a (±15) and a (0/22/0/-22) fiber orientation were considered. The miniature impact specimen tests of the 1100 aluminum and the ATAC material indicated that the (0/22/0/-22) orientation had higher impact strength than the (±15) orientation. The (0/22/0/-22) orientation met the design requirements except the first flexural frequency was only 10% above the 2/rev excitation line. The (±15) orientation did meet the design requirements. Later studies of the 1100 aluminum matrix material indicated that the impact resistance of the (±15) was higher than the (0/22/0-22) layup.

Consideration of the adaptability of the (0/22/0-22) orientation to J101 blade indicated that elimination of the -22° fibers may be desirable. The resulting (0/22) orientation is essentially a (±11) orientation skewed forward 11°. The resultant modulus of elasticity and first flexural frequency are less than a (±10) orientation but higher than a (±15) orientation. Addition of plies at higher orientation angles toward the airfoil

FOLDOUT FRAME

PLY OR LAM NO	ORIENT. ANGLE	WEIGHT	PLY OR LAM NO	ORIENT. ANGLE	WEIGHT	PLY OR LAM NO	ORIENT. ANGLE	WEIGHT
1A	.005 AL		34-9	15 WIRE MESH		56-27	[illegible] MESH	
2A	[illegible] AL TEST		35-9			57-27		
3A	.005 AL		36-9			58-27		
4A			37-9			59-27		
5A			38-9			60-27		
6A			10			61-27		
7A			11	0°		62-27		
8A	15 WIRE MESH		12	0°		63-27		
9A			13	0°		28	0°	
10A			14	0°		29	-20°	
11A			15	0°		30	0°	
12A			16	0°		31	-20°	
13A			17	0°		32	0°	
14A			18			33	-20°	
15A			39-18	15 WIRE MESH		34	0°	
16A			40-18			35	-20°	
17A			41-18			36	0°	
18A			42-18			648	15 WIRE MESH	
19A			43-18			658		
20A			44-18			668		
21A						678		
22A			45-18	15 WIRE MESH		688		
23A			45-18AL			698		
24A			46-18	15 WIRE MESH		708		
25A			47-18			718		
26A			48-18			728		
1	0°		49-18			738		
2	-20°		50-18			748		
3	0°		51-18			758		
4	-20°		19	0°		768		
5	0°		20	0°		778		
6	-20°		21	0°		788		
7	0°		22	0°		798		
8	-20°		23	0°		808		
9	0°		24	0°		818		
27-9	15 WIRE MESH		25	0°		828		
28-9			26	0°		838	.005 AL	
29-9			27	0°		848		
30-9			52-27	15 WIRE MESH		858		
31-9			53-27			868		
32-9			54-27			878		
33-9			55-27			888		
						898		

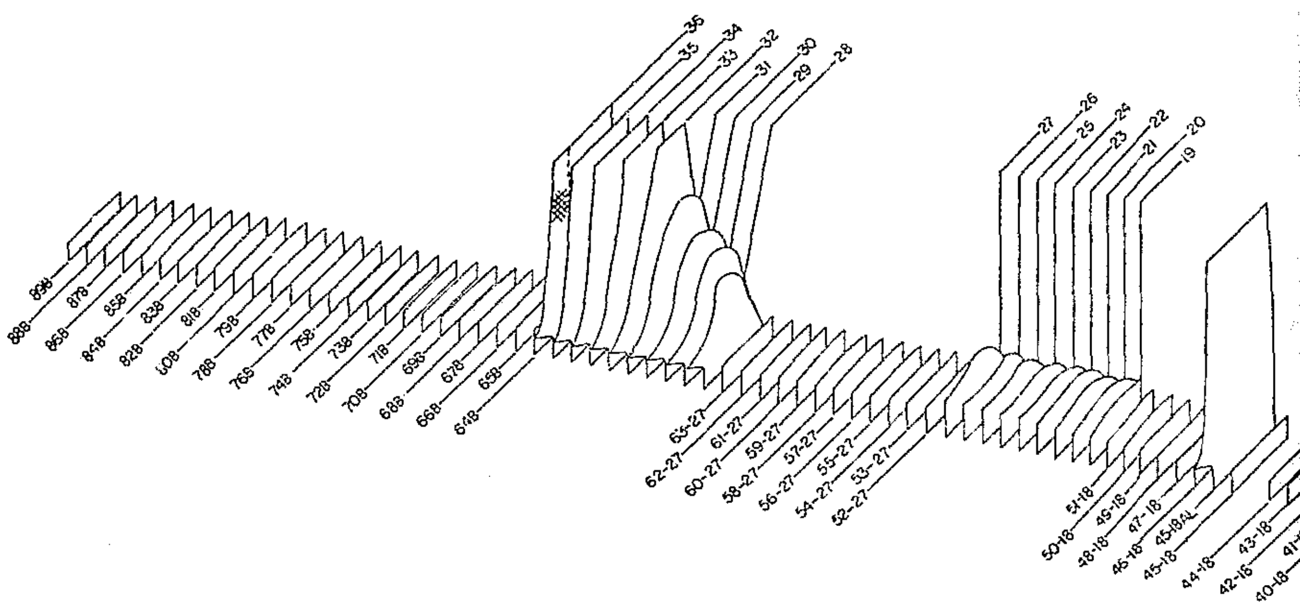

Figure 39. J101 Blad

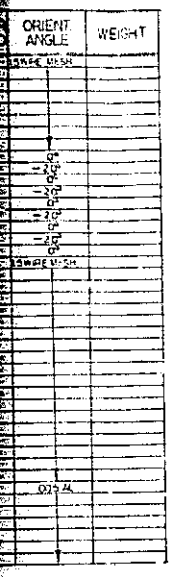

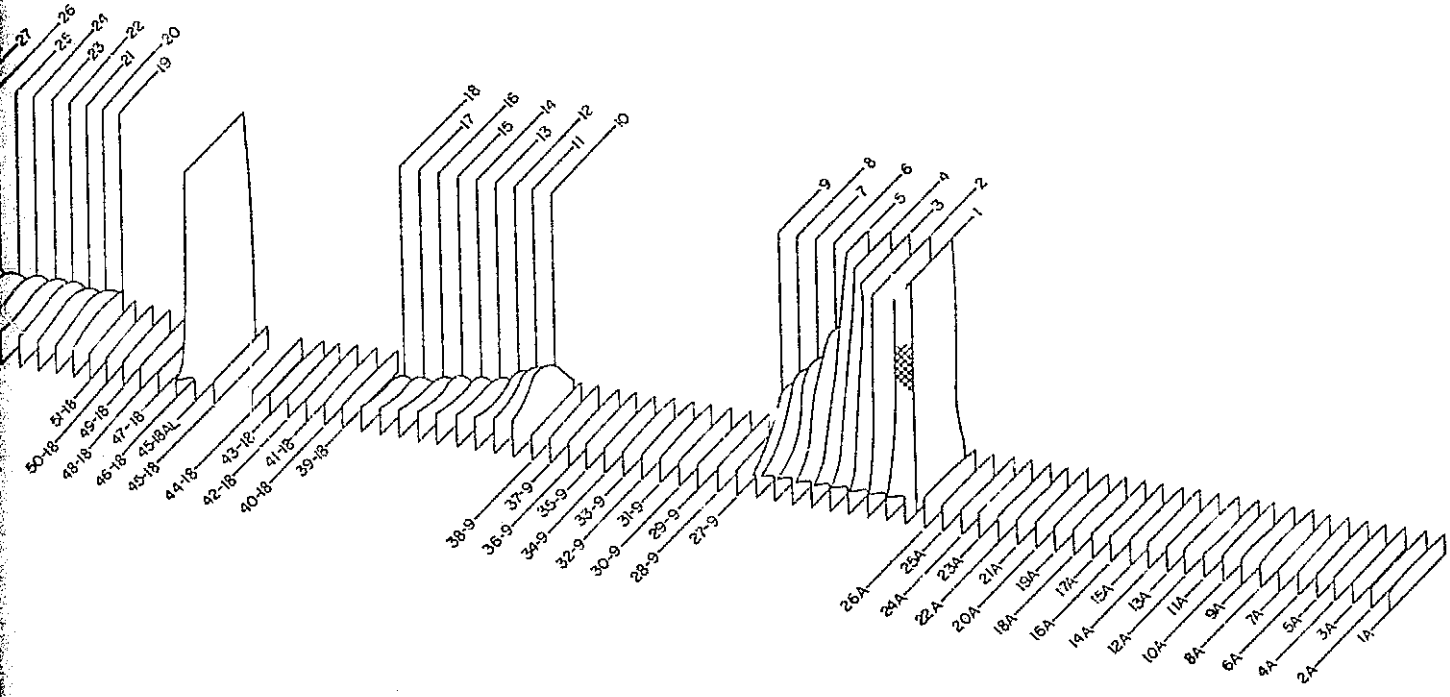

gure 39. J101 Blade Ply Stack-Up.

core to achieve chordwise stiffness and impact energy transfer is still possible and the first flexural frequency requirement can be met.

3.4.4 Material Properties

Material properties were calculated for two material designs, i.e., 8 mil diameter boron/±15° orientation and 8 mil diameter boron/0,°20 orientation. The two filament orientation angles were selected on the basis of preliminary aeromechanical stability calculations and impact resistance results which indicated these two orientations had good Charpy impact strength.

Table XV summarizes the B/Al material physical properties of the 57 percent volume fraction boron/aluminum material. Note, that for the two filament orientations, the modulus of elasticity and Possions ratios are quite similar. Further, there is very little change in properties due to temperature. The largest change due to temperature is in the shear modulus (G).

3.4.5 Blade Analysis

As discussed in the preceding section, the material selection had been reduced to 8.0 mil boron with either a (±15) or a (0/20) layup. The J101 B/Al blade was analyzed using the twisted blade computer program. This analysis is based on elastic beam theory with compensation for coupling of the torsional and flexural modes and included centrifugal stiffening. The analytical results of both material systems were nearly identical; the stresses and frequencies deviate less than 2%. Consequently, the analytical results of the (±15) layup are presented herein.

The first three J101 B/Al blade frequencies of interest for blade stability characteristics are indicated on the Campbell diagram, Figure 40. The calculated first flexural frequency is about 1% below the objective. Blades fabricated and tested on the NASA SCAR program had an average measured static first flexural frequency about 2% above the objective. The calculated second flexural natural frequency has good separation from the first torsional mode and does not cross any significant excitation lines within the engine operating range.

The first torsional frequency of the J101 B/Al blade has adequate margin over the 6/rev excitation at the engine design point. Furthermore, the J101 B/Al blade first torsional frequencies are essentially the same as the titanium blade which it replaces.

The 18 IGV's and 68 Stage 1 stator vanes produce a 3980 cps and a 15035 cps stimuli, respectively. These excitations are well out of the area of concern. Table XVI presents a comparison of the calculated and measured stage frequencies for the fabricated J101 B/Al blades.

Table XV. B/Al Material Properties Estimated Temperature Influence.

	±15° Layup		0/20 Layup	
	175° F	350° F	175° F	350° F
Tensile				
Ex 10^6 ksi	31.5	30.5	31.9	30.9
Ey 10^6 ksi	21.6	20.7	21.8	20.9
Gxy 10^6 psi	7.7	6.0	7.5	5.8
Mxy	0.236	0.184	0.220	0.171
Myx	0.163	0.140	0.152	0.130
Compression				
Ex 10^6 psi	31.5	32.5	31.9	32.9
Ey 10^6 psi	21.6	18.1	21.8	18.3
Gxy 10^6 psi	7.7	6.0	7.5	5.8
Mxy	0.236	0.127	0.220	0.127
Myx	0.163	0.163	0.152	0.163
Bending				
Ex 10^6 psi	31.5	31.5	38.9	31.9
Ey 10^6 psi	21.6	17.4	21.8	19.6
Gxy 10^6 psi	7.7	6.0	7.5	5.8
Mxy	0.236	0.155	0.220	0.145
Myx	0.163	0.151	0.152	0.141

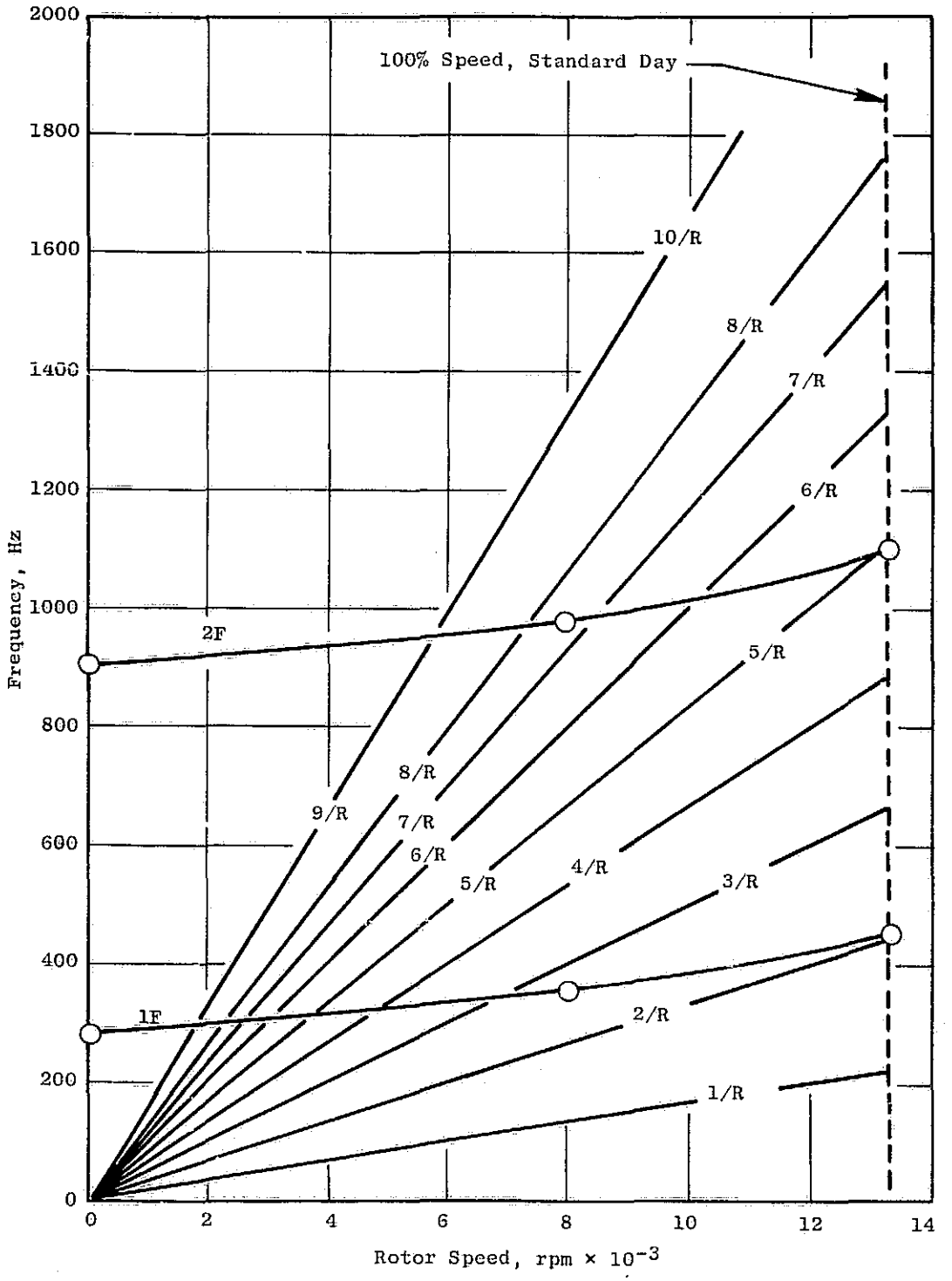

Figure 40. Hybrid B/Al Blade Campbell Diagram.

Table XVI. Comparison of Calculated and Measured Static Blade Frequencies.

S/N	Configuration	Calculated			Measured		
		1F	2F	1T	1F	2F	1T
1	ATAC [0/20]	346	1020	1580	342	1020	1404
2	ATAC [0/20] Full Chord Mesh	335	987	1553	338	942	1548
3	1100 [0/20]	346	1020	1580	348	968	1364
4	1100 [0/20]	346	1020	1580	328	872	1296
5	1100 [±15] Full Chord Mesh	323	969	1578	316	926	1564
6	*1100 [±15] Full Chord Mesh	323	969	1578	310	876	1450
7	1100 [0/20] Full Chord Mesh	335	987	1557	-	-	-
8	1100 [0.20] Full Chord Mesh	335	987	1553	-	-	-

*Tip section 10% thicker than other blades

A plot of Reduced Velocity (V/bW) versus incidence angle for the J101 Stage 1 fan blade is shown in Figure 41. Sufficient stability margin exists for inlet distortion and for capability of sustaining repeated stalls throughout the J101 operating regime.

A steady state stress analysis of this blade was completed for sea-level-static operation as shown in Figure 42. This computer analysis included appropriate boundary conditions to account for blade tilting. The maximum calculated centrifugal stress was 18,500 psi at 100% rotor speed (Figure 43). The maximum effective stress was 57,500 psi located at the trailing edge, concave surface, 3.5 inches above the dovetail pressure face (Figure 43). These stresses were well within the allowable limits for the B/Al material. An estimated Goodman diagram is shown in Figure 44.

The analytical techniques and results presented are normally adequate for metallic blades. However, this analysis does not explore interlaminate shear and transverse tensile stresses, which are a major concern in selecting the aluminum matrix material. A more sophisticated, three-dimensional finite element computer analysis is highly recommended, particularly for use of the rather low-strength 1100 aluminum matrix material.

3.4.6 Dovetail Design

The dovetail form is obtained by interspersing bulking plies of stainless steel mesh and aluminum foil between the primary load-carrying boron/aluminum plies. Additional pressure face plies are provided to allow machining of the dovetail flanks without removal of load-carrying plies. These mesh and foil layers also act as a pressure pad for properly distributing the dovetail bearing load. Results of the blade and disk dovetail analysis are presented in Figure 45. Figure 44 shows anticipated steady state and vibratory endurance limits for the J101 B/Al blade material at 350° F. This Goodman Diagram needs to be confirmed by bench testing of blades. Preliminary calculations indicate that if the stresses in the airfoil go to the material limit, the dovetail stresses are still well within the allowable dovetail limit.

3.4.7 Whirligig Design

Although no blades were impact-tested in this program, a complete whirligig impact facility (see Figure 46) capable of conducting such testing was designed and fabricated.

All design and detail drawings for the rotor disk, blade retention and drive shaft on the whirligig facility were completed. The disk has three slots at different incidence angles to simulate bird impacts at various aircraft flight conditions shown in Table XVII. Additional slots may be added to the disk to simulate other impact conditions as desired.

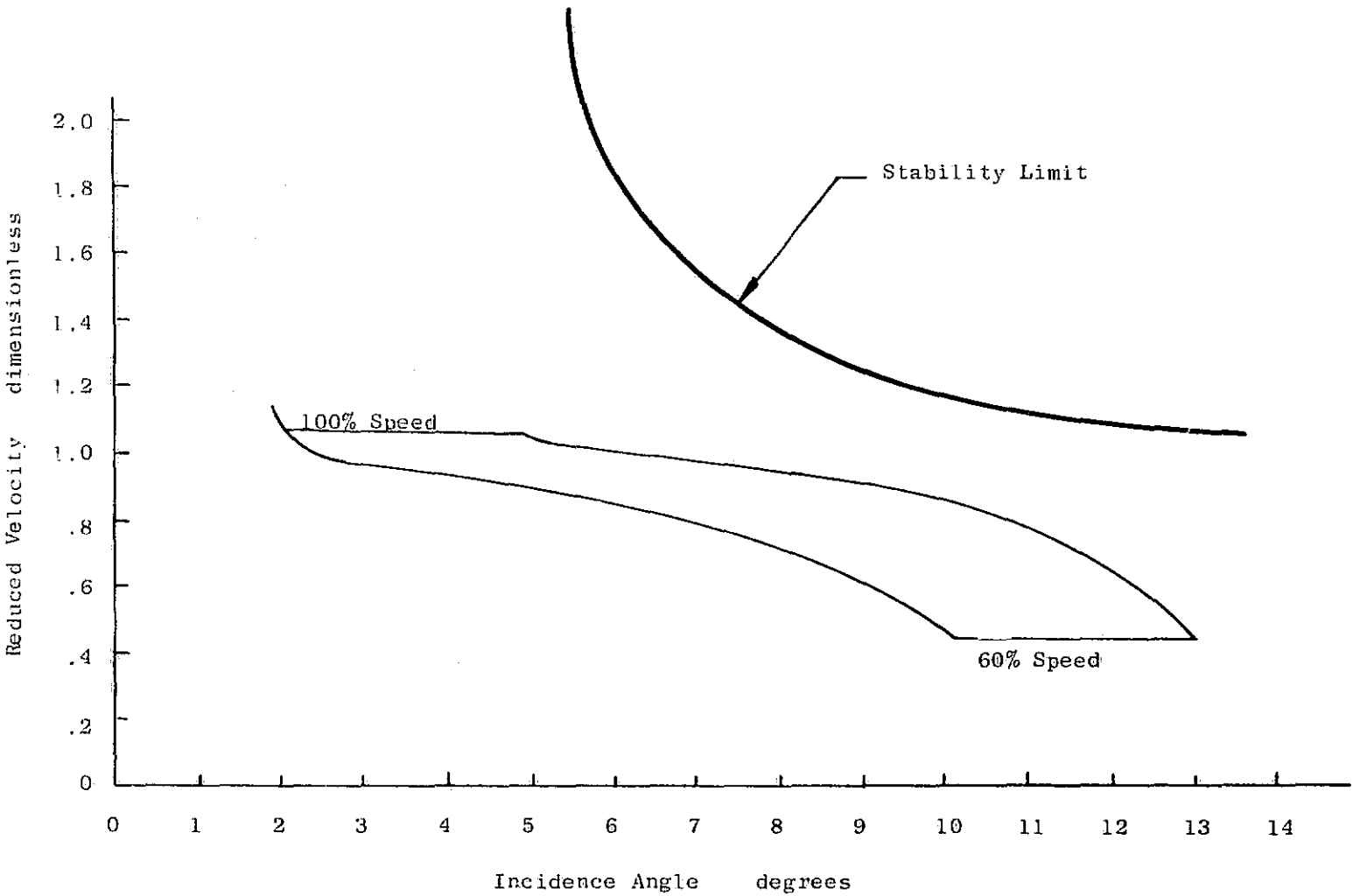

Figure 41. J101 Stage 1 B/Al Fan Blade, Torsional Stability Map.

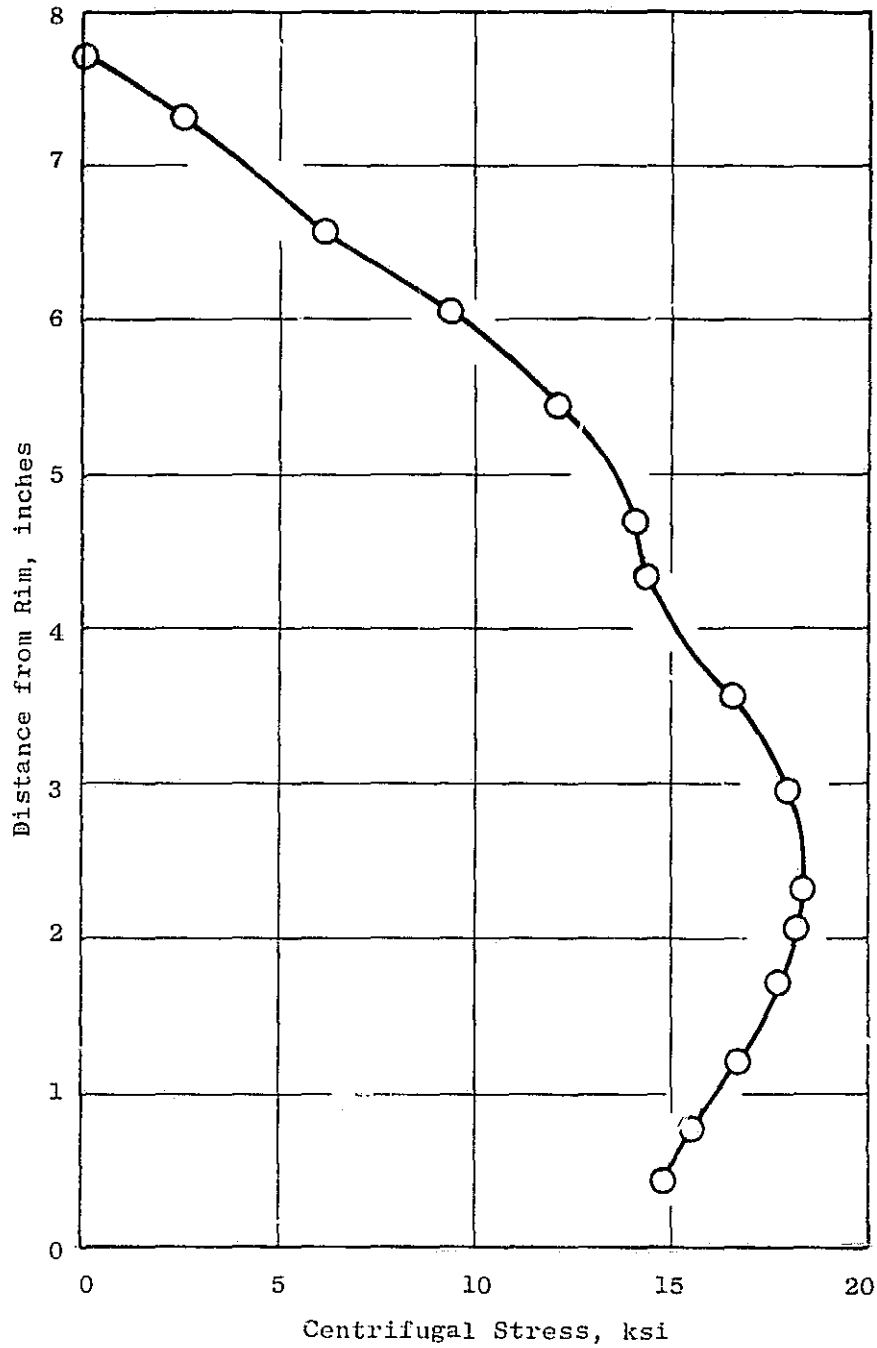

Figure 42. J101 Blade Calculated Centrifugal Stresses at 100% Speed (13,266 rpm).

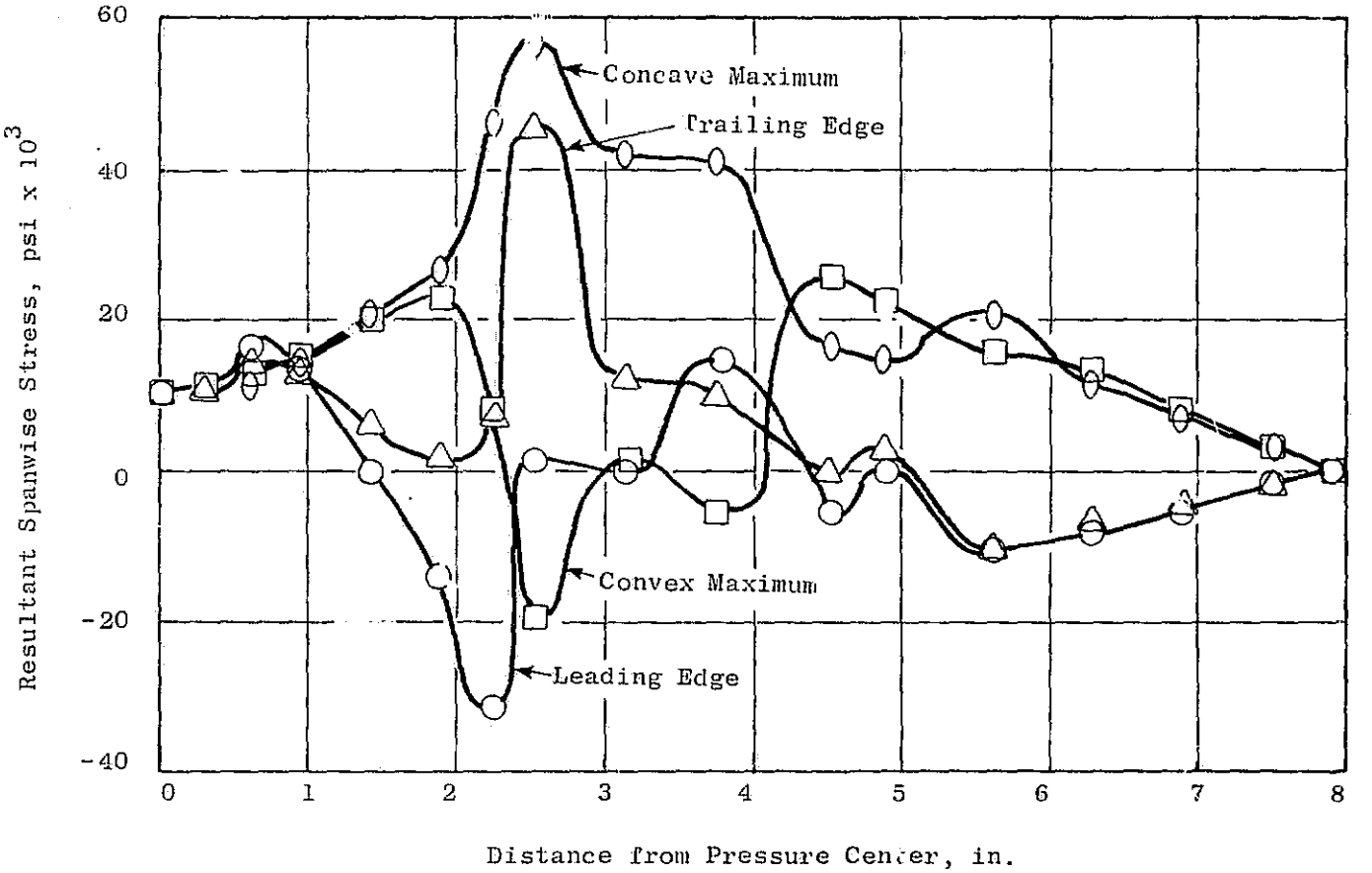

Figure 43. J101 B/A1 Blade Resultant Spanwise Stress Sea Level Static Blade Loading.

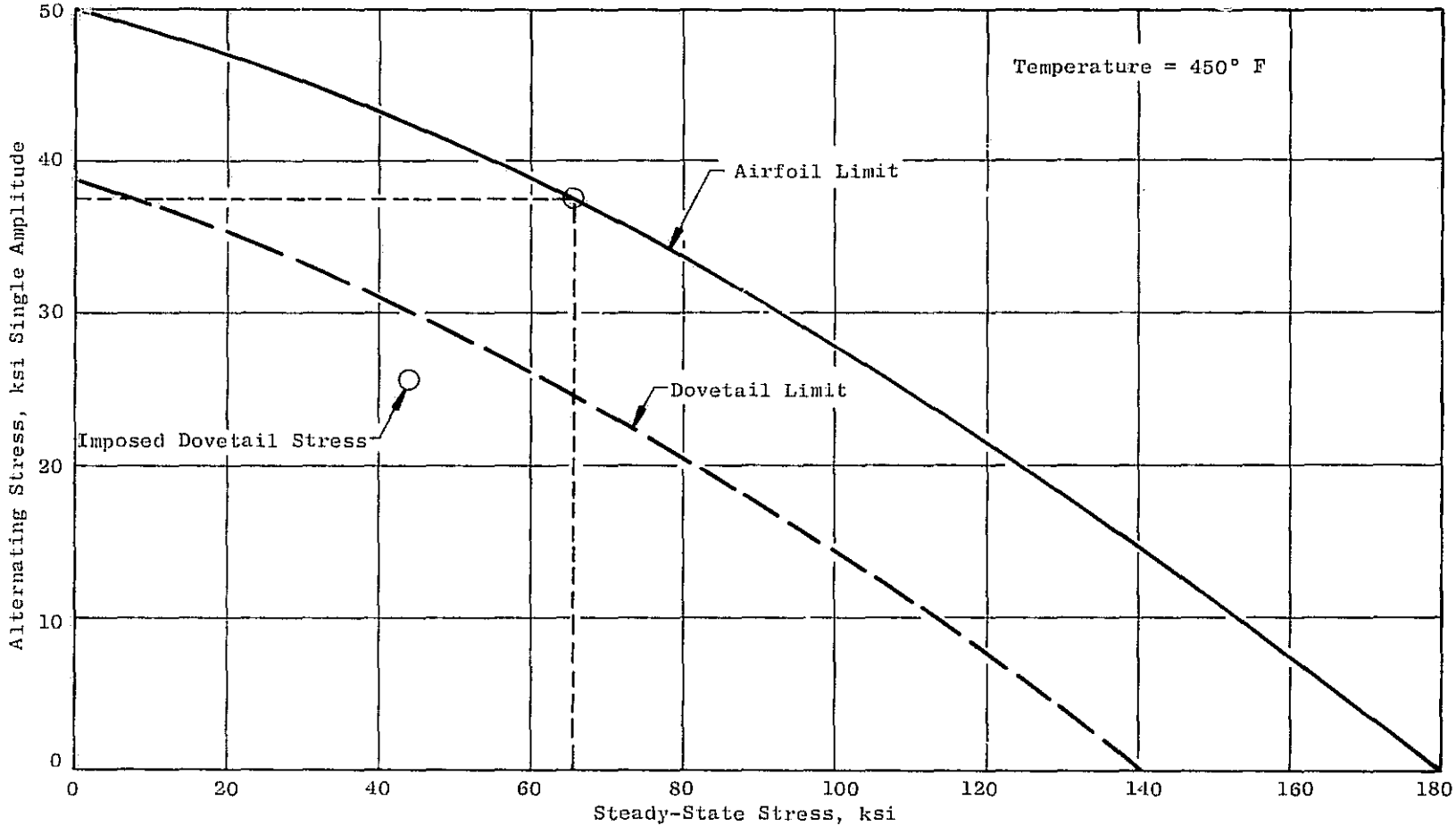

Figure 44. Goodman Diagram, J101 Stage 1 B/Al Fan Blade.

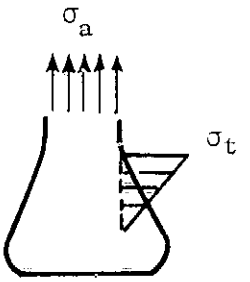

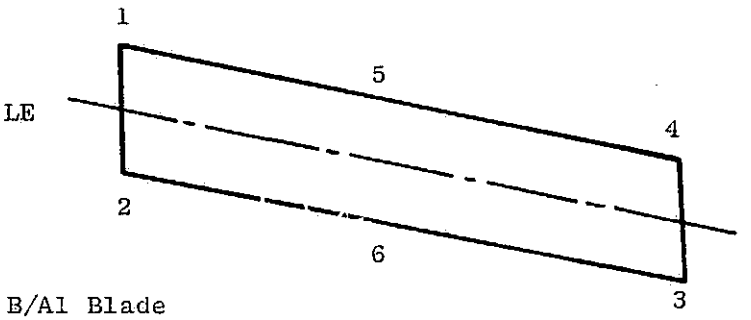

Stage 1 B/Al Blade

Stress, ksi	Location					
	1	2	3	4	5	6
σ_a = Dovetail Neck Stress	24.6	5.1	-11.5	28.5	-3.2	26.5
σ_t = Tang Bending Stress	-11.5	-9.3	-2.5	-10.9	-5.9	-11.2
σ_c = Combined Stress	24.6	-9.3	-13.4	28.5	8.9	26.5

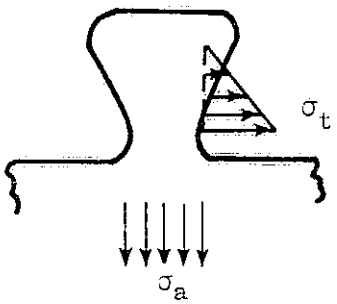

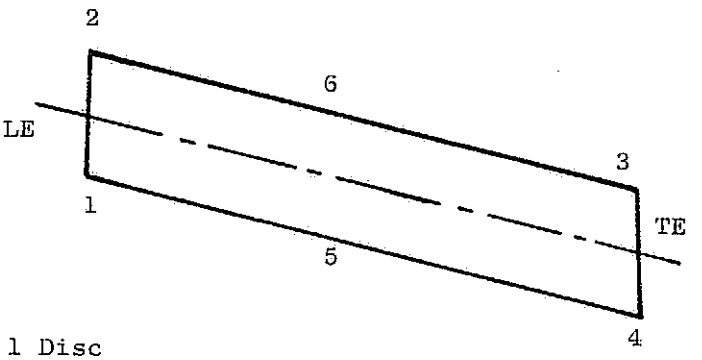

Stage 1 Disc

Stress, ksi	Location					
	1	2	3	4	5	6
σ_a = Neck Stress	34.3	5.2	-11.1	39.6	-2.9	36.9
σ_t = Tang Bending Stress	9.2	7.4	2.0	8.7	4.7	8.9
σ_c = Combined Stress	41.6	12.2	-11.1	46.1	35.9	56.5

Figure 45. J101 Stage 1 B/Al Blade and Disc Dovetail Tang Stresses at 100% Speed.

FOLDOUT FRAME

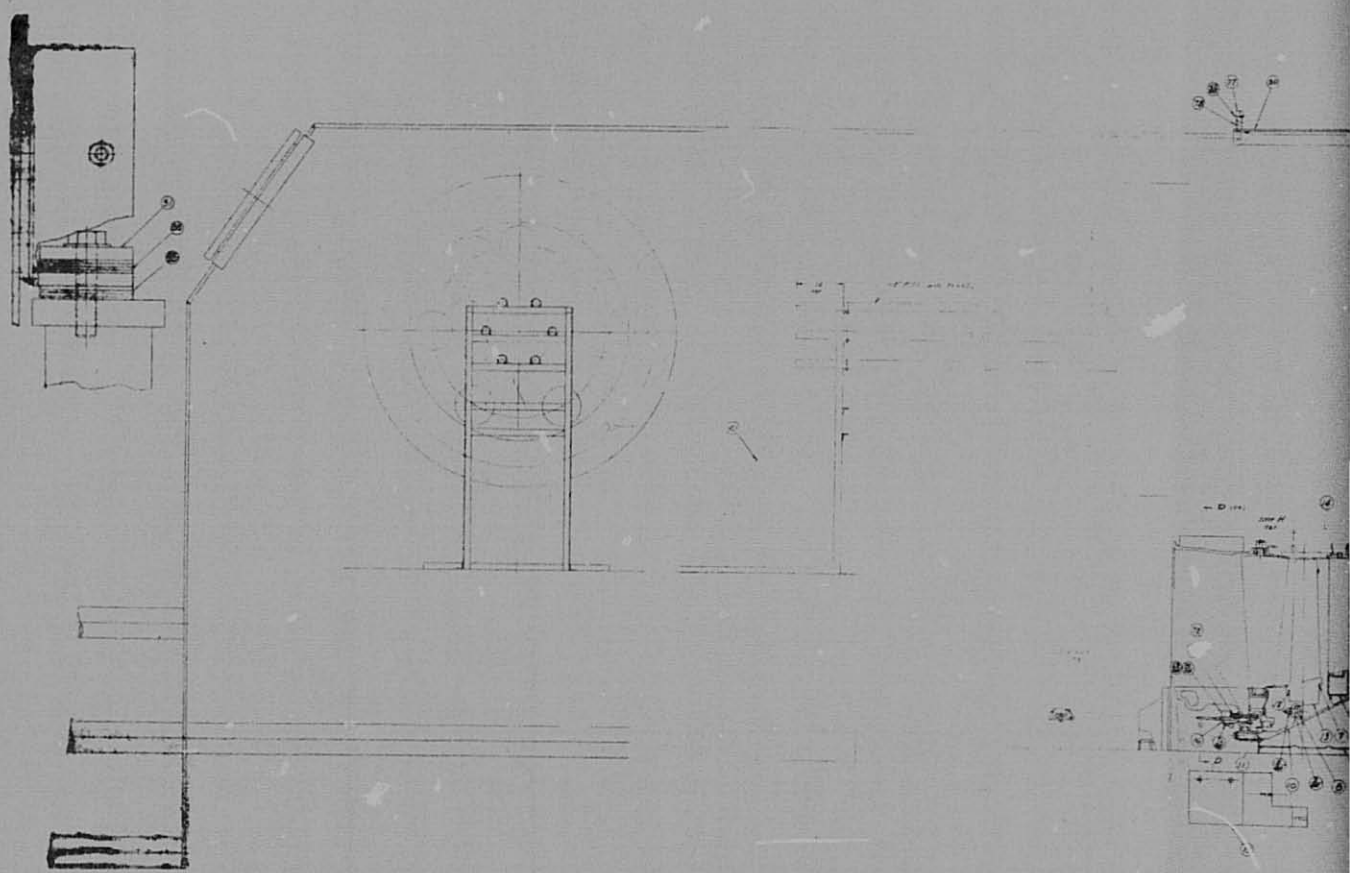

Figure 46. Whirilig Impact F

FOLDOUT FRAME 2

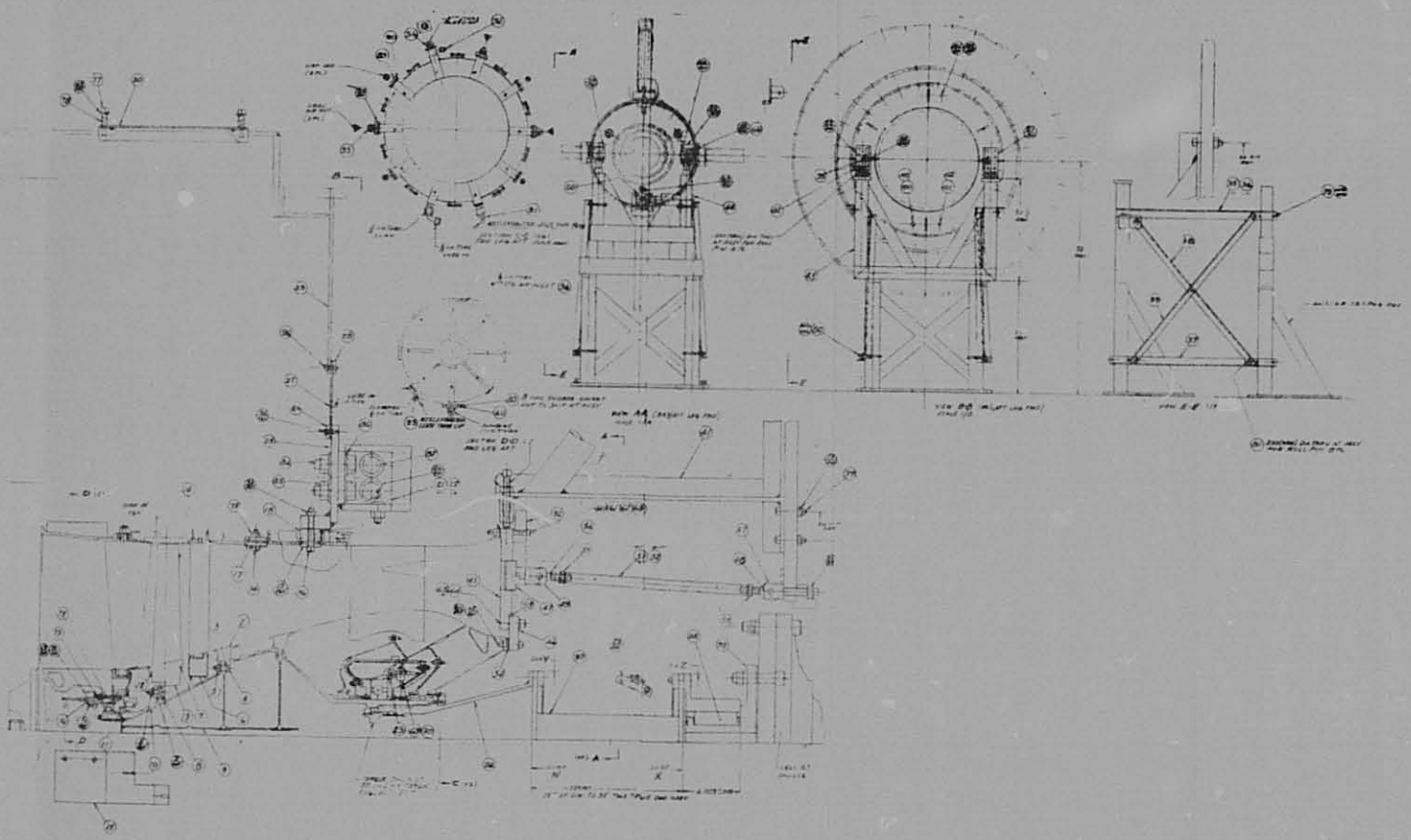

Whirilig Impact Facility Layout.

Table XVII. AST Single Blade Impact Test of J101 Blades.

Shot No.	Span, %	Engine Rotor Speed, %	Aircraft/ Bird Vel., ft/sec	Relative Velocity, ft/sec	Slot Angle Degrees	Simulated Incidence Angle, Degrees	Whirligig Rotor Speed, rpm	Bird Size/Slice Size Weights, oz
1	70	100	400	1322	37.5	17.5	13,500	4/2 16/12
2	70	100	400	1322	37.5	17.5	13,500	(3 Tests) *
3	70	100	400	1322	37.5	17.5	13,500	(1 Test) **
4	70	80	400	810	40.8	14.2	8,260	(3 Tests) *
5	70	80	400	810	40.8	14.2	8,260	(3 Tests) **
6	70	80	400	810	40.8	14.2	8,260	(1 Test) **
7	30	100	400	1030	42.75	30.25	13,850	4/2 16/12
8	30	100	400	1030	42.75	30.25	13,850	(3 Tests) *

* - Weights to be selected from previous test to bracket failure.

** - Weight to be selected from previous test.

Tip R = 13.2 in. 70% Span impact R = 11.2 in. 30% Span impact R = 8.5 in.

100% Engine Rotor Speed: 13,266 rpm
80% Engine Rotor Speed: 10,600 rpm

In order to balance the single B/Al blade, a short steel "dummy blade" will be inserted in the opposite side of the disk.

The SAE 4340 steel disk was designed to operate at speeds in excess of the specified burst speed of 16,345 rpm.

3.5 BIRD IMPACT ANALYSIS

The purpose of this study was to select the bird impact conditions which would be used for the blade dynamic impact analysis. The approach taken was to estimate the most severe bird impact conditions for the J101 B/A1 stage 1 fan blade. Using these severe conditions, four cases were identified which would identify stress and deflection as a function of bird size incidence angle and relative velocity.

J101 Bird Impact Characteristics

The J101 engine has inlet guide vanes (IGV's) upstream of the first stage fan blade. The trailing edge of the IGV's is approximately 0.5 inch upstream of the leading edge of the fan blade. Figure 47 shows a front view of the IGV's and the largest diameter bird that can pass through the IGV's. At the root, adjacent to the spinner, the largest bird that can pass through is 6.5 ounces. At the mid-span and 70% span, the bird sizes are 16 ounces and 25 ounces, respectively.

Using the bird sizes identified, the bird-blade impact conditions were calculated at the 17%, 50%, and 70% blade heights as a function of aircraft velocity. Figure 48 schematically shows the top view of the blade and the bird velocity vectors. It was assumed that the bird axial velocity was equal to the aircraft and the maximum bird slice would be taken by the blade. The bird was assumed to be an ellipsoid sliced perpendicular to its major axis and the slice taken is out of the center of the bird. Figure 49 shows the number of blades that could be impacted by various size birds at the 70% span location. In the analysis presented herein, the largest slice weight is being considered. It must be noted that the maximum slice weight is obtained when the bird is sliced parallel to its major axis; however, this was not considered for this analysis.

Figure 50 shows the largest bird slice weight, when the bird is sliced perpendicular to its major axis, as a function of bird weight and J101 aircraft velocity. Also shown are the radii of the birds. Figure 51 shows the bird-blade impact parameters; i.e., bird slice weight (Ws), relative velocity (Vr) incidence angle (o) and bird slice thickness to diameter ratio (tsDs) as a function of aircraft velocity for a 25 ounce bird impacting the J101 blade at the 70% span location. These parameters were used to calculate the change in bird slice momentum normal to the airfoil at the impact span and the change in bird slice kinetic energy as a function of aircraft velocity for the 17%, 50%, and 70% blade span height. These calculations are summarized in Figures 52 and 53, respectively. Note that the peak magnitude of the change in momentum (ΔMn) is high for all three span locations, but the peak occurs at different aircraft speeds. The change in bird slice kinetic energy (SK) has similar characteristics, but it's peaks occur at different aircraft velocities than the ΔMn.

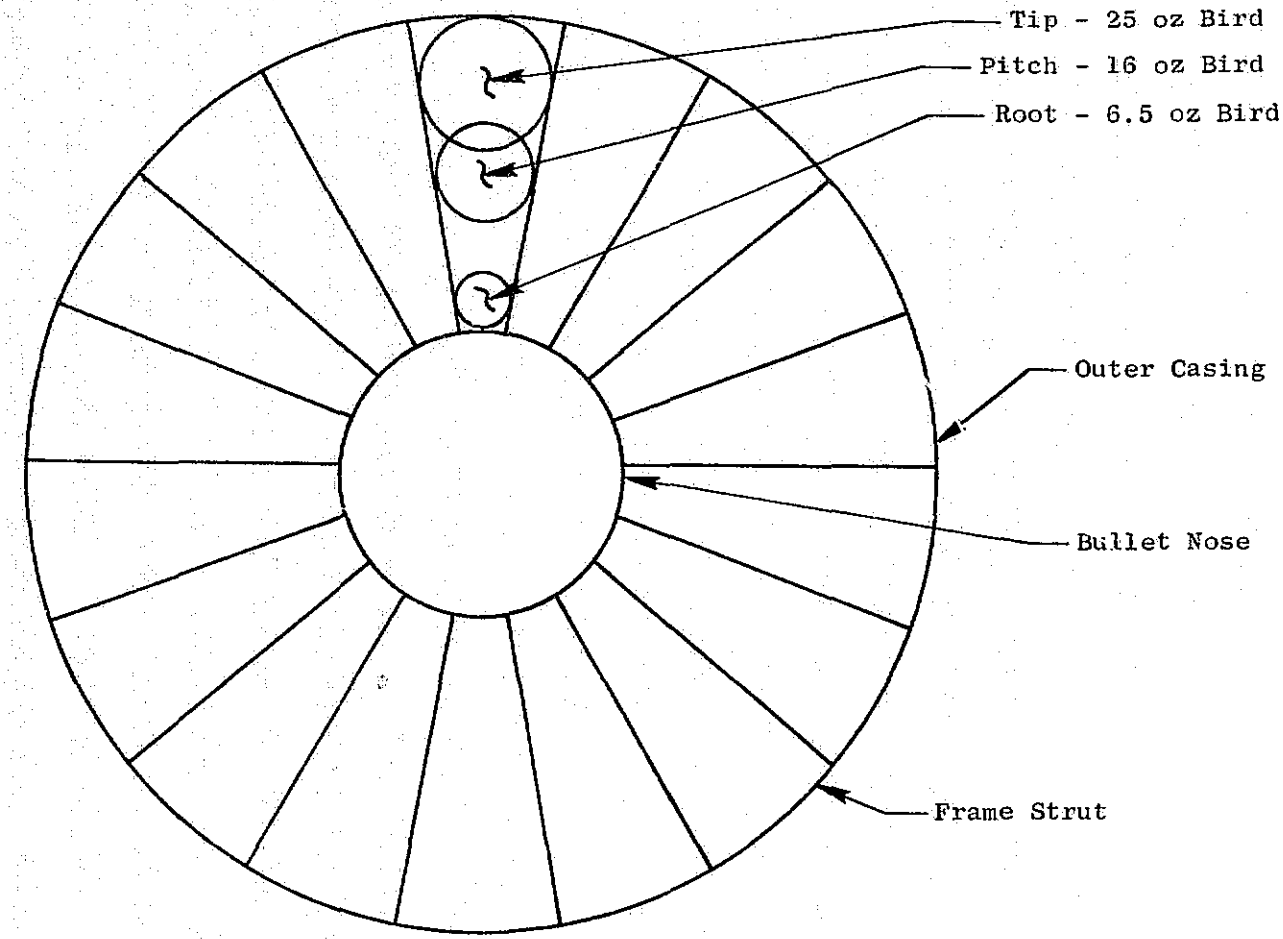

Figure 47. J101 Engine-Ingested Bird Size Limit.

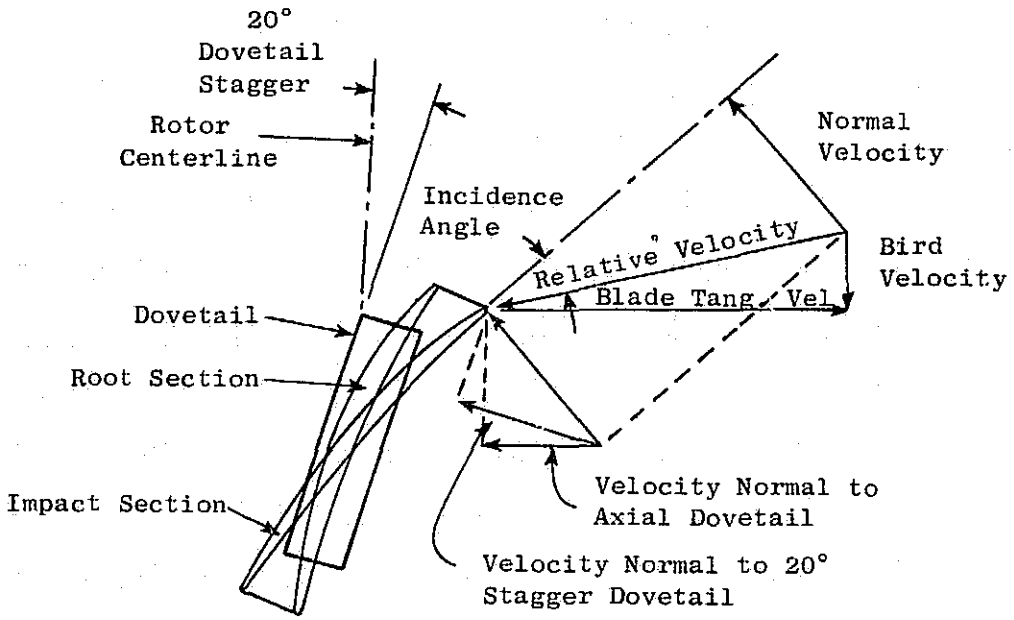

Figure 48. Bird Impact Diagram.

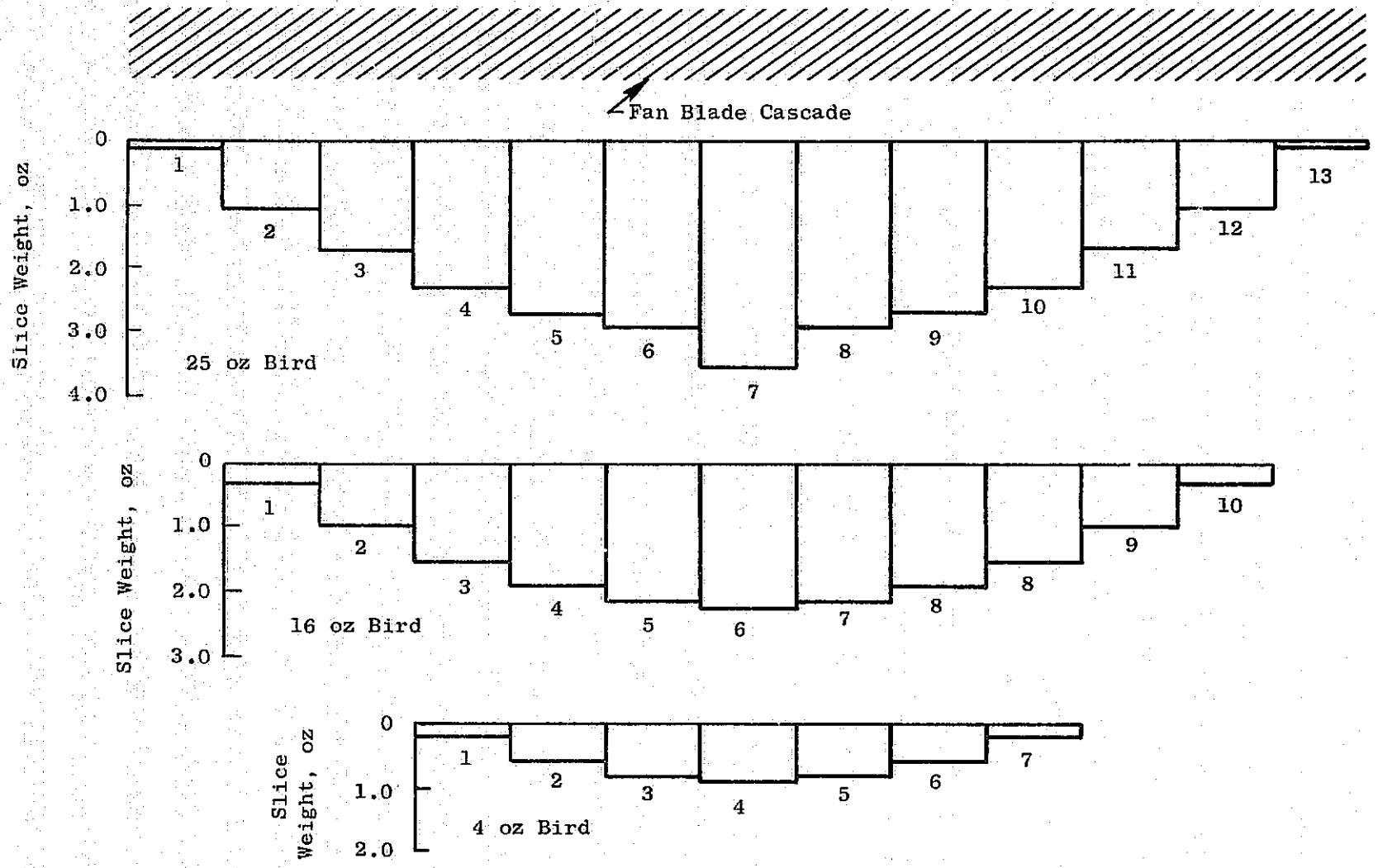

Figure 49. Number of Blades Impacted by Several Sizes of Birds J101 Blades, 70% Span, Aircraft Velocity 400 fps.

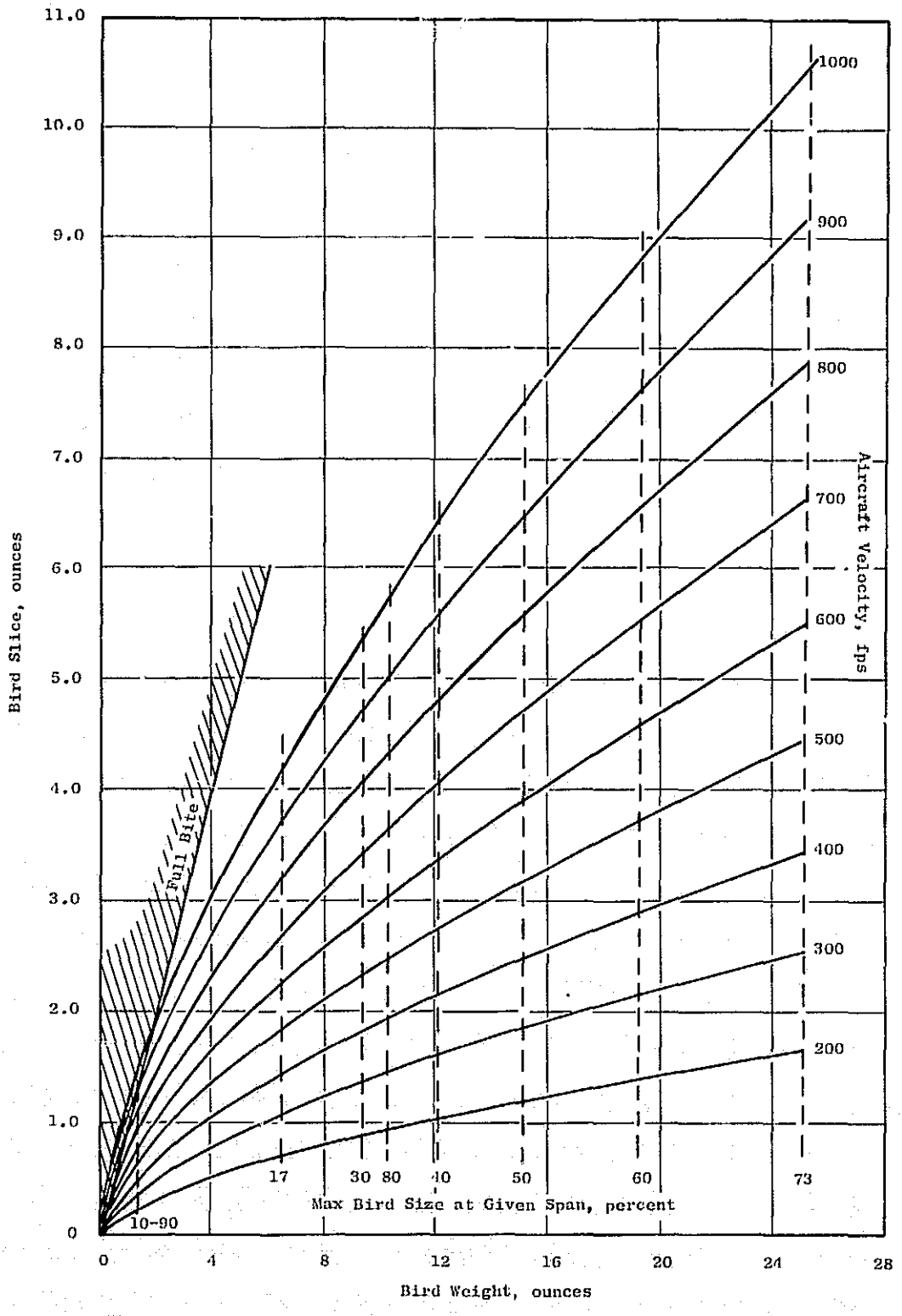

Figure 50. J101 Stage 1 Boron/Aluminum Fan Blade Bird Strike Parameters.

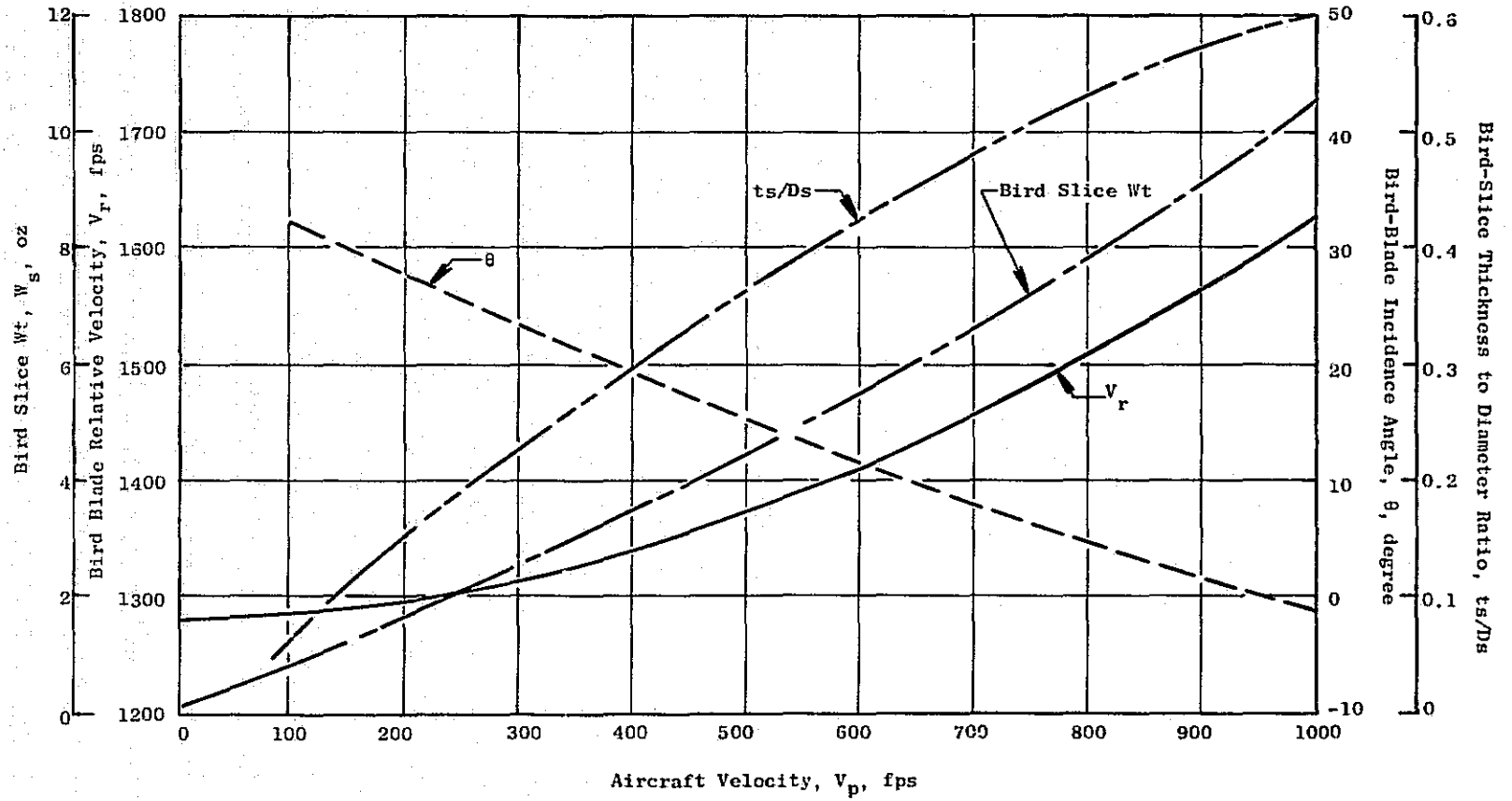

Figure 51. J101 Bird-Blade Impact Parameters for 70% Span and 25-oz. Bird.

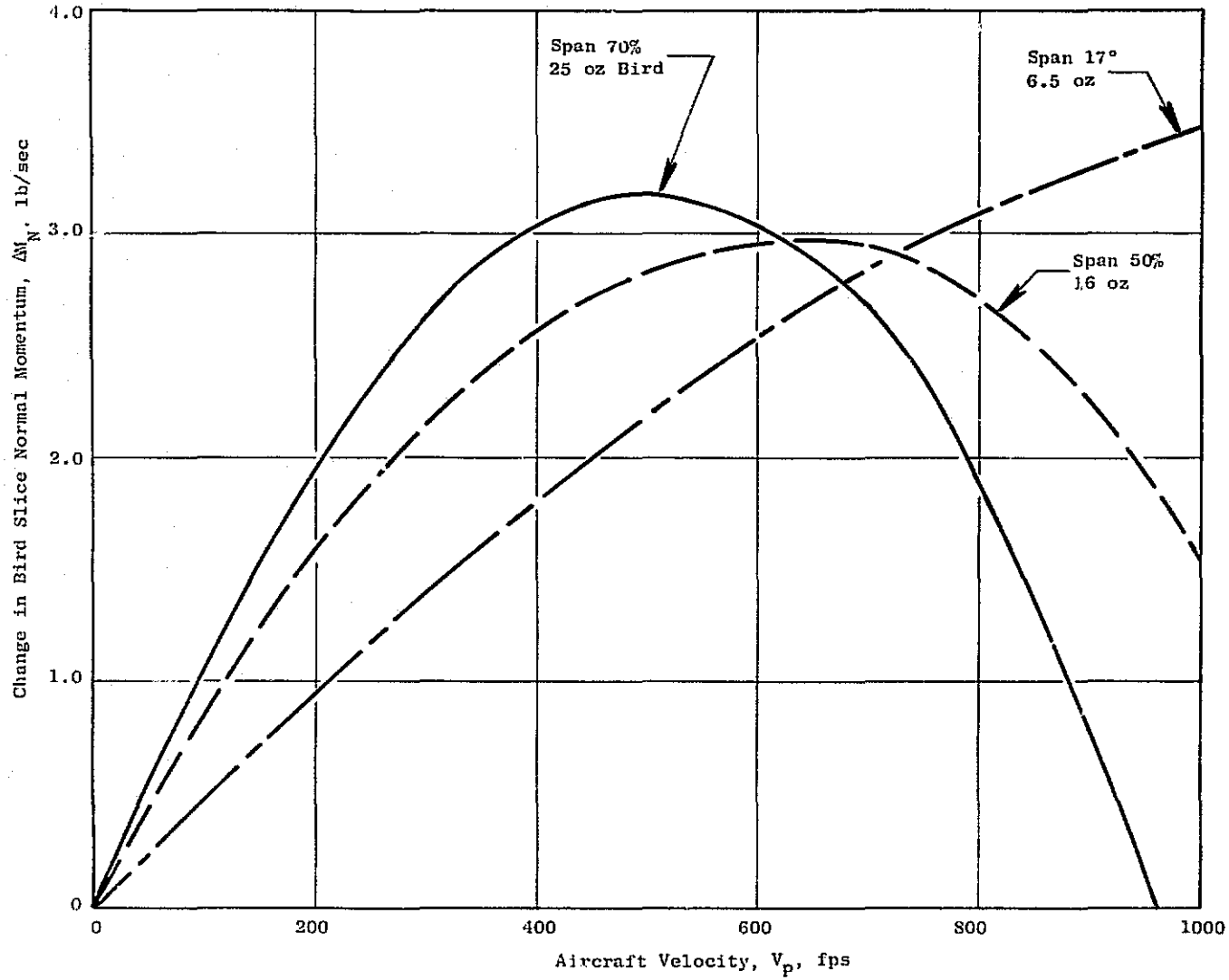

Figure 52. J101 Blade Impact - Change in Bird Slice Momentum.

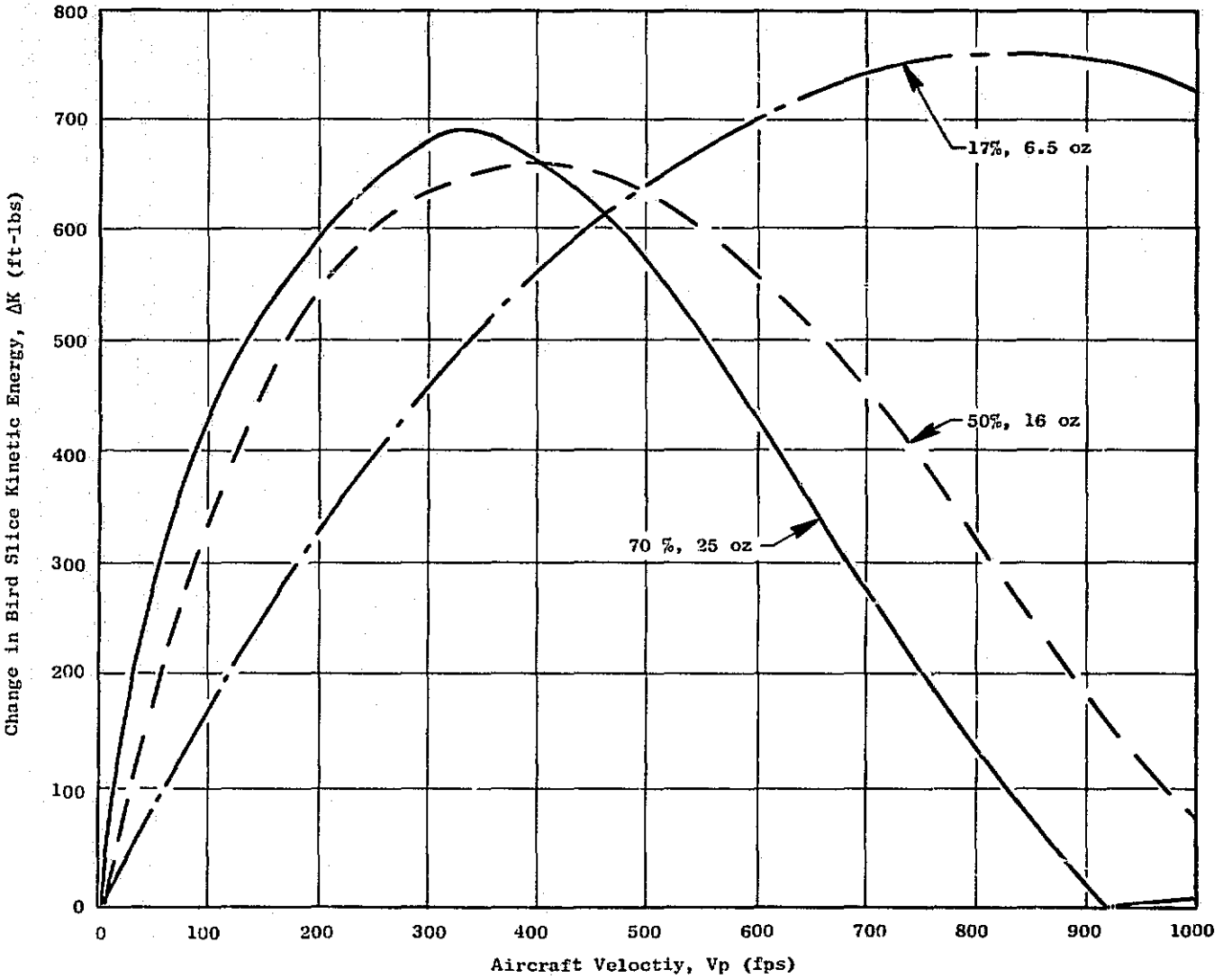

Figure 53. J101 Blade Impact - Change in Bird Strike Kinetic Energy.

Work done on the J79 B/Al blade has shown that good correlation between predicted and measured keyhole rotation was obtained by using the bird slice moment of momentum. However, it was also found in QCSEE blade studies that measured blade impact stresses correlated with changes in bird slice and changes in kinetic energy. Since this effort addresses the calculation of blade impact transient stresses and deflections, initial work attempted to use a Δ correlation, since it had been shown successful in the past. Shown below are the impact parameters for maximum Δ conditions at the three blade span locations.

Span %	ΔK	Vp (ft/sec)	Vr (ft/sec)	θ (degrees)	Ws (oz)	Wb (oz)	Ds (in)	Es/Ds
70	695	325	1321	22.5	2.8	25	3.94	0.13
50	661	400	1180	26.3	2.5	16	3.4	0.185
17	765	800	1153	25.5	3.2	6.5	2.5	0.385

3.6 SCAR BLADE SELECTION RATIONALE

The J101 fan was selected for application of B/Al in this program because of its similarity to the preliminary SCAR engine fan systems. The existing J101 and a preliminary SCAR fan configuration are shown in Figures 54 and 55. Both are axial flow, high tip speed fans designed for high efficiency, stall margin and inlet distortion tolerance. A comparison for the J101 and SCAR fans significant design parameters is presented in Table XVIII. The two fan blades are very similar, except in size. The J101 fan air weight flow is 127 lb/sec compared to 820 lb/sec for the SCAR fan. Physically, the J101 fan has a 26.32 inch inlet diameter compared to the SCAR inlet diameter of 66.328 inches, a scale factor of 2.52.

A twisted blade analysis of the SCAR stage 1 B/Al fan blade was conducted, using a 8.0 mil boron fiber with a (±15) layup. The resulting Campbell program is shown in Figure 56. The first flexural frequency lies 13% above the 2/rev excitation line at 110% rotor compared to the desired 115% margin. The decrease in the first flexural stability margin compared to the J101 stage 1 fan blade is due primarily to the higher blade tip tangential velocity (1640 ft/sec compared to 1504 ft/sec). A slight increase in the blade root maximum thickness could alleviate this problem.

A study was also conducted to determine the bird ingestion requirements. Using the same assumptions applied to the J101 fan analysis, a 25 pound bird can be ingested through the SCAR front frame. This is due to the very large inlet radius of the SCAR with only 18 frame struts (same as J101). However, the FAA specification (FAA Advanced Circular AC #33-18)* listed in Table XIX is more applicable to the SCAR engine. Ingestion of two birds of three to five pounds is required; this is normally interpreted

*This FAA regulation superceded by "FAA Part 33, 1975)" after above study way completed and reported.

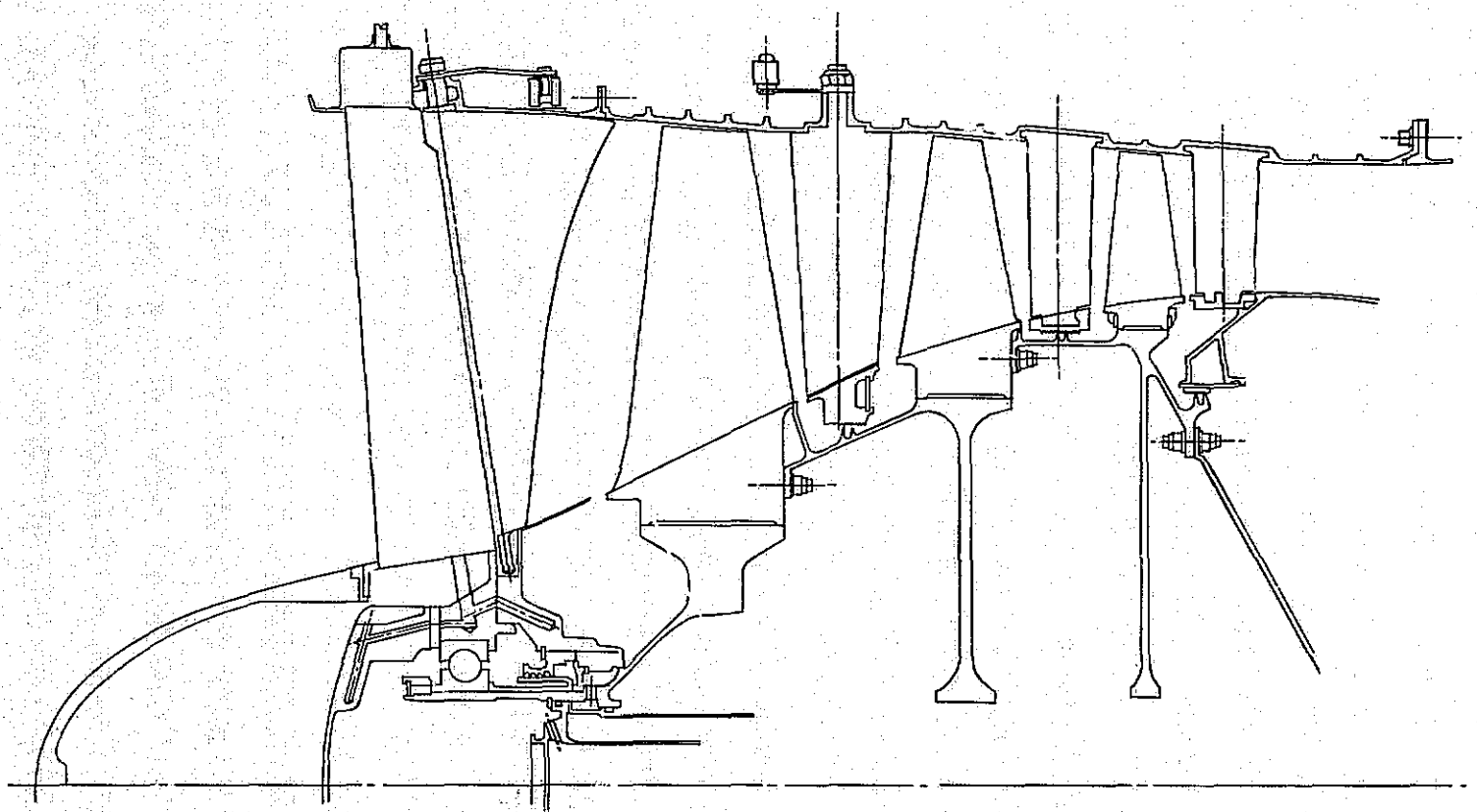

Figure 54. J101 Fan Rotor Assembly.

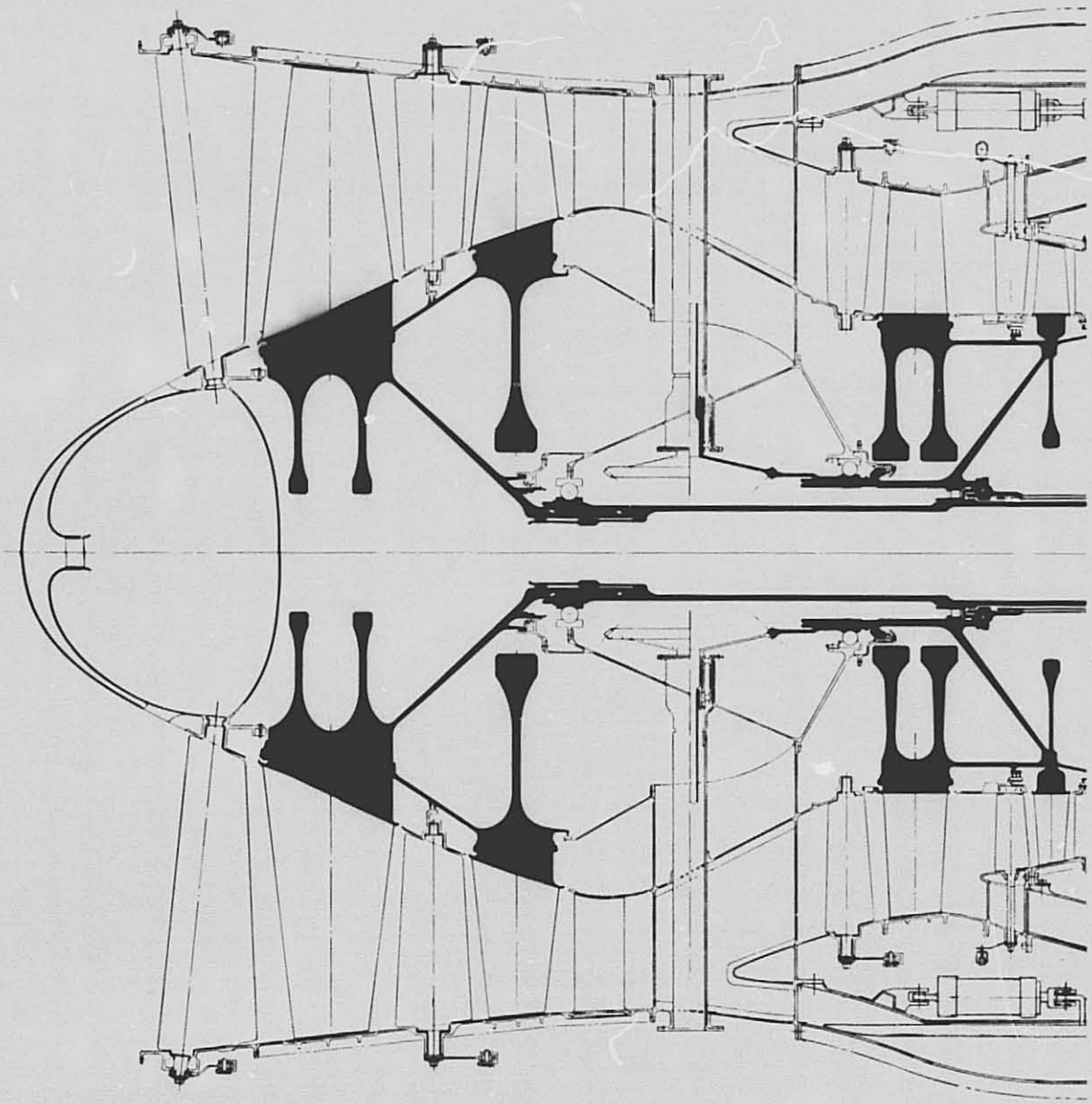

Figure 55. Preliminary SCAR Fan Configuration.

Table XVIII. J101 and SCAR Fan Comparisons.

Parameter	J101	SCAR
Weight Flow	127	820
Pressure Ratio		3.17
No. Stages	3	2
Inlet Diameter	26.32	66.328
100% Rotor Speed, rpm	13266	5650
Airflow per Frontal Area	42	42
Max. Operating Temperature, ° F	342	464

J101 and SCAR Stage 1 Fan Blade Comparisons

	Material	B/Al	B/AL
N	- No. Blades	32	32
V_t^b	- Tip Tangential Velocity	1504	1640
RR	- Radius Ratio	0.45	0.45
AR	- Aspect Ratio	1.77	1.73
L_{SA}	- Airfoil Length at Stacking Axis	6.24	14.45
	C_o - Root Chord	3.52	8.67
	C_t - Tip Chord	3.60	9.66
	S_o - Root Solidity	2.62	2.6
	S_t - Tip Solidity	1.40	1.4
	t_m/C_o - Airfoil Max. Thk/Root Chord	0.68	0.75
	t_m/C_t - Airfoil Max. Thk/Tip Chord	0.25	0.25
	β_o - Root Stagger Angle	18.72	29
	β_t - Tip Stagger Angle	60.89	71
	θ_o - Root Camber	99.7	
	θ_t - Tip Camber	2.93	
	t_e/C_o - Leading Edge Thk/Root Chord		
	t_e/C_t - Leading Edge Thk/Tip Chord		

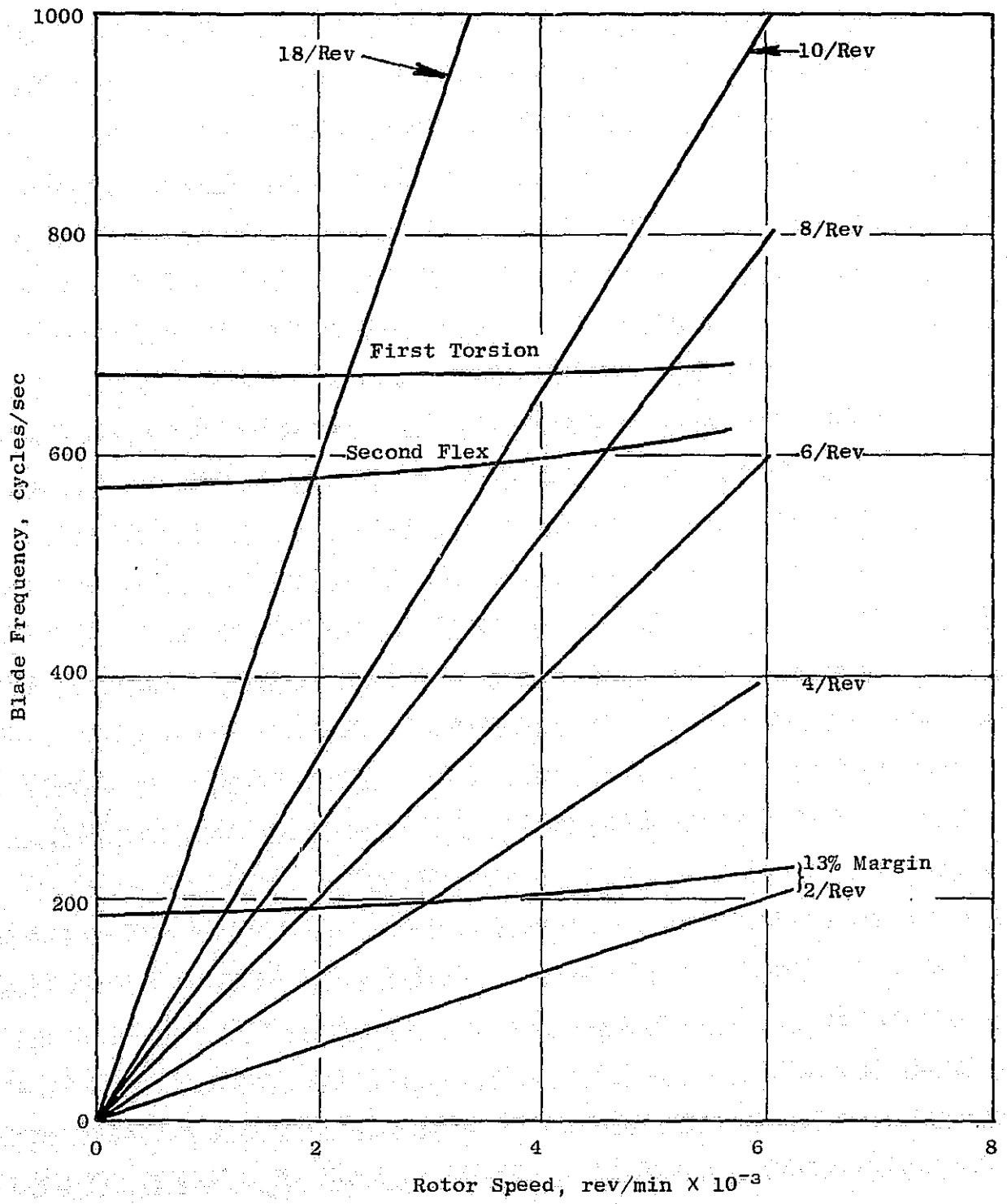

Figure 56. SCAR Stage 1 B/Al Fan Blade Campbell Diagram.

Table XIX. FAA Ingestion Requirements for SCAR Engine.

Group	Foreign Objects	Size	Amount	Occurrence	Power Recovery	Flight Condition
IID	Ice	Typical of Inlet Duct & Lip Formations	Typical Amount Ingested in a Single Flight	Single Flight All Engines	No Imminent Failure During Ingestion 75% Power	Cruise & Takeoff Power
E	Hail Stones	1 Inch 2 Inch	Two Per 150 Sq. Inches Inlet Area 46	Close Intervals	No Imminent Failure During Ingestion 75% Power	Max. Cruise
F	Birds, Small	2 to 4 Ounces	1 per 50 Sq. Inch Inlet Area 69	Close Intervals	No Imminent Failure During Ingestion 75% Power	Max. Takeoff
	Medium	1 to 2 lb	1 per 150 Sq. Inch Inlet Area 23	Close Intervals	No Imminent Failure During Ingestion 75% Power	Max. Climb & Max. Cont. Up to 8000 ft.
	Large	3 to 5 lb	1 per 2000 Sq. Inch Inlet Area 2	Close Intervals	None Established	Max. Climb & Max. Cont. Up to 8000 ft.

as a four pound bird. The impact parameters as a function of aircraft velocity for a four pound bird striking the SCAR blade at 70% span are presented in Figure 57. This impact results in the momentum and kinetic energy transferred to the blade shown in Figure 58.

Although the kinetic energy and momentum are much higher than a 25-ounce bird strike on the J101, the SCAR blade is larger than the J101. Table XX presents the relative severity of various size bird impacts on several blades as compared to a 3-ounce bird impacting a J79 blade as the baseline (1.0).

This comparison was based on the leading edge tearout shear stress resulting from the impulse force and assuming a cubic bird. The relative local impact severity of 2.07 for a four-pound bird strike on the SCAR compares to 1.75 for a 25 ounce bird strike on the J101. Thus, the SCAR impact severity is only 20% higher than the J101.

A similar study, presented in Figure 59, assumes a spheroidal bird of 2:1 radius ratio. In this case, a four pound bird striking the SCAR is less severe than a 25-ounce bird striking the J101 by about 11%.

The cubic bird results in a more severe impact than the spheroidal bird because the basic dimension of the cubic is equal to the minor diameter of the spheroid. This results in a 28% layer max slice weight for the cubic bird if the spheroid bird is assumed to be sliced across its major axis. Since the spheroidal shape more closely represents the bird shape, the impact severity resulting from the spheroidal bird shape most closely represents an actual bird strike of the two studies. However if the spheroidal bird is sliced across its minor axis the calculated slice weight is appoximately 60% larger than that of a cubic bird. This approach is not normally visualized as a realistic representation of how the bird would be sliced.

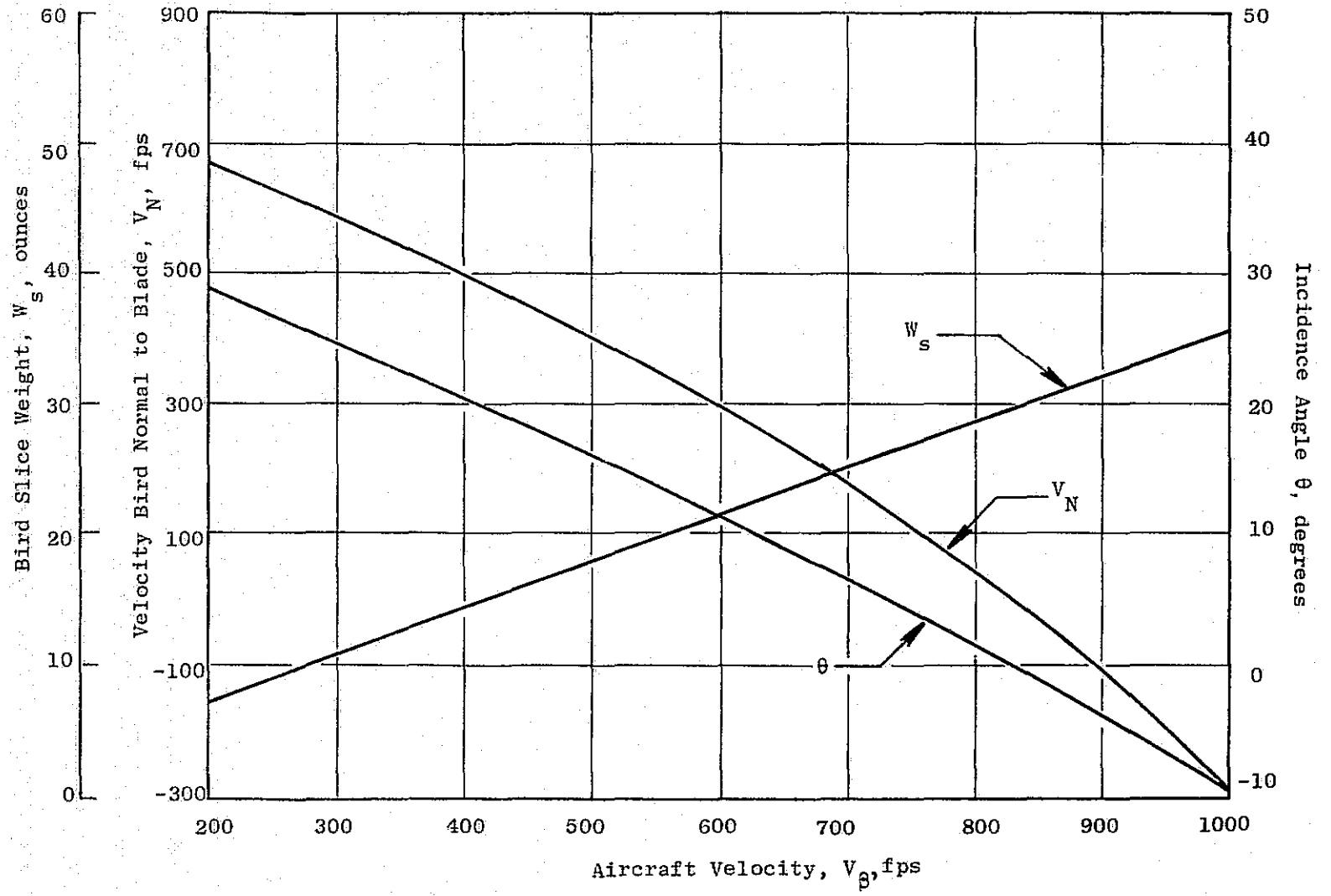

Figure 57. SCAR Stage 1 Fan Bird Impact Parameters.

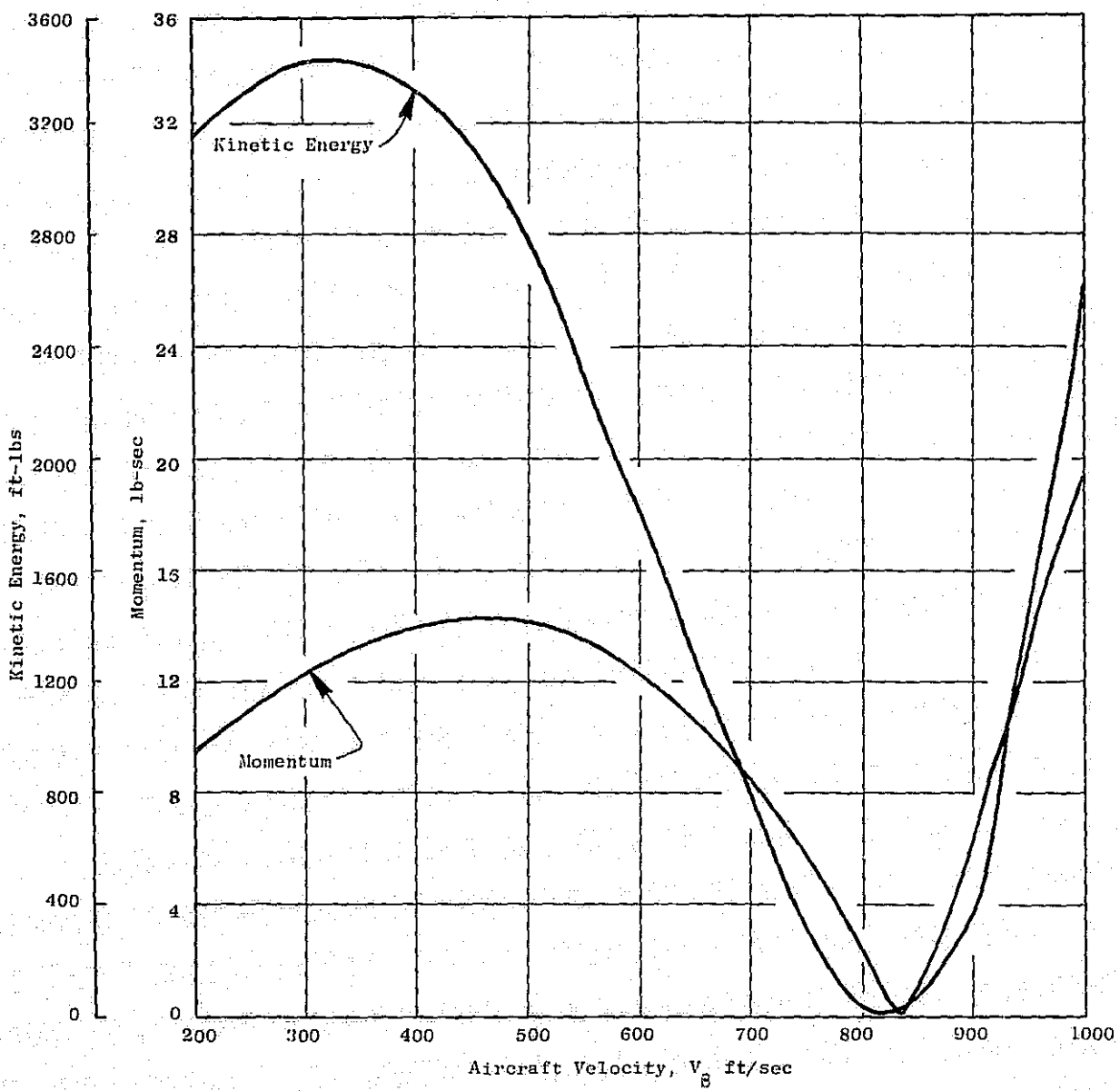

Figure 58. SCAR Stage 1 Fan Bird Impact Momentum and Energy.

Table XX. Comparison of Local Impact Parameters for Several Fan Blade Designs.

	J79	J101	CF6	TF39	QCSEE	F103	SCAR
Bird Size	3 oz	1.5 lb	2 lb	2 lb	2 lb	2 lb	4 lb
Tip Speed - Ft/Sec	1000	1500	1500	1000	978	1500	1640
Normal Momentum - Lb/Sec	1.88	3.6	10.8	12.8	20.4	18.1	18.50
Percent Span	70	75	75	75	75	75	75
Leading Edge Thickness	0.08	0.040	0.07	0.120	0.155	0.105	0.101
Thickness 1" From Leading Edge	0.12	0.085	0.12	0.155	0.205	0.235	0.214
Average Thickness (Unit Area)	0.10	0.062	0.095	0.138	0.180	0.170	0.156
Local Impact Severity	1.0	1.75	3.19	1.89	2.40	2.98	2.07

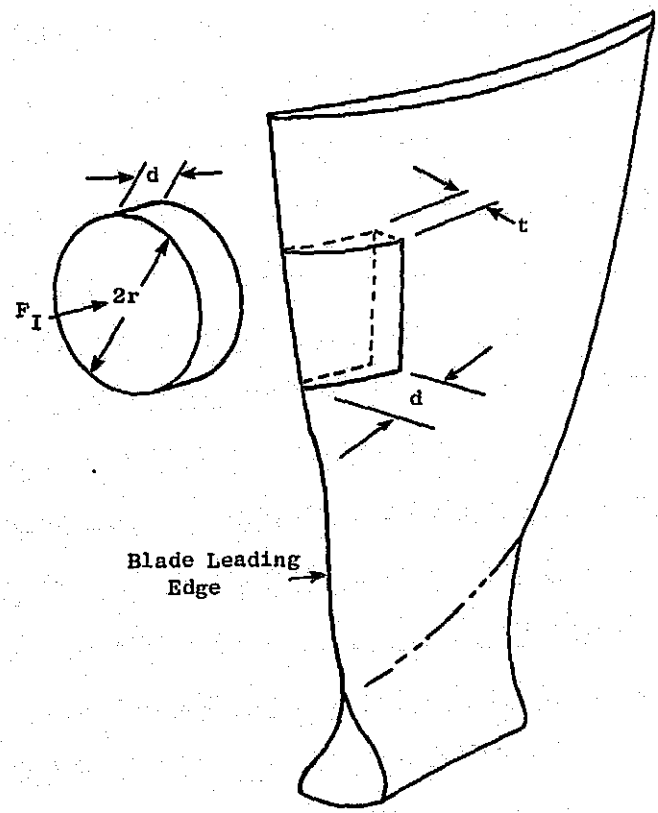

SCAR

4-lb Bird Strike at
70% Span

J101

25-oz Bird Strike at
70% Span

Assume:

Spheroidal Bird 2:1
Radius Ratio

te/c (J101) = te/c (SCAR)

V_{Bird} = 500 ft/sec

Impulse Force = $F_I \approx \frac{\text{Momentum}}{\Delta t}$

$\Delta t \approx 2r/V_R$ where V_R = Relative Velocity Between Bird and Blade

Shear Tearout Stress = $\tau = F_I/(2d + 2r)t$

Parameter	J101	SCAR
d, in.	0.513	11.92
2r, in.	3.88	5.30
t, in.	0.062	0.156
V_R, ft/sec	1,287	1,401
Momentum, lb-sec	3.2	14.25
F_I, lbs	12,732	45,204
τ, lb/in.^{2}	41,868	37,704
Local Impact Severity	1.75*	1.58

* Based on 3-oz Bird Impact on J79 as 1.0

Figure 59. Local Impact Severity of J101 and SCAR Blades.

3.7 BLADE FABRICATION PROCESS DEVELOPMENT

Two series of blades were fabricated in this development. The first ten J101 blades consisted of the initial fabrication performed prior to the advanced surface process treatment. The second 6 blades incorporated the newly developed surface processing along with the rapid band cycle for blade consolidation.

3.7.1 Materials and Blade Pressing Sequence

A summary of the first ten consolidated J101 blades is given in Table XXI. In the initial trial run at 920 F/6 ksi/20 an all 2024 aluminum blade without boron, was consolidated. This was done by cutting out the ply patterns using 0010 inch thick 2024 aluminum foil. These patterns were generated from the Tridea computer program masters. The purpose of this trail pressing was to demonstrate the conformance of the ply patterns in filling the die cavity as well as a check of the die tooling. The pressing cycle went very smoothly. However, difficulty caused by the shuttlebox cocking and locking onto the upper die section was encountered when the press was opened. Upon removing the shuttle box, indications were that the two clamps anchoring the box to the lower shoe did not satisfactorily perform. A minor box modification and clamp change were made.

In the second pressing, again an all-2024 Al alloy blade was consolidated at 920° F/6 ksi with the clamp-down modifications incorporated. The main problem was presumed to be the inability of the clamping mechanism to secure the matrix box to the bottom die assembly. Consequently, it was felt that the matrix box and the pressing cycle proceeded smoothly without any problems. The product was a well consolidated all - 2024 Al blade.

On the third pressing, the first B/Al blade, K52*82/1-2, herein to be designated as S/N2, was consolidated from the CRB B/Al tape. The purpose of pressing this blade was to further define possible ply modifications, to determine temperature distribution, and to identify any other die problems related to consolidating B/Al blades. This blade was an ATAC matrix (2024Al/1100Al) matrix blade with the [0°/20°] filament orientation with 55 v/o of the 8 mil diameter boron. The selection of this material system was based upon our prior panel results and the results of design studies which indicated that this filament layup, in reality a [±10°] orientation with a 10° bias, could increase the bird strike capabilities of the J101 blade. This blade was pressed without the outer stainless steel mesh sandwiched within the 2024 Al foil. Consequently, since a limited amount of outer layer was available to fill in irregularities, the blade exhibited considerable surface perturbations. Upon opening the press, the matrix box again hung up and necessitated a more extensive die modification to open the tolerance between the matrix box and the die assembly. The blade surface indicated regions of extensive material flow and heavily bonded areas. Consequently ply pattern modifications were made.

Table XXI. Summary of Consolidated J101 B/Al Blades.

Blade S/N	Material System	Fabrication Parameter	Outer S.S. Mesh	Orientation
KAL1	Al	920°/6ksi/20 min.		
KAL2	Al	920°/6ksi/20 min.		
K52*8 2/1-1[1]	ATAC	920°/6ksi/30 min.	No	[0/20]
K52*8 2/1-2	ATAC	920°/6ksi/30 min.	Yes	[0/20]
K52*8(2/1R-1T)-3	2/1R-1T[2]	920°/6ksi/40 min.	No	[0/20]
K52*8(2/1R-1T)-4	2/1R-1T	920°/8ksi/35 min.	No	[0/20]
K558(2/1R-1T)-5	2/1R-1T 2/1R-1T	920°/8ksi/35 min. 920°/8ksi/35 min.	Yes Yes	[±15]
K558(2/1R-1T)-6	2/1R-1t	920°/8ksi/35 min.	Yes	[±15]
K52*8(2/1R-1T)-7	2/1R-1T	920°/8ksi/35 min.	Yes	[0/20]
K52*8(2/1R-1T)-8	2/1R-1T	920°/8ksi/35 min.	Yes	[0/20]
Second Series of 6 Blades				
K5581-X1	2/1R-1T[3]	910°/8ksi/20 min.[4]	Yes	[±15]
K5581-X2	2/1R-1T	910°/8ksi/20 min.	Yes	[±15]
K5581-X3	2/1R-1T	910°/8ksi/20 min.	Yes	[±15]
K5581-X4	2/1R-1T	910°/8ksi/20 min.	Yes	[±15]
K5581-X5	2/1R-1T	910°/8ksi/20 min.	Yes	[±15]
K5581-X6	2/1R-1T	910°/8ksi/20 min.	Yes	[±15]

(1) The designation for orientation of 2* is [0/20]
(2) (2/1R-1T) - 2/1R is the ATAC system in the Root and the 1T is the 1100 AC material in the blade's tip
(3) Plies formed from bonded monotapes (BMT)
(4) Consolidated preformed by rapid bond cycle (RBC)

After the die and matrix box were modified, the blade designated, K52*82/1/2 or S/N 2, was consolidated. Again, the blade had a 55 v/o of 8 mil diameter filament at the [0/20°] orientation. In addition, the blade had an outer covering of the stainless steel 2024 Al material. Visual examination of the blade reveals a good surface. However, again, cordwise regions of heavily bonded areas were detected and additional ply modifications were made. As for the first B/Al blade, this blade appeared to be well bonded.

The remaining six B/Al blades were formed with the airfoil containing the all-1100 Al matrix while the root section contained the ATAC system of alternate layers of 1100 Al and 2024 Al matrix. One of these blades S/N 4, is shown in Figure 60 immediately following pressing and in Figure 61 after a bench cleaning operation. This blade appeared to be sound as evidenced by the metallic "ring". However, after the tip section was EDM machined, the blade no longer exhibited this metallic sound.

A detailed visual inspection of this blade revealed that five additional ply modifications were required. Ultrasonic C-scans were obtained on this blade along with blade K52*82/IR-IT)-3 or (S/N 3). Extensive defect indications were observed on the S/N 3 scans, but these areas appeared to have lessened on the S/N 4 blade.

Blade K558 (2/IR-IT)-5 or S/N5 contained a [±15] ply orientation along with the ply modifications from blade S/N 4. In addition, a sacrificial sheet was incorporated in the tip region to affect better tip bonding. This blade, again as with blade S/N 4, exhibited a metallic "ring", indicating a well-consolidated composite structure. After the tip was removed with a diamond cut-off saw, the blade still displayed the metallic "ring". From visual inspection, six relatively minor ply modifications were made. This blade, S/N5, was repressed to attempt to achieve a better consolidation. After this blade S/N 6, containing the same [±15°] orientation along with the ply modifications, was assembled and consolidated. Again, after the tip was cut off, the blade continued to display the metallic "ring" as evident in the as-consolidated condition.

With only minor modification, two more blades were consolidated. These blades contained the [0°/20°] orientation and were designated K52*8 (2/IR-IT)-7 and -8. As before, these blades were consolidated in an identical manner as blades S/N 5 and 6 at 920° F/8 ksi/35 minutes and contained the tip sacrificial sheet. Upon removal from the press, both blades had a metallic "ring," but after the tip cut off they no longer exhibited this "ring." As a consequence, the blade fabrication program was curtailed until the surface bonding treatments were identified for the 1100 aluminum. This effort, outlined earlier, permitted the consolidation of fully bonded, B/Al material with the use of the S/F9 surface treatment. The blade fabrication was reinitiated and a total of six blades fabricated. All six blades were made with the 8-mil boron and the 1100 aluminum matrix and were consolidated from the bonded monotape (BMT) described earlier, at 910° F/8 ksi/20 minutes using a Rapid Bond Cycle (RBC). In this fabrication cycle, the entire die assembly was preheated to 700° F and the matrix box contain-

Figure 60. Blade S/N K52*8(2/IR-IT)-4 After Pressing.

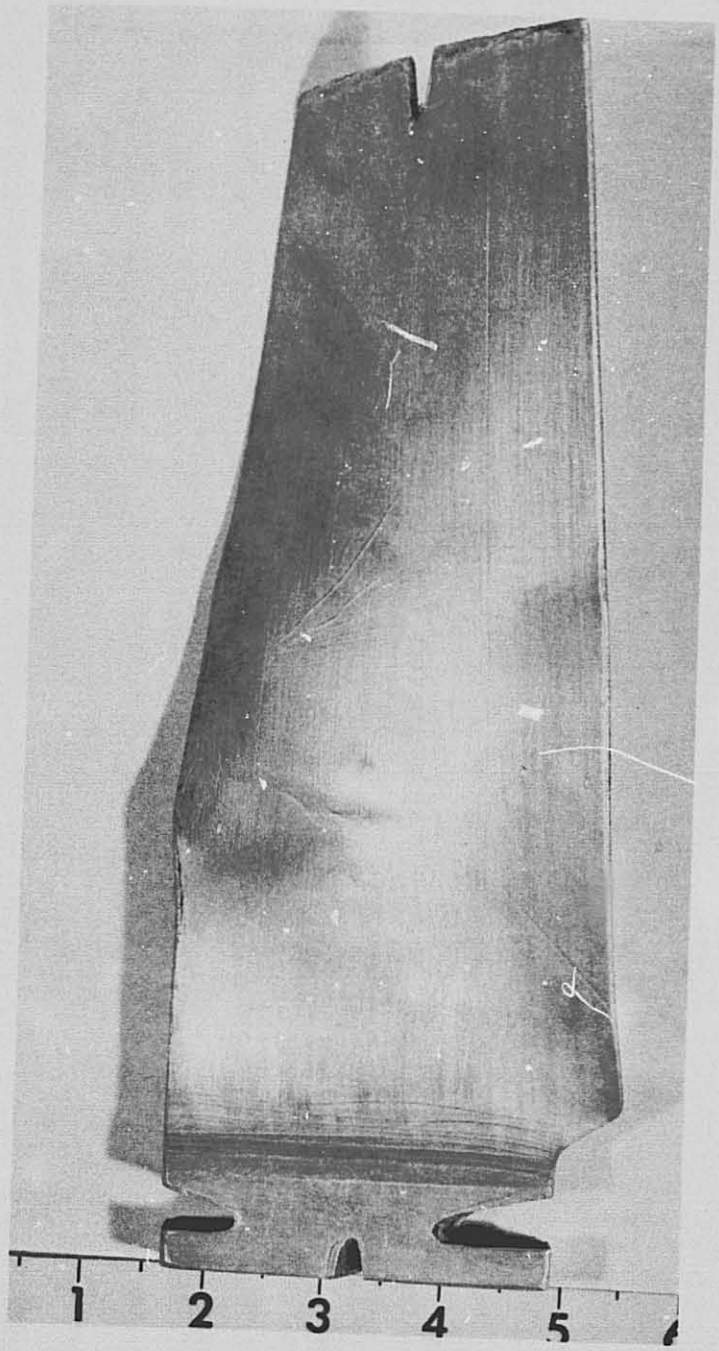

Figure 61. Blade S/N K52*8(2/IR-IT)-4 After Bench Cleaning.

ing the stacked ply assembly was inserted into the chamber within the die envelope. Next the chamber was closed and the assembled plies treated to 910° F. Finally, the ply assembly was pressed at 8 ksi for 20 minutes to form the consolidated blade.

3.7.2 Quality Control

As part of the overall quality control process, each blade was thoroughly inspected by a visual examination. An integral facet of the visual examination was to evaluate the surface characteristic of the outer sacrificial sheets. Such examinations indicated the ply adjustments needed to more completely fill the die cavity containing surface asperities. In the course of this program, a great number of ply modifications were made; however, even after consolidation of the original eight B/Al blades, additional adjustments were still required.

In addition to the visual examination, dimensional inspections were made on each blade. A summary of these dimensional inspection results are tabulated in Table XXII for blades S/N 4 through S/N 8, along with the drawing tolerance at the select locations. The measurements indicate that the blades were oversized compared with the drawing tolerances by about 0-020 inch relative to the maximum tolerance. As mentioned earlier, blade S/NK558 (2/IR-IT)-5 was repressed again at 920° F/8 ksi/35 minutes to further consolidate the blade. It was believed that the flash during consolidation restricted the dies from properly closing. As seen in Table XXII, the repressed blade's dimensions at the maximum thickness (T_m) were reduced by only 0.00/to 0.005 inch. Consequently, the ply assembly was reviewed and, as seen in Table XXIII, the number of plies in the assembled stack are in agreement with the observed measurements. Hence, it was concluded that the Tridea ply patterns did not accurately predict the die cavity dimensions. From this evaluation, an alternate method of ply pattern generation, was incorporated and employed in consolidation of the six added blades. This ply generation method consisted of scaling the plies from a mold casting of the die cavity. The newly developed plies in general were smaller than the original ply masters and appeared to more accurately follow the cavity contours.

The dimensional inspection for the second set of six blades, see Figure 62, as documented in Table XXIV, indicated a significantly thinner blade at all stations and show that the dimension at the blade's lower stations are within or close to the maximum tolerance, while the dimensions at the higher stations are about 10 mils over the tolerance, possibly as a result of the nonuniform BMT plies.

Ultrasonic "C" scan and radiographic inspections were conducted on all blades. Except for the first two B/Al blades (fabricated from the ATAC material), all of the initial 8 blades exhibited extensive delamination indications. The second series of six blades reveal some U/S indication but were believed to be due largely to surface characteristics. To further evaluate possible filament degradation during the processing cycle, boron

Table XXII. Dimensional Inspection of B/A1 J101 Blades - Initial Eight Blades

Blade Section	Leading Edge					Max Thickness (T_M)					Trailing Edge					
	E-E	H-H	L-L	N-N	R-R	E-E	H-H	L-L	N-N	R-R	E-E	H-H	L-L	N-N	R-R	D/T Root
Drawing	0.034	0.027	0.018	0.015	0.012	0.194	0.152	0.103	0.089	0.079	---	0.038	0.026	0.022	0.020	---
Tolerance	0.054	0.047	0.038	0.035	0.032	0.214	0.172	0.123	0.109	0.099	---	0.058	0.046	0.042	0.040	0.760
Blade S/N																
S/N 4	0.066	0.055	0.052	0.053	---	0.240	0.188	0.143	0.125	---	---	0.070	0.074	0.055	---	0.760
* S/N 5	0.077	0.068	0.058	0.063	0.059	0.235	0.191	0.142	0.127	0.119	---	0.077	0.070	0.066	0.069	0.757
* S/N 5 (Repressed)	0.070	0.060	0.055	0.058	0.055	0.230	0.182	0.140	0.125	0.118	---	0.066	0.060	0.060	0.062	0.757
* S/N 6	0.075	0.066	0.058	0.062	0.062	0.234	0.190	0.144	0.131	0.136	---	0.078	0.064	0.067	0.064	0.758
* S/N 7	0.074	0.066	0.060	0.067	0.061	0.245	0.194	0.147	0.136	0.126	---	0.081	0.073	0.068	0.067	0.764
* S/N 8	0.074	0.061	0.056	0.061	0.056	0.243	0.195	0.146	0.133	0.122	---	0.069	0.062	0.066	0.064	0.762

*Includes SS Mesh

Table XXIII. Dimensional Inspection of B/Al J101 Blades - Six Additional Blades.

Blade Section	Leading Edge					Max Thickness (T_M)					Trailing Edge					
	E-E	H-H	L-L	N-N	R-R	E-E	H-H	L-L	N-N	R-R	E-E	H-H	L-L	N-N	R-R	D/T Root
Drawing	0.034	0.027	0.018	0.015	0.012	0.194	0.152	0.103	0.089	0.079	---	0.038	0.026	0.022	0.020	---
Tolerance	0.054	0.047	0.038	0.035	0.032	0.214	0.172	0.123	0.109	0.099	---	0.058	0.046	0.042	0.040	0.760[1]
3K-5581-X1	0.061	0.047	0.042	0.047	0.048	0.218	0.174	0.132	0.118	0.116	---	0.058	0.055	0.054	0.060	0.740
X2	0.057	0.047	0.038	0.045	0.045	0.226	0.174	0.130	0.116	0.113	---	0.055	0.055	0.051	0.053	0.740
X3	0.058	0.049	0.045	0.048	0.050	0.227	0.176	0.132	0.120	0.120	---	0.050	0.049	0.050	0.048	0.745
X4	0.059	0.049	0.042	0.047	0.048	0.226	0.177	0.132	0.118	0.114	---	0.051	0.051	0.052	0.054	0.745
X5	0.059	0.049	0.041	0.049	0.049	0.230	0.175	0.082	0.119	0.119	---	0.055	0.048	0.050	0.058	0.745
X6	0.058	0.051	0.046	0.048	0.047	0.221	0.175	0.126	0.120	0.118	---	0.061	0.052	0.052	0.054	0.747

[1] Includes the sacrificial B/Al ply plus two 0.005 inch Al plies.

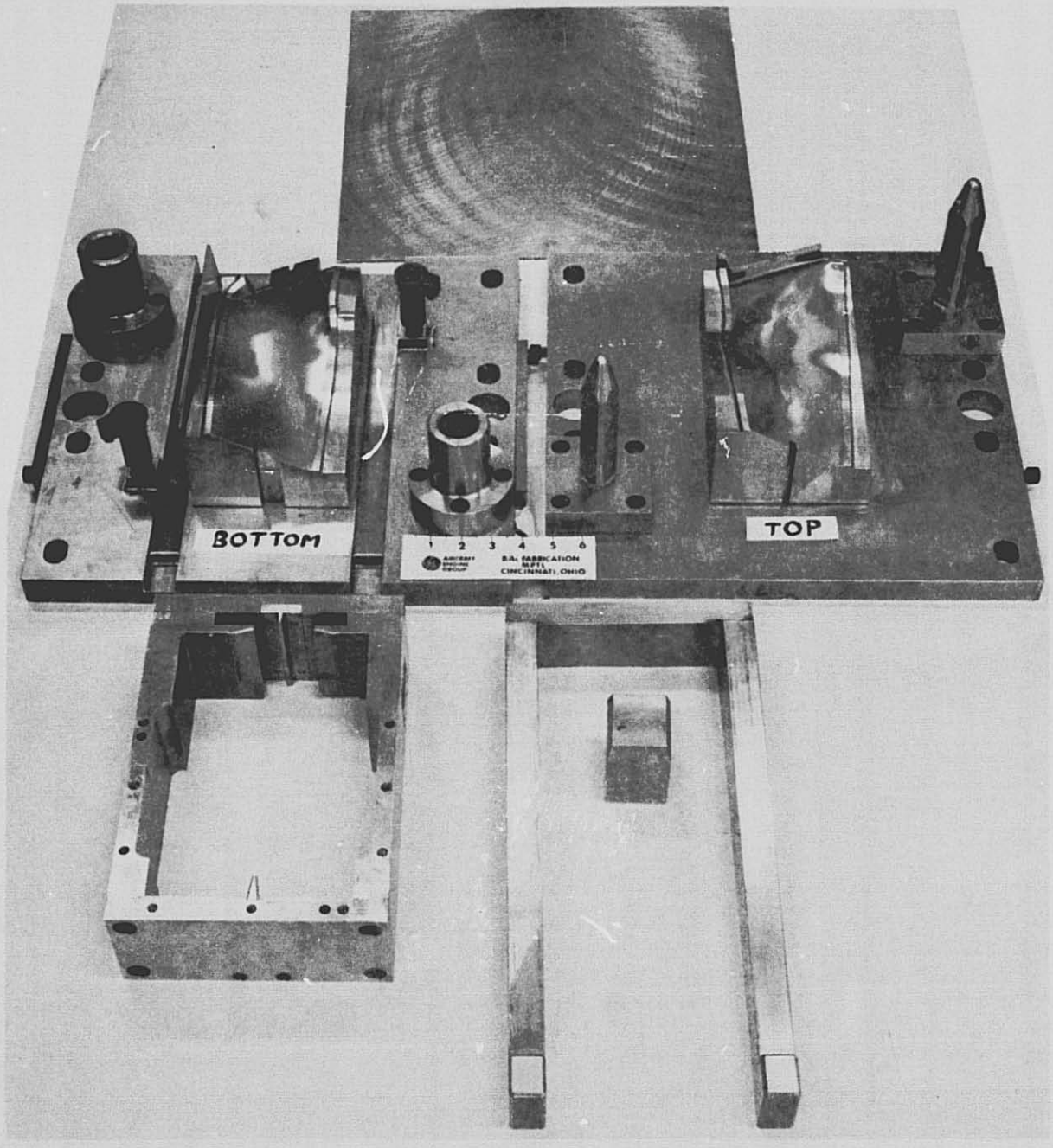

Figure 62. Consolidation Cycle on YJ101 Boron/Aluminum Compressor Blade.

Table XXIV. Ply Thickness Measurements versus Inspection Thickness at Ti.

Blade Section (Drawing Tolerance)	E-E (0.194/0.214)	H-H (152/172)	L-L (0.103/0.123)	N-N (0.089/0.109)	R-R (0.079/0.099)
(+ SS + Center Ply)					
No. B/Al Plies (0.0094 inch/ply)	23 (0.2162)	18 (0.1692)	13 (0.1222)	12 (0.112)	10 (0.094)
No. SS Mesh Plies (0.0056 inch/ply)	2 (0.0112)	2 (0.0112)	2 (0.0112)	2 (0.0112)	2 (0.0112)
Center Ply (0.005 inch)	1 (0.0051)	1 (0.005)	1 (0.005)	1 (0.005)	1 (0.005)
Calculated Ply Thickness	0.2324	0.1854	0.1384	0.1282	0.1102
Observed Thickness S/N 5 Repressed	0.230	0.188	0.140	0.125	0.118

filaments were extracted from a sacrificial root ply of the consolidated blades and tensile tested. The tensile strengths of the boron filaments before and after consolidation as shown in Table XXV for the first eight blades and Table XXVI for the second series of six blades reveal no filament degradation.

3.7.3 Tooling

The J101 blade die assembly is shown in Figure 63. The two halves of this hard, notched-metal die were permanently secured in position by bolting to the top and bottom press platens contained within a William White Vacuum Hot Press. The guide pins provided accurate alignment between the top and bottom die shoes and this, in turn, prevented die rotation, thereby producing close alignment of the die's faying surfaces. A unique characteristic of the pressing tooling is the capability of using the shuttle box as a ply location fixture, a die alignment tool and a matrix box for the subsequent blade machining operation. Accurate positioning of this matrix box between the two die surfaces allowed the ply assemblies to be accurately and consistently consolidated. The shuttle box with the ply patterns assembled in position can be readily installed into the die. In the consolidation cycle, the B/Al ply assembly contained within the shuttle box was positioned on the lower die. The Williams White press was then closed to obtain a seal on the vacuum chamber flange and the chamber was then evacuated. After heating the ply assembly to the desired temperature, the pressure was applied to form the composite blade.

3.7.4 Fabrication Processes

In this program, two fabrication processes were employed. The first series of eight B/Al blades were fabricated from continuous roll bonded (CRB) tape containing the acrylic cement binder. A schematic illustration of the bond cycle is shown in Figure 61. At the outset of the cycle, the temperature, was slowly increased with a constant loss of vacuum to remove the fugitive cement at about 500 to 700° F.

At the completion of the out gas cycle, the vacuum again returns to the 10^{-3} torr range. Heating was continued until a temperature of 800° F was reached at which time a 5% load is applied and the temperatures at the different die location coverage. After a temperature of greater than 875° F was reached, the full load of 5000 psi was applied. The heating continued until the desired temperature of 920° F was obtained and the 20 minute time at temperature under pressure was reached. The consolidated blade was then cooled in an organ atmosphere to below 400° F before the shuttle box containing the blade was removed. The entire bond cycle was of the order of 5 hours with an additional 2 to 3 hours for the cool-down cycle.

Table XXV. Boron Filament Tensile Strengths Before and After Consolidation.

Blade S/N	Tensile Strengths (Before Consolidation)	(ksi) (After Consolidation)
1	461	477
2	460	467
3	476	469
4	470	461
5	462	441
6	443	491
7	443	469
8	413	485

Table XXVI. Boron Filament Tensile Strengths Before and After Consolidation 10/11/76.

Blade S/N	Tensile Strengths (Before Consolidation)	(ksi) (After Consolidation)
X1	461.2	526.6
X2	528.3	514.0
X3	464.1	492.6
X4	475.3	472.4
X5	487.4	468.9
X6	436.9	448.1

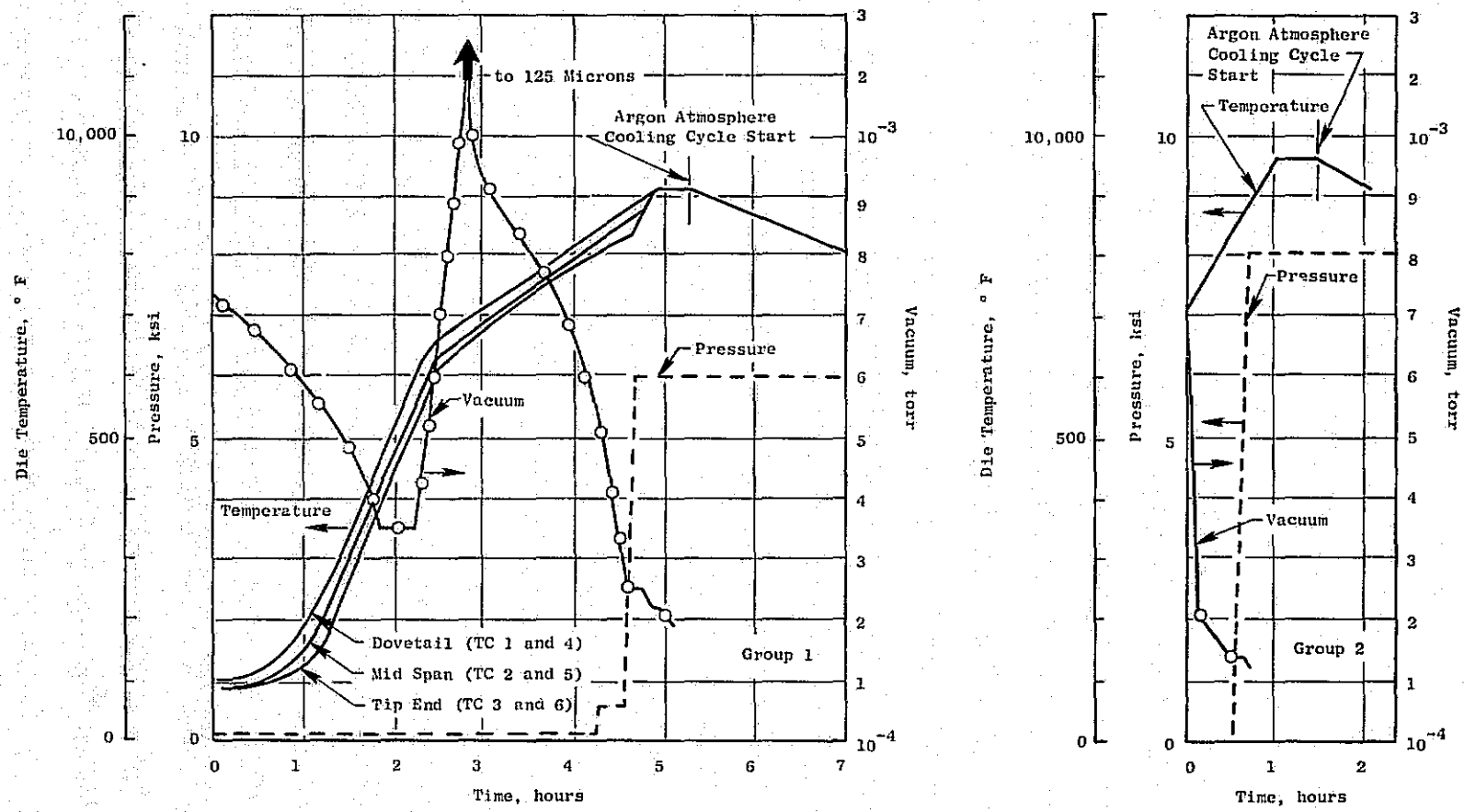

Figure 63. J101 Stage 1 B/Al Blade Molding Die and Matrix Box.

The second fabrication process is referred to as the Rapid Bond Cycle (RBC). In this process, the bonded monotape (BMT) plies aligned in the shuttle box, are inserted into a pre-heated die assembly at temperatures of the order of 700° F. The chamber is closed and the air evacuated to pressures below 10^{-3} torr. Upon heating to the pressure temperature of 910° F, the full bonding pressure of 8000 psi is applied for 20 minutes and the B/Al plies consolidated. The bonding schedule for this process is less than 1.5 hours. It is anticipated that the process time can be reduced to less than 0.5 hours, however this has yet to be demonstrated in blade fabrication.

3.7.5 Blade Evaluation

The initial set of eight B/Al blades consolidated from the CRB tape displayed poor bond qualities, particularly with the 1100 aluminum matrix. This low quality was due in part to insufficient bonding of the 1100 aluminum bonding within the confines of our correlation parameters, an internally funded program was initiated and was directed at solving the bond problem. This internal program identified special surface treatments such as the S/F9 treatment.

Following the successful surface evaluation, the SCAR program was again activated and a second series of six, all-1100 aluminum matrix blades fabricated. As before, these blades contained 8 mil boron filaments oriented at [±15°]. All six blades were determined to be well bonded and four blades were finished machined.

SECTION 4.0

CONCLUSIONS AND RECOMMENDATIONS

4.1 CONCLUSIONS

1. The impact strength of B/Al metal matrix materials can be affected by the boron fiber orientation and the aluminum matrix material. Greatest increases in impact strength were obtained from changes in aluminum matrix materials.

2. Two aluminum matrix materials were identified which yielded significant increases in 8 mil diameter B/Al composite material impact strengths relative to 2024 aluminum matrix material; they were 1100 aluminum and ATAC, (a two alloy (1100 Al/2024 Al) composite matrix material).

3. The 1100 Al matrix material yielded the highest impact strength B/Al, as measured by Charpy impact tests. A value of 55 ft-lbs was obtained. However, it is necessary to use special surface preparations in order to obtain adequate bonding of the 1100 Al matrix material.

4. For the 1100 Al matrix material B/Al, it was found that impact strength, tensile and shear strengths are affected by processing cycle conditions. Further the trends are as impact strength increases, tensile and shear strength decrease.

5. The impact, tensile and shear strength of the ATAC matrix material B/Al were intermediate between those of 2024 Al and 1100 Al. The affect of processing cycle conditions on properties was less pronounced than 1100 Al, however, it was found that the impact strength of the ATAC was directional, that is higher when impacted on the 2024 Al surface.

6. Of the six ply orientations investigated, $[0^\circ]$, $[\pm 10^\circ]$, $[\pm 15^\circ]$, $[\pm 20^\circ]$, $[0^\circ/20^\circ]$ and $[0^\circ/22^\circ/0^\circ/-22^\circ]$, the highest combination of impact and tensile strengths were derived from the $[\pm 15^\circ]$ orientation.

7. The matrix enhancement studies, including the stainless steel wire mesh in aluminum and the nickel plate, showed no significant improvement in soft body impact resistance.

8. Six full size J101 blades with 8 mil diameter Boron/1100 Al matrix material, and a $[\pm 15^\circ]$ fiber orientation were fabricated and are ready for whirling arm testing. The quality of the blades was good, based on ultrasonic "C" scan non destructive evaluations. In order to obtain good quality blades, it

was found that the generation of ply master patterns is extremely critical and must take into consideration the die contour irregularities.

9. A total of 18 J101 blades were fabricated. In the first series of pressing inadequate bonding was evident as a result of ply irregularities and poor bond characteristics of 1100 Aluminum matrix. Better ply definition and surface preparation led to fabrication of six J101 blades with 8 mil diameter 3/1100 Al at [±15] orientation, which are now ready for whirling arm testing.

10. Analysis indicated that the use of B/Al results in a shroudless fan blade design, for both the J101 and SCAR first stage blades, which satisfy aeromechanic stability design requirements.

11. Although increased Charpy Impact Strength was obtained by the development of the fabrication processes of 1100 Al matrix B/Al, but not being a part of this program, no data was obtained to identify whether blade FOD resistance is proportional to most Charpy Impact Strength.

4.2 RECOMMENDATIONS

1. The blades fabricated in Task IV should be subjected to whirling arm impact tests, with birds to establish their impact resistance.

2. Greater blade impact resistance improvements are potentially available by further refinement of material processing, improved control of pressing parameters, and mechanical design. Programs to develop and evaluate these improvements should be defined and carried out.

3. The current approach of using material specimen Charpy Impact strength to assess material impact strength does not result in meaningful blade design data for use in delineation of blade impact behavior. More meaningful material specimen test methods are needed to allow composite fan blade development to escape from the realm of build and bust.